

# DISSERTATION

## **A Topographic Mars Information System**

Concepts for Management, Analysis and Visualization of Planet-Wide Data

ausgeführt zum Zwecke der Erlangung des akademischen Grades eines Doktors der  
technischen Wissenschaften unter der Leitung von

Ao.Univ.Prof. Dipl.-Ing. Dr.techn. Josef Jansa  
Institut für Photogrammetrie und Fernerkundung (E122)

eingereicht an der Technischen Universität Wien  
Fakultät für Mathematik und Geoinformation

von

Dipl.-Ing. Peter Dorninger  
Matr. Nr. 9425300  
Emil Kögler-Gasse 13  
2511 Pfaffstätten

Wien, am 3. Juni 2004

The participation of the Institute of Photogrammetry and Remote Sensing (I.P.F.) in the Mars Express project was supported by the Federal Ministry of Technology (BMVIT) under project number GZ 190.174/2-V/B/10/2000. The following thesis is based on investigations in this project. Further on the author received a two years scholarship by the Neumaier Foundation from March 2001 to March 2003.

Die Beteiligung des Institutes für Photogrammetrie und Fernerkundung (I.P.F.) am Mars Express Projekt wurde durch das Bundesministerium für Verkehr, Innovation und Technologie (BMVIT) unter der GZ 190.174/2-V/B/10/2000 finanziert. Die vorliegende Arbeit basiert auf wissenschaftlichen Ergebnissen dieses Projektes. Außerdem erhielt der Autor ein zweijähriges Stipendium, finanziert durch die Neumaier Stiftung.

## Acknowledgements

I would like to thank all those who have contributed their time and effort to realize this research thesis. First of all, I would like to thank Josef Jansa, my supervisor, for his untiring encouragement and support of my study. Further, I am especially grateful to Georg Gartner for constructive discussions and Jörg Albertz for reviewing this thesis.

I am much obliged to Laszlo Molnar; without his encouragement this work probably would not have been finished. I further wish to thank Christian Briesse and Gottfried Mandelburger for their assistance and for proof-reading and all my colleagues at the I.P.F. for supporting me whenever necessary. A special thank goes to Hans Thüminger for his professional assistance in computer related problems.

I would also like to thank Thomas Roatsch, Marita Wählich and Frank Scholten as representatives of the Institute for Planetary Research, DLR, Berlin for their cooperation concerning the realization of TMIS and their assistance in Mars related matters.

Finally, I would like to express my utmost appreciation to my parents, my wife Angela and my son Christoph for their unwavering support and encouragement.

## Abstract

The *Institute of Photogrammetry and Remote Sensing (I.P.F.)* is participating at the project *Mars Express* which is supported by the *European Space Agency (ESA)*. Task of the I.P.F. is the development of a *Topographic Mars Information System (TMIS)* for efficient management and distribution of the high amount of image data provided by the *High Resolution Stereo Camera (HRSC)* on board the spacecraft, and also of surface point data as derived from these images using feature-based image matching methods, as well as subsequently derived digital terrain models (DTMs). Thus, the TMIS acts as the main interface for data exchange among the Co-Investigators of the *HRSC on Mars Express* project group.

The first part of this thesis deals with *concepts of spatial data modeling and management* and with data formats and data exchange with respect to available standards, mostly based on the *Extensible Markup Language (XML)*. Special attention is paid to the *Geography Markup Language (GML)* for data representation and exchange and to *Scalable Vector Graphics (SVG)* for web presentation of spatial data. Web presentation formats based on static images provided by a *Web Map Service (WMS)* are compared to object-based presentation formats. Further on, shortcomings as well as possible improvements and extensions to enhance the capability for efficient application of XML and related technologies in the area of geodata management are presented. Finally, the realization of the TMIS framework is described.

In the second part, methods for *topographic data manipulation and analysis* are investigated. For testing purposes, image and topographic data acquired by the NASA probe *Mars Global Surveyor (MGS)* has been used. Since the original surface point cloud contained gross errors due to incorrect referencing of the sensor platform, a method to detect and eliminate the erroneous points became essential. The computation of DTMs for further analysis is described afterwards. Ever since the surface of Mars is investigated in detail, scientists are discussing if liquid surface water was involved in the surface forming process in former times. To help answering this question, raster-based hydrological analysis methods were applied to regions which were possibly formed by water. The results are prepared for visual presentation. Finally, 3D visualizations of these results, e.g. for web presentation, are provided.

## Kurzfassung

Das *Institut für Photogrammetrie und Fernerkundung (I.P.F.)* ist am *Mars Express Projekt* der Europäischen Raumfahrtsbehörde ESA beteiligt. Die Aufgabe des I.P.F. ist die Entwicklung eines *Topographischen Mars Informationssystems (TMIS)*. Dieses soll die enormen Mengen an Bilddaten, welche vom hochauflösenden Kamerasystem *High Resolution Stereo Camera (HRSC)* erfasst werden, effizient verwalten. Die Verwaltung topographischer Daten als Originalpunktwolken sowie auch davon abgeleiteter digitaler Geländemodelle (DGMe) soll ebenfalls möglich sein. TMIS stellt somit die zentrale Datendrehscheibe innerhalb der Projektgruppe *HRSC on Mars Express* dar.

Im ersten Teil der Arbeit werden *Konzepte zur Modellierung und Verwaltung räumlicher Daten* unter Berücksichtigung vorhandener Standards und Normen beschrieben. Die Möglichkeiten auf *Extensible Markup Language (XML)* basierten Formaten für Datenhaltung und Datenaustausch raumbezogener Daten sowie für deren kartographische Aufbereitung zur Darstellung im Internet werden im Detail untersucht. Derzeitig verfügbare Implementierungen von *Web Map Services (WMS)* liefern meist statische Kartendarstellungen, obwohl seitens der Spezifikation von WMS auch objekt-basierte Ausgabeformate wie z.B. *Scalable Vector Graphics (SVG)* unterstützt werden. Im Rahmen der Entwicklung einer kartenbasierten Benutzerschnittstelle für TMIS wurden die Möglichkeiten von SVG eingehend untersucht. Basierend auf den resultierenden Erkenntnissen werden mögliche Erweiterungen zur Verbesserung der Anwendbarkeit vorhandener XML basierter Formate im Bereich der Geodatenmodellierung und -verwaltung präsentiert. Abschließend wird der gegenwärtige Implementierungsstand von TMIS als Anwendungsbeispiel der beschriebenen Methoden gezeigt.

Im zweiten Teil der Arbeit werden Methoden zur *Bearbeitung und Analyse topographischer Marsdaten* untersucht. Als Testdatensatz dienten Bild- und Topographiedaten welche im Rahmen der NASA Mission *Mars Global Surveyor (MGS)* erfasst wurden. Zunächst wird eine Methode zur Detektion und anschließenden Elimination grober Datenfehler, welche in den Originalpunkten enthalten sind, vorgestellt. Die Ableitung homogener und von zufälligen Fehlern bereinigter DGMe als Grundlage für weiterführende Analysen wird ebenfalls näher beschrieben. Seit die Oberfläche des Mars erkundet wird drängt sich die Frage auf, ob es in früheren Zeiten Oberflächenwasser gab. Um der Beantwortung dieser Frage näher zu kommen, wurden rasterbasierte, hydrologische Analysemethoden an ausgewählten, möglicherweise durch Oberflächenwasser geformten Bereichen des Mars angewandt und die Ergebnisse visuell aufbereitet. Als Abschluss der Arbeit werden dreidimensionale Visualisierungen dieser Resultate, unter anderem zur Darstellung im Internet, präsentiert.

# Contents

<b>1</b>	<b>INTRODUCTION.....</b>	<b>1</b>
1.1	MOTIVATION .....	1
1.2	OBJECTIVES .....	2
1.3	OVERVIEW.....	3
<b>2</b>	<b>MARS EXPRESS 2003 – THE SEARCH FOR WATER .....</b>	<b>5</b>
2.1	THE PLANET MARS .....	5
2.2	SCIENTIFIC GOALS.....	6
2.3	HRSC ON MARS EXPRESS .....	7
<b>3</b>	<b>CONCEPTS FOR SPATIAL DATA MANAGEMENT .....</b>	<b>9</b>
3.1	INITIAL SITUATION.....	9
3.1.1	Topographic Information Systems .....	9
3.1.2	Related Work .....	9
3.2	SPATIAL DATA MODELING .....	10
3.2.1	Database Management Systems.....	10
3.2.2	Database Models .....	11
3.2.3	Modeling Spatial Data Structures .....	13
3.2.4	Realizations of Spatial Data Modeling using Extended Relational Models .....	15
3.3	EXTENSIBLE MARKUP LANGUAGE FOR SPATIAL DATA REPRESENTATION .....	20
3.3.1	Introduction to XML .....	20
3.3.2	Geography Markup Language .....	21
3.3.3	Scalable Vector Graphics .....	22
3.3.4	Improving XML Performance .....	27
3.3.5	XML and Topographic Data .....	29
3.3.6	Integration of XML Documents in Databases .....	32
3.3.7	XPath Performance Considerations .....	33
3.4	CONCEPTS FOR WEB APPLICATIONS .....	34
3.4.1	Web Services .....	34
3.4.2	Web Services and Spatial Data .....	35
3.4.3	Spatial Data Presentation using Web Map Services .....	36

<b>4</b>	<b>REALIZING THE TOPOGRAPHIC MARS INFORMATION SYSTEM .....</b>	<b>38</b>
4.1	SYSTEM ARCHITECTURE .....	38
4.2	DATA MANAGEMENT .....	39
4.2.1	Meta Data Catalogue .....	39
4.2.2	Topographic Data Server .....	41
4.3	DATA ACCESS AND MANIPULATION .....	42
4.3.1	Requesting Footprint Maps .....	43
4.3.2	Requesting HRSC Images .....	45
4.3.3	Requesting Topographic Data .....	45
4.3.4	Integration of DTM Analysis and Visualization Tools .....	46
4.4	DATA PRESENTATION .....	47
4.4.1	Object-Based Visualization Methods .....	48
4.4.2	Image-Based Visualization Methods .....	49
4.4.3	Object- vs. Image-Based Visualization Methods .....	51
<b>5</b>	<b>MODELING THE TOPOGRAPHY OF MARS .....</b>	<b>52</b>
5.1	INITIAL SITUATION .....	53
5.1.1	Topographic and Image Data from the Mars Surface .....	54
5.1.2	Referencing Considerations .....	55
5.2	DTM COMPUTATION FROM ORIGINAL MARS SURFACE POINTS .....	57
5.2.1	Method for DTM Interpolation .....	57
5.2.2	Error Elimination .....	58
5.2.3	Comparison of Error Elimination Methods .....	66
5.2.4	DTM Computation .....	67
5.2.5	Results .....	70
<b>6</b>	<b>HYDROLOGICAL ANALYSIS OF THE MARS SURFACE .....</b>	<b>72</b>
6.1	HYDROLOGICAL ANALYSIS .....	73
6.1.1	Hydrological Map of Tharsis Region and Valles Marineris .....	73
6.1.2	Outflow Channel Detection in the Elysium Region .....	76
6.1.3	Simulated Outflow Behavior in Ma'adim Vallis and Gusev Crater .....	80
6.2	DERIVING STRUCTURE LINES FROM POINT CLOUDS .....	84
6.3	VISUALIZATIONS .....	85
6.3.1	Perspective Views .....	86
6.3.2	Virtual 3D Modeling .....	87
6.3.3	3D Hardcopy of Olympus Mons .....	89

---

<b>7</b>	<b>CONCLUSIONS.....</b>	<b>91</b>
7.1	SUMMARY AND ACHIEVEMENTS .....	91
7.2	FURTHER INVESTIGATIONS.....	92
	<b>APPENDIX.....</b>	<b>94</b>
A	MARS FACT SHEET.....	94
B	CHRONOLOGY OF MARS EXPLORATION.....	97
C	MARS EXPRESS FACT SHEET .....	99
D	SCIENTIFIC OBJECTIVES OF THE I.P.F. AS HRSC CO-INVESTIGATOR.....	100
E	HRSC PERFORMANCE .....	101
F	SCIENTIFIC PUBLICATIONS AND PUBLIC RELATIONS .....	102
	<b>ACRONYMS AND ABBREVIATIONS.....</b>	<b>103</b>
	<b>REFERENCES.....</b>	<b>106</b>
	<b>CURRICULUM VITAE .....</b>	<b>114</b>



# 1 Introduction

*"The exploration of other worlds underscores our responsibility to deal more kindly and compassionately with one another and to preserve and cherish that pale blue dot, the only home we've ever known."* (Carl Sagan 1934-1996)

On 14<sup>th</sup> of July 1965, the NASA probe *Mariner 4* passed the Mars and transmitted 21 images, covering about 1 % of the Mars surface. The era of Mars photogrammetry has begun. Since then, almost 30 Mars missions were accomplished and about half of them were successful. From a topographic point of view, the most important one is *Mars Global Surveyor (MGS)*, supported by the NASA as well (NASA-MGS, 2004)<sup>1</sup>. Among other results, it provided 112.000 coloured, high-resolution images (1.4 m/pixel at 400 km altitude) covering about 3 % of the surface and images covering almost the whole planet at a resolution of 280 m/pixel from 400 km altitude, using a wide-angle camera (NASA-MOC, 2004). Further on, more than 600 million individually measured surface points were determined, using a laser profiling altimeter. This point cloud describes the topography of the planet's surface. It allows to derive a digital terrain model (DTM) with a resolution of 1/128° grid width. This is equivalent to 463 m at the Martian equator (NASA-MOLA, 2004).

*Mars Express (MEX)*, the first European Mars mission, was successfully launched on 2<sup>nd</sup> of June, 2003. Since 25<sup>th</sup> of December 2003, it is in an orbit around Mars and on 10<sup>th</sup> of January 2004, the operational phase has started. The mission is supported by the *European Space Agency (ESA)*. Among other instruments on board the spacecraft, the *High Resolution Stereo Camera (HRSC)* is the instrument for photogrammetric surveying. Its scientific aim is high-resolution mapping of the whole Martian surface at a resolution of down to 10 m/pixel in color and stereo and about 1 % of the Martian surface in grayscale at a resolution of down to 2.5 m/pixel. The stereo images are to be used for deriving highly accurate surface points which will lead to an improvement of the currently available topographic models.

## 1.1 Motivation

As this work was started in 2001, most web-based image archives of Mars related data were based on file archives, available via FTP (e.g. Planetary Data System archives, MGS archives at the web servers of the related institutions, ...). Other approaches provided static image maps at the client-side. Furthermore, most of these solutions were implemented for a specific purpose and it turned out, they will not be applicable to solve the given task without major modifications and adaptations.

---

<sup>1</sup> Results of the current NASA orbiter *Mars Odyssey* are not considered within this thesis, as data for improving the topographic description of the Mars surface is not provided. The *THERMIS (Thermal Emission Imaging System)* acquires promising high resolution daylight image data from sampled areas and thermal images from almost the whole surface; potentially, they will allow to improve the current geological model (NASA-ODYSSEY, 2004).

In order to provide the best capabilities for managing and distributing the expected huge amount of HRSC topographic and image data – as well as of derived higher level products such as map projected images or DTMs – in an efficient manner, building up of a *Topographic Mars Information System (TMIS)* has been included into the project preparations.

The conceptual design and following realization of an information system for management and distribution of image and topographic data from the project group *HRSC on Mars Express* constitutes the central theme of this thesis. The original task of this research can be outlined as finding answers to the following two questions:

---

*“Which realizable and, if possible, standardized methods for management and for presentation of planet-wide image and topographic data do exist? How can they be applied to implement a web portal as central data provider for the project group “HRSC on Mars Express” in order to increase the efficiency of the HRSC experiment?”*

---

The first part of the thesis focuses on this task. Different models for data management and their historical development are described with a special view on the object-relational model. Furthermore, current trends are introduced such as object-oriented models or XML based data management. Afterwards, the concept for the realization of the web-based TMIS framework is described. In particular, vector and raster-based methods for the representation of spatial information using common web browsers are compared.

It was intended to integrate analysis and visualization functionality in the TMIS. Hence, the following question arose:

---

*“Are raster-based hydrological analysis methods (rain simulation) appropriate to improve the interpretation of available and future DTMs of the Mars surface in order to determine hydrologically originated surface structures?”*

---

Consequently, the second part of this thesis describes the development of new and the adaptation of already available methods and algorithms for hydrological analysis and following visualization of Mars DTMs and their integration into the TMIS environment. As the surface point cloud used for testing purposes contained gross errors due to incorrect referencing of the sensor platform, a method to detect and eliminate the erroneous points was investigated.

## **1.2 Objectives**

Starting from a single-user, single-machine topographic database application based on a relational database enhanced by topological data types and access methods, a concept for a multi-user, web application had to be developed for efficient management and distribution of the data provided by the HRSC experiment. The interoperability between implemented modules and the new methods had to be guaranteed. As a matter of course, a graphical user interface based on both, parameter selection forms and interactive maps had to be provided.

An important matter of research was the integration and application of available and future standards, mostly based on the *Extensible Markup Language* (XML) for data transport (e.g. *Geographic Markup Language – GML*) and visualization (e.g. *Scalable Vector Graphics – SVG*). The capabilities of web presentation formats based on static images provided by a *Web Map Service (WMS)* according to the OpenGIS Consortium (OGC) implementation specifications are compared to object-based presentation formats.

This thesis describes the conceptual design and the realization of the TMIS. The advantages and shortcomings of the standards and methods used in relation to commercially used and already available other solutions are discussed. Possible improvements and extensions to enhance the capability for efficient application of XML and related technologies in the area of geodata management are presented.

A current focus of research at the I.P.F. concerns interpolation, management, application and visualization of nation-wide terrain data. Many scientific results were implemented in the commercially available software package SCOP++ (IPF-SCOP, 2004). The participation in the Mars Express Team was the first attempt to investigate the capabilities of these methods as applied to extraterrestrial data in a planet-wide context and to improve the already existing methods, technologies and applications in order to be able to apply them to Mars and, later on, receive a feedback for further Earth related problems.

For about ten years, *Airborne Laser Scanning* has become an effective method for topographic data acquisition with a high degree of automation. In 2001, when the research for this thesis began, the Mars-wide surface point cloud, acquired by the MGS, represented a new dimension of amount of laser-scanner points. On the one hand, by then it was one of the largest laser scanner projects in terms of measurements (more than 600 Mio. points) and on the other hand, this point cloud covers a whole planet. Besides being able to manage data on a complete sphere, organizing data describing the extensive surface area of Mars, which is equivalent to 1/3 of the Earth's surface or the total area of our continents, has become a challenging task.

Therefore, new methods for data management and access had to be found. As the original points contained gross errors due to incorrect referencing of the spacecraft, a method for detecting and eliminating those erroneous points was necessary. And last but not least, the application of methods for analysis and visualization of the derived DTMs were investigated, as they might facilitate finding some answers concerning the evolution of the Mars surface, possibly influenced by the appearance of liquid surface water.

### 1.3 Overview

The following chapter 2 introduces the reader to Mars-related research from ancient times until today. The scientific goals of the *Mars Express* mission are described and the contributions of the HRSC experiment to them discussed.

Chapter 3 presents concepts for spatial data modeling and results of investigating the *Extensible Markup Language (XML)* for spatial data representation and visualization. A closer look is taken on *Geography Markup Language (GML)* for data exchange and on *Scalable Vector Graphics (SVG)* for data representation and web visualization. As *Web Services* are emerging as the basic concepts for web applications, they are discussed finally.

The *Topographic Mars Information System (TMIS)* is a multi-user web application for management, distribution, analysis and visualization of planet-wide topographic data in combination with image datasets. The provided functionality has been separated into two different groups:

- *data management and distribution and*
- *analysis and visualization.*

*Data management and distribution* are provided by a web application, based on a database management system (DBMS). This system represents the kernel of TMIS and thus, it is referred to as *TMIS* in the following. The concepts of the system's realization are presented in chapter 4. Special attention is paid to the visualization of planet-wide shape information (polygonal boundaries of regions as used for footprints of images) within a web browser environment using standardized vector- and raster-based methods. Furthermore, planet-wide topographic data is management by TMIS and the way of distribution via the Internet is presented.

The *analysis and visualization* functionality is provided by a package named *TMIS-Extended Functionality (TMIS-EF)*. The investigation of new algorithms and methods for deriving homogeneous, "error-free" digital terrain models (DTMs) and subsequently their analysis and visualization are described in the chapters 5 (topographic data processing) and 6 (application and results).

The final chapter 7 summarizes the results and gives outlook to further investigations.

## 2 Mars Express 2003 – The Search for Water

*"Mars Express is the first fully European mission to any planet. It is an exciting challenge for European technology." (Rudolf Schmidt, Mars Express Project Manager, ESA).*

This chapter concentrates on general issues concerning Mars and the mission *Mars Express*. After a brief introduction to the historical knowledge of the planet, the mission *Mars Express* and its scientific goals, in particular the project objectives of *HRSC on Mars Express*, are described. Additionally information such as a *Mars Fact Sheet*, a *Chronology of Mars Exploration Missions* and a *Summary of Mars Express* as well as facts about *HRSC on Mars Express* may be found in the Appendix.

### 2.1 The Planet Mars

Mars is our immediate neighbor out from the Sun and the outermost of the hard, rocky terrestrial planets before the asteroid belt and the gas giants, such as Jupiter and Saturn (Battrick, Talevi, 2001). Since he can be observed by the naked eye, he was always known as one of the seven "planets" (Mercury, Venus, Mars, Jupiter, Saturn, Moon and Sun) which seemed to be moving around the fixed Earth, which was considered as center of the universe in former times. Inspired by its red color, which was already known 4000 years AD, he was associated with war. Within the Greek mythology he was named Ares, the god of war, always accompanied by Phobos (fear) and Deimos (panic). The name Mars was introduced by the Romans.

From these first observations to our present knowledge, a very long process of technological progress took place. During the Dark Ages, this progress was nearby stopped, due to the fact that the Church was not prepared to accept that the Sun, rather than the Earth, is the center of gravitation within our solar system, and billions of such systems are existing within the universe. They referred to Aristoteles who did not believe in the plurality of worlds. The astronomer Carl Sagan said once: *"Without Aristoteles, maybe Greek spacecrafts would travel between Mars and Earth nowadays"* (Puttkamer, 1997, p. 42).

Nevertheless, the fundamentals of current space science were established at that time. *Nikolaus Kopernikus* (1473 – 1543) defined the Sun as the center of gravitation, *Tycho Brahe* (1546 – 1601) observed the Mars with the naked eye and defined an empirical basis for *Johannes Kepler* (1571 – 1630), who derived his three laws about the moving of the planets using this information. *Galileo Galilei* (1564 – 1642) was the first who observed the Moons of Jupiter using a telescope. Based on observations of planets using telescopes, *Isaak Newton* (1643 – 1727) was able to define the law of gravity and to improve Kepler's third law considering the mass of the planets.

The first "albedo map" of Mars was drawn by *Christian Huygens* (1629 – 1695), who discovered *Syrtis Major*, a large, dark highland at the equatorial region of the planet. 1877 became a special year concerning Mars observations, as an advantageous opposition did occur. During this approach *Giovanni Schiaparelli* (1835 – 1910) produced the first detailed Mars map and named numerous

features. These names are still used nowadays. Furthermore, he was convinced to see rifts and channels (ital. canali) of natural origin. This experience was misinterpreted, and the story of large, artificial water channels and vegetation along them was born! Many well-known scientists (even Wernher von Braun, one of the most famous and important Mars scientists ever, who was involved into NASA's Mars exploration program until the 1970s) believed into this misinterpretation, until *Mariner 4* took the first close range images of the Mars surface during its fly-by in 1965. The reality was disillusioning. David Knight said: "*After the publication of the images, the scientific world was shocked. They found out, that the red planet – the only one in our solar system which allowed for the speculation for any kind of extraterrestrial life – has a Moon-like surface full of craters; a dead world as it seemed.*" (Eisfeld, Jeschke, 2003, p. 171).

During the 1970s the scientific image of Mars changed again. Orbiting spacecrafts – first *Mariner 9* (1971) and then the two *Viking* missions (1975) – showed there was much more to the Martian surface than craters. *Mariner 9* saw volcanoes twice as tall as on Earth. There were canyons as deep as the Earth's deepest ocean trenches. There were what appeared to be desiccated river systems. There were plains scoured by floods large enough to drain the Mediterranean in a month (Morton, 2004, p. 14).

After the following almost two decades without successful Mars missions, a new era of Mars investigation started with NASA's *Mars Global Surveyor (MGS)*, launched in 1996. This mission captured data with a degree of detail not available until then. Followed by the results of *Mars Odyssey*, scientists were able to discover surface features which seem to be of rather young age. Some of them appeared to be evidence that liquid water could have flowed on the surface in the recent past (Morton, 2004). This led to confusion by the Mars scientists, as they thought so far, that most of the surface forming processes took place in the planet's distant past.

In order to answer the upcoming questions raised by the new information, further missions are intended to observe the planet. As the year 2003 provided a very close up opposition of Earth and Mars (55,4 Mio km), three missions were launched: *Mars Express (MEX)*, the first European Mars mission and two similar so-called *Mars Exploration Rovers (MER)* sent by the NASA (NASA-MER, 2004). Whereas the primary aim of MEX is the search for current water as well as for signs of past or current life, the task of the rovers is to determine, if liquid water persisted long enough to make Mars hospitable for life. Unfortunately the lander of MEX, *Beagle2* was lost after its insertion into the Martian atmosphere, and the Japanese *Nozomi* spacecraft, which was on its way to Mars since 1998 in order to observe the Martian atmosphere, was lost in December 2003 as well.

## 2.2 Scientific Goals

*Mars Express* was launched on 2<sup>nd</sup> of June, 2003 in Baikonur, Kasachstan. It consists of an orbiter which reached its operating orbit in January 2004 and the above mentioned lander, *Beagle2*. Most of the instruments were taken over with some modifications from the unsuccessful Russian mission Mars96. An operational phase of one Martian year (687 Earth days) is funded. The spacecraft is designed for a further Martian year's operation.

The scientific goals of *Mars Express* are global high-resolution photogeology and mineralogical mapping, the search for subsurface water and the analysis of atmospheric composition and circulation. The following list describes them in more detail:

- *Global high-resolution photogeology (including topography, morphology, paleoclimatology, etc...) at 10 m resolution*
- *Super-resolution photogeology of selected areas of the planet (2 m/pixel)*
- *Global high spatial resolution mineralogical mapping of the Martian surface at kilometer scale down to several 100 m resolution*
- *Global atmospheric circulation characterization, and high-resolution mapping of the atmospheric composition*
- *Subsurface structure characterization at kilometer scale down to the permafrost (a few kilometers)*
- *Surface-atmosphere interaction; interaction of the atmosphere with the interplanetary medium (solar wind)*
- *Structure of the interior, atmosphere and environment via radio science measurements*
- *Surface geochemistry and exobiology*

(from: ESA, 2004)

The following Tab. 2.1 lists the instruments aboard the *Mars Express* spacecraft and their intended focus of investigation. Details are available at the ESA homepage (ESA, 2004).

<i>Instrument</i>	<i>geology topology</i>	<i>water</i>	<i>atmosphere</i>
<i>ASPERA – Energetic Neutral Atoms Analyser</i>		(X)	X
<i>HRSC – High/Super Resolution Stereo Camera</i>	X	(X)	X
<i>MaRS – Radio Science Experiment</i>	X		X
<i>MARSIS – Subsurface Sounding Radar/Altimeter</i>	X	X	
<i>OMEGA IR – Mineralogical Mapping Spectrometer</i>	X	(X)	X
<i>PFS – Planetary Fourier Spectrometer</i>		X	X
<i>SPICAM – UV and IR Atmospheric Spectrometer</i>		X	X

Tab. 2.1: Instruments aboard the *Mars Express* spacecraft and focus of investigation (X = direct, (X) = indirect).

### 2.3 HRSC on Mars Express

*“The HRSC experiment will directly address three of the scientific goals of the Mars Express mission, namely high-resolution and super-resolution photogeology including topography as well as surface-atmosphere interactions. It will provide significant support for atmospheric studies and mineralogical mapping and provide important information for studying the Martian subsurface.”* (Hoffmann et al., 2003, p. 5). A table of HRSC performance is provided in Appendix E.

The scientific objectives and measurement goals of the HRSC experiment on Mars Express have been formulated by the international team of 43 Co-Investigators from 10 countries under the leadership of the Principal Investigator Prof. G. Neukum. The major scientific objectives are:

- 
- *Evolution of the Martian surface morphology through time and geologic processes involved*
    - *Climate and the role of water throughout the Martian history*
    - *Evolution of volcanism on Mars*
    - *Evolution of tectonism and the structure of the crust*
    - *Atmosphere / surface interactions and Eolian processes*
  - *Atmospheric characteristics and dynamic atmospheric phenomena,*
  - *Characteristics of past, present, and future landing sites*
  - *Potential resources on Mars*
  - *Support for exobiological studies*
  - *Observation of Phobos and Deimos*
- 

(Hoffmann and Neukum, 2003, p. 9)

By comparing the already existing Martian imagery and the expected performance of cameras and altimeters aboard ongoing or planned missions, the imaging data to be acquired by the HRSC experiment should close the existing gap between medium- to low-resolution coverage and the very high-resolution images of the *Mars Observer Camera* on *Mars Global Surveyor* as well as the in-situ observations and measurements by landers.

The following imaging data and surface coverage will be achieved during the nominal mission lifetime of one Martian year:

- 
- *Medium to high-resolution imaging at 10-20 m/pixel: ~ 50% of the Martian surface, targeted observations*
  - *“Super” resolution imaging at 2-5 m/pixel: ≥ 1% of the Martian surface, targeted observations*
  - *Medium resolution imaging at 20-40 m/pixel: 70 % of the Martian surface, global and multiple coverage*
  - *“Low” resolution at ≤ 100 m/pixel: 100 % of the Martian surface, global and multiple coverage*
  - *Limb sounding (resolution variable) 2 to 3 times per month*
  - *“Spot Pointing” (EPFL) observations for atmospheric and photometric studies*
  - *In-flight calibration and commissioning*
  - *Phobos imaging at high-resolution = ≤ 30 m/pixel ~ 50% of Phobos surface*
  - *Phobos imaging at “low”-resolution = ≤ 100 m/pixel ~ 100% of Phobos surface*
  - *Deimos imaging as feasible*
- 

(Hoffmann, Neukum, 2003, p. 11)



## 3 Concepts for Spatial Data Management

In this chapter, different concepts for spatial data modeling are introduced. Afterwards, the capabilities of the *Extensible Markup Language (XML)* for spatial data representation and visualization are discussed. A closer look is taken on two already standardized XML applications: *Geography Markup Language (GML)* for data exchange and *Scalable Vector Graphics (SVG)* for data representation and web presentation. Current shortcomings of XML related technologies are outlined. As *Web Map Services (WMS)* are widely used for cartographic web presentation, this technology is investigated as well. The chapter concludes with general concepts for the realization of web applications.

### 3.1 Initial Situation

#### 3.1.1 Topographic Information Systems

For more than 10 years, one of the I.P.F.'s focus of research has been in the area of *Topographic Information Systems (TIS)*, a category of spatial information systems concentrating on digital data and models of natural and artificial topography at a scale of 1:2,500 to 1:100,000 (Kraus, 2000, pp. 1f.). *TopDB* is a realization of such a system, first presented by Loitsch and Molnar (1991). It is a relational database with additional data types and operations enabling topological relations. Loitsch and Molnar (1991) named this concept "*Topology in terms of relationality*", thus, *TopDB* is a topologic-relational database. Hochstöger (1996) introduced and implemented the database application *TopDM (Topographic Data Management)* in order to manage data, stored in *TopDB*, in a consistent state. Therefore, *TopDM* represents a Database Management System (DBMS) for consistent and efficient management of country-wide topographic data upon *TopDB*. Although this system would, from the conceptual point of view, enable concurrent user management, it was never implemented.

The *Topographic Mars Information System (TMIS)* is a multi-user web application for management, distribution, analysis and visualization of planet-wide available topographic data in combination with image datasets. It has been developed to increase the efficiency of the HRSC experiment working group of *Mars Express*. When setting up the TMIS concept, the main intention was the extension of the single-user, single-machine database application of *TopDM* to a distributed storage, multi-user web application, based on the commercial database kernel Oracle (Oracle, 2004). Furthermore, the realization should take into account XML related standards.

#### 3.1.2 Related Work

When this work started in 2001, most web-based image archives of Mars-related data were based on file archives, available via FTP from the investigating institutes. As an example the *Planetary Data System (PDS, 2004)* should be mentioned, which archives and distributes scientific data from NASA planetary missions (e.g. MGS), astronomical observations, and laboratory measurements. Other approaches provided static image maps at the client-side. The Arizona State University (ASU) operates the THEMIS archives in such a way (ASU, 2004). Furthermore, most of these solutions were

implemented for a distinct purpose and it turned out, that they will not be applicable to fulfill the given task without major modifications and adaptations. Therefore, the Data Processing Working Group of the HRSC project group decided to develop a web-based information system.

An approach, similar to the TMIS concept is provided by Gilbert (2002). The Centre for Topographic Information in Sherbrooke (CTI), Canada, distributes digital topographic data using a web application entirely implemented in Java. The user interface is realized using HTML pages and the map-based data access is provided through a WMS serving static image presentations. But this system is restricted to the management of country-wide datasets.

Another interesting realization of a so-called spatial data infrastructure describe Fitzke et al. (2004). The Free Software project *degree* started as a framework for integrating software products of different vendors on base of OpenGIS (OGC, 2004) and ISO standards (ISO, 2004).

In 2001, fat clients were not yet used for security reasons. Therefore, although providing a high degree of functionality, Java-Applets were not considered for TMIS. Most of the Co-Is were not willing to permit Java functionality in their browsing environment then. Nevertheless, new web-based database interfaces are realized using the Applet technology (e.g. EOLI-Web Envisat Catalogue, 2004). Therefore, another method to include client-side functionality, the *Scaleable Vector Graphics (SVG)*, is investigated in this thesis. Obviously the best reference for SVG examples is carto:net (CARTONET, 2004).

## 3.2 Spatial Data Modeling

### 3.2.1 Database Management Systems

According to Reinhart (1995, p. 32) a *database system (DBS)* consists of two parts:

- a *Database (DB)* representing a structured collection of data and
- a *Database Management System (DBMS)*, an application for handling the data.

A list of advantages of a centralized data management using a DBMS as compared to decentralized file storage gives Date (1990, pp. 15 ff.):

- Due to the fact, that the data can be provided to different applications, data redundancy can be decreased to a necessary extent and hence the amount of secondary storage capacity is reduced.
- Control and maintenance of remaining (intended) redundancy is simplified and the danger of inconsistent content is reduced.
- The preservation of the integrity (content correctness) of the data is supported.
- Unified data security and data backup concepts are realizable in a more simple way.
- Standards, concerning data representation such as naming or type conventions, can be realized easier.

According to the “ANSI/X3/SPARC Study Group on Database Management Systems (1970)”, a DBMS has to support two aspects of data independence:

- *Implementation independence = physical data independence*: The conceptual view on the data is independent from the internal (physical) data storage.
- *Application independence = logical data independence*: separation from DB and application interface.

In order to realize this independence, a 3-Tier-Schema-Architecture was proposed (Tsichritzis and Klug, 1978, pp. 173-191):

- The *internal schema* describes the system specific realization of the database. It is dependent on the operation system.
- The *conceptual schema* includes the logical modeling of the database structure using e.g. the relational model.
- The *external schema* defines the application dependent data view.

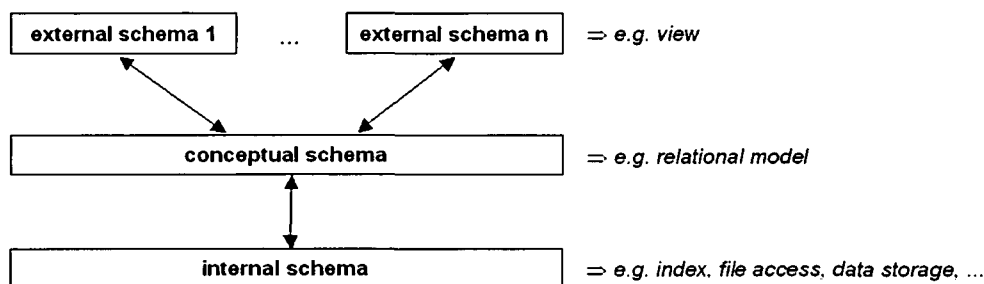


Fig. 3.1: Three-Tier-Architecture of a DBMS.

In the following, especially the conceptual and the external schemas of TMIS's concept are described. The conceptual schema has great impact on database consistency and performance. Thus, the following three sections (3.2.2 to 3.2.4) are introducing fundamentals which are used to realize the data management of TMIS. The realization of the external schema is discussed in chapter 4. The internal schema defining the physical data storage and the data access mechanisms such as index realizations shall not be discussed, as they are dependent on the implementation of the DBMS.

### 3.2.2 Database Models

#### *Hierarchical and Network Model*

The first generation of database models were *hierarchical models*, based on hierarchically structured data formats, and *network models*, based on chained datasets (records) which describe a network using binary functional relations. Further information can be found in Heuer and Saake (2000, pp. 105 ff.).

### Relational Model

In 1970, Edgar F. Codd (1970) invented the *relational database model* as the first abstract model for database management. This model describes real world *object types* (often named entities) using *relation schemata*  $R = \{A_1, A_2, \dots, A_n\}$  with the *attributes*  $A_i$  representing common properties of an object. *Domains* (value ranges) are associated with the attributes, mostly using standard data types such as integer, string, real or boolean ( $\text{dom}(A_i)$ ). A database schema consists of a set of relation schemata. A *relation* ( $r$ ) represents a subset of the Cartesian product over the domain of the attributes of the relation schema. Hence, it represents the current data of a relation schema being an *instance* of this schema. A relation according to a relation schema is named  $r(R)$ . One element of a relation is named *tuple*. A relation can be visualized as a table as shown in Fig. 3.2. The representation as Cartesian product has the disadvantage, that the order of the rows is fixed. Therefore, another representation is commonly used, defining  $r(R)$  as assignment of the attribute values to the attributes, resulting in tuples  $t_1, t_2, \dots, t_n$  and therefore providing independency from the order of the attributes.

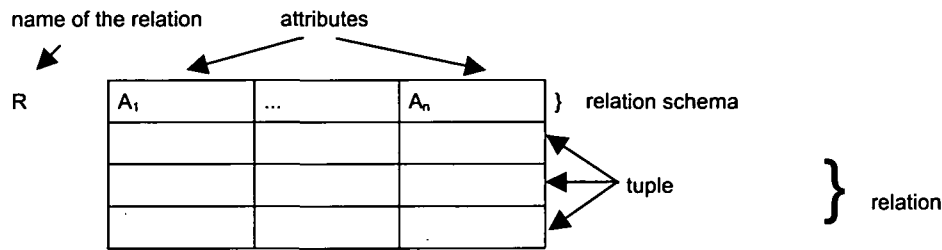


Fig. 3.2: Tabular visualization of a relation schema and the corresponding relation.

*Normal forms* (NF) try to avoid update anomalies within relations. According to Schrefl and Bichler (1995), a relation schema is in

- *first normal form*, if the domains of its attributes consist of atomic values,
- *second normal form*, if no non-key attribute is dependent on part of the primary key,
- *third normal form*, if no non-key attribute is transitively dependent on the primary key.

According to the first normal form, which requires atomic attribute values, neither data fields (arrays) nor complex objects or so-called nested tables are allowed. Thus, each geometric structure has to be separated into single points, and the coordinate values of each point have to be introduced as distinct attributes. Multipoint objects (e.g. polyline) require a tuple per point resulting in very large relations containing the geometry information of such objects. The following Fig. 3.3 shows a relation containing spatially referenced objects. The location of the villages is represented by the attributes  $x$ ,  $y$  and  $z$ .

ZIP	name	x	y	z
2481	Achau	603505	5326194	172
2511	Pfaffstätten	594338	5318896	218
...	...	...	...	...

Fig. 3.3: Modeling spatial information using the relational model.

The following section introduces alternative models as well as “extensions” to the relational model for more efficient modeling of complex structures.

### 3.2.3 Modeling Spatial Data Structures

„Almost everything that happens, happens somewhere. Knowing where something happens is critically important.” (Longley et al. 2001). About 80 % of available data can be associated to a spatial context. This can be the position of data acquisition defined by coordinates, or neighborhood relationships, referred to as topology as well. As shown in section 3.2.2, the core relational model is not appropriate to store spatial structures.

#### **NF<sup>2</sup> Model**

The 1<sup>st</sup> normal form (NF) is important in order to avoid database anomalies, but it prevents the definition of complex objects. An attempt to overcome this problem is the *NF<sup>2</sup> model*. NF<sup>2</sup> stands for *Non First Normal Form*, and allows to define non-atomic attribute data types. A relation schema  $R = \{A_1, A_2, \dots, A_n\}$  may be defined using  $\text{dom}(A_i) \in D$  of standard data types or  $A_i = \{A_{i1}, \dots, A_{im}\}$ , being recursively a set of attributes. On the one hand, this enables the definition of nested relations using constructors such as *set of* and *tuple of* and on the other hand, of array data types using the constructor *array of*. A realization of spatial data management using an array data type is presented in section 3.2.4.

#### **Semantic Data Model**

*Semantic data models* support further concepts of abstraction. According to Heuer and Saake (2000, pp. 125 ff.), currently no commercial database system realizes a semantic data model. A representative is the *Enhanced Entity Relationship Model (EER)*, defined by Engels et al. (1992, pp. 157-204). The semantic data models are not further discussed in this work.

#### **Object-Oriented Model**

The *object-oriented (OO) database model* is the consequent enhancement of semantic and nested relational models. Thus, it extends the concept of modeling complex structures by

- *complex data type constructors* enabling to model complex real world entities as one abstract object,
- *object-identity* enabling the distinction of objects and their values,
- *inheritance* of attributes and methods between objects

and it provides concepts to realize object specific operations such as

- *access methods*.

The first commercial object-oriented database systems (OODBS) were released in 1987. Beerli (1989) published a theoretical description for OO database models. There are three different directions of development

- extensions to object-oriented *programming languages* (e.g. C++, Java),
- extensions to *relational database systems* (PostgreSQL (POSTGRESQL, 2004), Oracle Spatial (ORACLE, 2004), IBM DB2 (IBMDB2, 2004), ...),
- *new developments* (O<sub>2</sub> (Bancilhon et al., 1992), ...) using OO database models.

The following example shows the specification of a point object using the algebraic specification of abstract data types as described by Ehrig and Mahr (1985).

---

```

datatype point based on real;
sorts point;
operations distance :      (point x point): real;
          xcoord, ycoord : (point): real;
          createpoint :    (real x real): point;
          add :            (point x point): point;
          ...
variables p,q : point ;
          x,y,x1,y1 : real ;
equations
  x = xcoord(createpoint(x,y));
  y = ycoord(createpoint(x,y));
  distance(createpoint(x,y),createpoint(x1,y1)) = sqrt((x-x1)*(x-x1)+(y-y1)*(y-y1));
  add(p,q) = createpoint(xcoord(p)+xcoord(q),ycoord(p)+ycoord(q));
  ...

```

---

This example is taken from Heuer and Saake (2000, p. 185) and shows the point constructor as well as the associated functions such as distance computation or add.

The *Object Data Management Group (ODMG)* tries to standardize the heterogeneous object-oriented database systems since the early 1990s. The current attempt of this group is the ODMG 3.0 standard, released in 2000 (Cattell et al., 2000). The structure of the standard consists of four parts:

- the *object model* defining the semantic of the object-oriented data model,
- the *database languages* Object Definition Language (ODL) and Object Query Language (OQL),
- the *bindings* of programming languages (C++, SMALLTALK, Java),
- the definition of a relation to the OMG (Object Management Group – standardization of object-oriented operating systems), to CORBA and to ANSI-C++.

### **Object-Relational Model**

The object-oriented model provides sophisticated concepts to model complex objects. The relational model is mainly implemented by commercial systems, because it provides a simple but efficient way to model real world entities. Therefore, the combination of these two models improves the capabilities of relational database systems by object-oriented concepts. This development resulted in so-called *object-relational database models*. In the following, the main concepts of this model are described, as TMIS is based on it.

The relational model is strongly associated with the *SQL (Structured Query Language)* standard. SQL is a relational database language. It may be separated into different groups of languages according to their functionality: e.g. the *Interactive Query Language (IQL)* to formalize database queries, the *Data Definition Language (DDL)* to define the conceptual database schema and the *Data Manipulation Language (DML)* to insert and manipulate managed data. It was first standardized in 1989 as SQL89-standard and enhanced in 1992 as SQL2, which was then accepted and implemented by the majority of the commercial vendors of relational databases. A new version, SQL3, is in progress, but has not been released yet. SQL99 realizes parts of SQL3, enhancing SQL's capabilities, for example, by object-oriented concepts, hence supporting

- abstract data types (ADT),
- object identifiers,
- ADT hierarchies,
- table hierarchies,
- definition of methods and functions on ADTs,
- overriding of functions and
- definition of complex data types.

Heuer and Saake (2000, pp. 142 ff.) separate object-relational implementations into different groups, according to what degree the above listed object-oriented concepts are realized. The following Tab. 3.1 lists obligatory and optional criteria for the distinction of extended relational DBSs in RDBS with Abstract Data Types (ADT) and "real" Object-Relational DBSs (OR-DBS).

part	concept	RDBS + ADTs	OR-DBS
structure	type constructors	must	must
	object identity	optional	must
	classes	optional	optional
	relations	optional	optional
	structure inheritance		must
	integrity constraints	must	must
operations	generic	must	must
	relational	must	must
higher concepts	methods	must	must
	inheritance		must
	overriding		optional
	encapsulation	must	optional

Tab. 3.1: K.O. criteria (must) and optional criteria for the distinction of extended relational DBSs in RDBS with Abstract Data Types (ADT) and "real" OR-DBSs (according to Heuer and Saake, 2000, p. 142).

### 3.2.4 Realizations of Spatial Data Modeling using Extended Relational Models

This section describes three implementations of RDBMS extended by different concepts, in order to increase their efficiency of managing spatial objects. The realizations of the academic software

package *TopDM*, the commercial system *Oracle* and the open source system *PostgreSQL* are introduced and discussed.

### ***Topographic Data Management – TopDM:***

*TopDM* is a topographic database application, intended for long time storage and archiving in a consistent way. It provides a GUI (graphical user interface) based access to topographic data managed by an RDBMS. To increase the quality of the managed data, the concept of *TopDM* supports the storage of a wide range of meta data such as accuracy, compilation method, authorized data users, and so forth (Hochstöger, 1996). Currently, two DBSs are supported through an abstract interface: *TopDB* and *Oracle Spatial*. It is not visible to the user, which database system is used. All necessary settings are defined during the initialization of the application. Thus, this system supports the distinction of logical and physical schema according to the ANSI/X3/SPARC model.

*TopDB* is an RDBS, extended by geometric/topologic elements (objects) and geometric/topologic operators in order to handle those elements. Topological data types include AREA (closed polyline), LINE (open polyline), POINT (single point) and WINDOW (rectangle parallel to coordinate system axis). Additional operators (.X. , .<. , .>. , ...) enable the intersection and selection of geometric/topological datasets.

The communication between *TopDB* and the application *TopDM* is realized by a database language called "TOPSQL". Its current functionality is on the one hand a subset of ANSI-SQL but on the other hand an extension regarding the geometric/topological data types and operators. A typical data selection could be to extract all data from a specified table, which are at least partially inside a given area, where the height accuracy is better than 30 cm and have been compiled later than 2004-05-03. This query can be formulated by using TOPSQL as follows:

---

```
SELECT * FROM DHMDATA
WHERE (COORDINATES .X. AREA (10000 50000
                             15000 60000
                             20000 40000)
      AND (ZACCURACY < 0.30)
      AND (COMPILEDATE > 03.05.2004);
```

---

The *logical schema* is realized by *TopDM*, defining a complex system of summary tables to guarantee data integrity and efficient data querying by providing a diversity of meta-information. Tab. 3.2 shows the table definition of a table type named TDXYZTAB. Tables of this type can store spatial objects. The geometry is stored as attribute COORDINATES. The objects may be 2D or 3D. The topological relationality is 2D as a grid-based indexing mechanism is used in order to increase the access performance. The coordinate information itself is stored as an array of coordinate tuples or triples (PERIOD) of a predefined accuracy (RESOLUTION = nr. of digits). IDOBJ is a unique system number comparable to an object-identifier as used by the object-oriented model. It may be used as primary key, but need not. All other columns are used to define meta-information such as type of geometry object (OBJECTTYPE), original data format (DATAFORMAT) and many more.



Name	Datatype	Unique Index	NULLs	Specification
IDOBJ	INTEGER	UNIQUE INDEX	NOT NULL	SYSNUM IDENTIFIER ,
DATAFORMAT	CHAR(16)	INDEX	NOT NULL	, ,
AGGREGATE	CHAR(64)	INDEX	NOT NULL	, ,
OBJECTNAME	CHAR(16)	INDEX	NOT NULL	, ,
OBJECTTYPE	CHAR(16)	INDEX	NOT NULL	, ,
COORDINATES	LINE	INDEX	NOT NULL	PERIOD(3) RESOLUTION(2,2,2) ,
FEATURECODE	CHAR(32)	INDEX	NULL	, ,
STATUS	CHAR(16)	INDEX	NULL	, ,
PROJECT	CHAR(32)	INDEX	NULL	, ,
MODEL	CHAR(32)	INDEX	NULL	, ,
XYACCURACY	NUMBER(12.2)	INDEX	NULL	, ,
ZACCURACY	NUMBER(12.2)	INDEX	NULL	, ,
CREATOR	CHAR(32)	INDEX	NULL	, ,
OWNER	CHAR(32)	INDEX	NULL	ARRAY ,
COMPILEMODE	CHAR(32)	INDEX	NULL	, ,
PROPERTIES	CHAR(32)	INDEX	NULL	ARRAY ,
COMPILEDATE	DATE	INDEX	NULL	, ,
COMPILETIME	TIME	INDEX	NULL	, ,
INSERTDATE	DATE	INDEX	NOT NULL	, ,
INSERTTIME	TIME	INDEX	NOT NULL	, ,
UPDATEDATE	DATE	INDEX	NULL	, ,
UPDATETIME	TIME	INDEX	NULL	, ,

Tab. 3.2: TopDM table definition of a TDXYZTAB enabling for storage of spatial objects.

Tables of type TDXYZTAB can store arbitrarily distributed topographic data. A dataset in one of these tables corresponds to exactly one terrain object represented by a series of 3-dimensional coordinates and additional data properties. This part of TopDM is named *Topographic Data Market*. It is used to manage “original data” describing the topography of an area according to the data sampling method used. Large amounts of randomly distributed points (e.g. bulk-data), additional linear structure information (e.g. break-lines) and further descriptive information (e.g. boundaries) can be managed, edited (pre-processed) and visualized.

Digital Terrain Models (DTMs) can be derived from original topographic datasets using different methods. In section 5.2.1 an appropriate method is described. Consequently, DTMs can be referred to as derived products. TopDM provides a functionality named *Derived Products Market*, for efficient storage and access of such datasets together with a set of meta-information parameter, comparable to those of the Topographic Data Market. Actually only 2.5D data can be managed, because the height information is treated as attribute and therefore only one z-value can be stored for each x/y location.

In order to apply reference frame transformations to the managed data, TopDM provides a variety of referencing systems, based on user defined reference ellipsoids, map projections and datum transformation parameter.

### Oracle Spatial

The commercial RDBMS Oracle provides a more complex concept for spatial data modeling. It allows to define abstract data types and provides functions, methods and stored procedures to create those and interact with them. Currently, Oracle neither supports the definition of class or type hierarchies nor

inheritance. As already mentioned, Heuer and Saake (2000) call such systems 'Database System with Abstract Data Types' and not object-relational as they define those object-oriented characteristics as essential (see section 3.2.3). For reasons of simplicity and because the vendor himself defines his system as OR-DBS, it will be named an OR-DBS in the following.

TMIS is based on Oracle 9i. The following considerations are related to this version of Oracle, although currently Oracle 10g is released. But this does not matter as it is not intended to give an introduction into this commercial system; only the concepts for spatial data management using this software are discussed.

The 'Oracle Spatial Users's Guide and Reference' (Oracle Spatial, 2003) defines Oracle Spatial as follows:

---

*Oracle Spatial is an integrated set of functions and procedures that enables spatial data to be stored, accessed, and analyzed quickly and efficiently in an Oracle9i database. Spatial data represents the essential location characteristics of real or conceptual objects as those objects relate to the real or conceptual space in which they exist.*

*Oracle Spatial, often referred to as Spatial, provides an SQL schema and functions that facilitate the storage, retrieval, update, and query of collections of spatial features in an Oracle9i database. Spatial consists of the following components:*

- *A schema (MDSYS) that prescribes the storage, syntax, and semantics of supported geometric data types*
- *A spatial indexing mechanism*
- *A set of operators and functions for performing area-of-interest queries, spatial join queries, and other spatial analysis operations*
- *Administrative utilities*

*The spatial component of a spatial feature is the geometric representation of its shape in some coordinate space. This is referred to as its geometry*

---

Fig. 3.4 shows the abstract definition of a spatial object as defined by the MDSYS schema of Oracle Spatial.

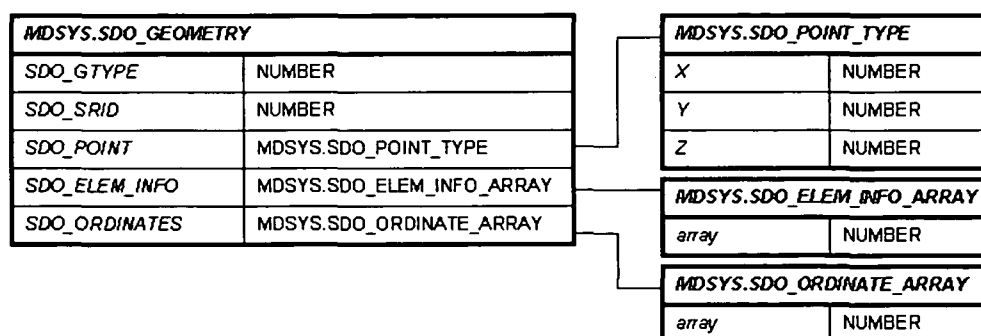


Fig. 3.4: Concept of a spatial object within Oracle Spatial 9i.

The geometry object represents a nested object with five attributes, from which three are non atomic data types. The access to the values of a spatial object is realized in an object-oriented manner. The following SQL code shows an INSERT command invoking the insertion of a spatial object:

---

```

INSERT INTO "TMIS"."SPATIAL_TAB" VALUES(
  [...],
  "MDSYS"."SDO_GEOMETRY"(
    2003, -- 2-dimensional polygon
    NULL, -- no spatial reference system (SRS) defined
    NULL, --
    MDSYS.SDO_ELEM_INFO_ARRAY(1,1003,1), -- one polygon (exterior polygon ring)
    MDSYS.SDO_ORDINATE_ARRAY(12.23,23.45,34.56,45.56,56.67,67.78,12.23,23.45)
  ),
  [...]
)

```

---

The first attribute, `SDO_GTYPE`, indicates the type of the geometry according to the “Geometry Object Model for the OGC Simple Features for SQL specifications” (OGC, 2004). The presented example defines a 2D polyline. The `SDO_SRID` attribute can be used to identify a spatial reference system (SRS). If no SRS is associated to the geometry, the value is set to `NULL`. Either the third attribute `SDO_POINT` or the following two, `SDO_ELEM_INFO` and `SDO_ORDINATES`, have to be `NULL`. The `SDO_POINT` attribute is used to define a simple point using the `SDO_POINT_TYPE`. This geometry type is recommended by Oracle for randomly distributed points; but it is not applicable to a large amount of single points as discussed in section 4.2.2. The other two attributes allow to define more complex geometries. `SDO_ELEM_INFO` is of type `ELEM_INFO_ARRAY` and defines the geometry type. `SDO_ORDINATES` stores the geometry information using an array type.

To enable spatial queries on attributes of spatial data type, a spatial index has to be created. Oracle supports two different implementations: *R-Tree* and *Quadtree* (Oracle, 2003, pp. 4-1 pp.). The spatial query operator is realized as a two-step process. The first step performs a selection according to the index information only. The second step realizes a selection according to the geometry information of the set of results determined by step one. *R-Tree*-indexed attributes can be queried in 3D. Unfortunately, only the first filter step is implemented for 3D queries.

In order to create a spatial index, metadata, defining the dimension, extension and resolution of the geometry types to be managed within an attribute, has to be stored within a global metadata table. This has to be realized by the application and is not performed by the index creation method.

Oracle Spatial is used as DBMS for the metadata catalogue of the TMIS. The realization of the conceptual schema as well as the data access is described in chapter 4.

### PostgreSQL

According to its documentation, *PostgreSQL*, currently available as version 7.4.2, is an OR-DBMS, (POSTGRESQL, 2004). According to the definitions presented in section 3.2.3, it is an RDBMS enabling ADTs, as no object or nested data types are supported. The realization of spatial data modeling is based on array data types. The fundamental building block for all geometry types is

Point. Supported geometry types are LineSegment, Box, Path, Polygon, Circle. Several index types (R-Tree, B-Tree) and geometric functions and operations on geometric objects are provided (intersection, area, isopen, ...). Core *PostgreSQL* supports only 2D geometries. *PostGIS*, developed by Refractions Research (POSTGIS, 2004), adds support for 2.5D geometries to the PostgreSQL server. Both systems are open source projects, distributed under the *GNU General Public License* (GNU, 2004). Therefore, it may be an interesting, possibly cheap, opportunity compared to commercially distributed systems.

### 3.3 Extensible Markup Language for Spatial Data Representation

This section gives an introduction to data management, exchange and visualization standards based on the *Extensible Markup Language (XML)*. Their main characteristics and capabilities are described.

#### 3.3.1 Introduction to XML

XML as data exchange format for the Internet tries to overcome the shortcomings of HTML (Hypertext Markup Language). These are syntax limitation (the HTML Document Type Definition (DTD) is fixed without the possibility of extension) and mixture of formatting information and data (XML allows to separate them). Furthermore, XML is especially built for reusability and it supports the Unicode character set, increasing its capability for internationalization.

An XML document consists of three different logical structures: *Tags*, *Attributes* and *Data*. A simple document might look like the following:

---

```
<person gender="male">
  <firstname>Peter</firstname>
  <lastname>Dorninger</lastname>
</person>
```

---

Tag names are enclosed with angle brackets '<' and '>'. They either occur in pairs as start and end tag or, for empty elements, as an empty element tag closed by a slash '/'. Start tags may include attributes. Attribute values have to be bounded by quotes. Data can be stored as attribute values. However, normally attributes are used to hold some meta-information which is used for several purposes (e.g.: language information) by the parser when interpreting the document.

XML documents represent their content as semi-structured data. Semi-structured data have one or several of the following characteristics:

- the schema definition is not stored in a central data dictionary. It is included into each document
- the data structure might change (different attributes, left attributes, different order)
- data itself has no further structure
- data types are not part of integrity constraints
- large number of attributes
- no strict distinction between data and schema

The *valid structure* of an XML document can be defined using two different mechanisms: *Document Type Definitions (DTD)* and *XML Schema Definition Language (XSD)*. The XSD is generally used to define XML applications, as it is standardized by the W3C, it is defined in XML and it provides more flexibility than DTDs.

The following list gives an overview of further XML related technologies (from: W3C-XML, 2004).

<i>namespaces</i>	restrict the scope of validity of XML objects
<i>XSD</i>	<i>XML Schema Definition Language</i> – defines valid structures and data types of an XML document
<i>XLink</i>	allows for linking of documents (extended HTML hyperlink functionality)
<i>XPath</i>	object selection language
<i>XQuery</i>	query language for XML documents (interface to databases)
<i>XSL</i>	<i>Extensible Stylesheet Language</i> – describes how to display / render documents; it consists of two parts:
<i>XSLT</i>	defines the transformation from one XML format into another
<i>XSL:FO</i>	<i>formatting objects</i> – allow to format an XML document

The acceptance and application of XML-based formats in the commercial market is growing. Unfortunately, there are still shortcomings within the available XML-based software solutions. For example, the current implementations of XPath have great performance shortcomings. As Gottlob (2002) shows in his tests, the evaluation time grows exponentially with the complexity of a query. This problem will be discussed in particular in section 3.3.7.

Currently several promising XML standards concerning geodata exist. In the following sections, an introduction to two already standardized XML applications for geodata is given:

- *Geography Markup Language (GML)* for data storage, management and distribution and
- *Scalable Vector Graphics (SVG)* for data visualization.

### 3.3.2 Geography Markup Language

The *OpenGIS Consortium (OGC)* was founded in 1994 in order to define standards for inter-vendor exchange of geodata. The OpenGIS Interface Specifications have become a successful foundation for interoperable geodata processing (e.g.: OpenGIS Simple Feature Specification). The increasing importance of the World Wide Web (WWW) as data exchange medium and the development of XML as a framework for the definition of proprietary data exchange formats lead to the development of the *Geography Markup Language (GML)*. GML can be characterized as follows:

---

*Geography Markup Language (GML) is an XML extension for encoding the transport and storage of geographic information, which includes geometry and properties of geographic features (Reichardt, 2001).*

---

This definition uses the expression 'XML extension' as a synonym for 'XML application'. The GML standard models the world according to the OGC Abstract Specifications, which define a geographic

feature as "*an abstraction of a real world phenomenon; it is a geographic feature, if it is associated with a location relative to the Earth.*" (Cox et al., 2004). The GML 2 specifications (latest version: 2.12) are concerned with the OGC Simple Features, features whose geometry properties are restricted to 'simple'. *Point, line, linestring* or *arc* are good examples for such objects. The current version, GML 3 (version 3.0 was released in January 2003 and version 3.1 is available as committee draft) overcomes many of the former restrictions. Thus, GML 3 allows to represent non-linear geometries (e.g. cubic, spline, bspline, bezier, clothoid, ...), 3D objects (e.g. building models), features with 2D topology, features with temporal properties, dynamic features, coverages and observations. GML 3 tries to fulfill the guidelines defined by the ISO 19100 standards (ISO, 2004). On the one hand, this important extension of the GML standard provides more flexibility in its application. On the other hand, the schema definitions became twenty times longer, making them much more difficult to be applied.

As one of the main characteristics of XML applications, GML supports full extensibility. Therefore, individual types can be defined. Another benefit of XML is the separation of content and presentation, and, as described in the previous section, there are several concepts to transform GML documents into appropriate formats for visualization such as SVG (to be discussed in the following section) or X3D, an XML application that can easily be transformed into VRML (Virtual Reality Modeling Language is the commonly used visualization standard for web presentation of 3D data. Further considerations relating to VRML are given in section 6.3.2).

GML is currently not integrated in the TMIS framework for several reasons: Most data to managed by TMIS can be characterized as structured according to the definitions for semi-structured data given in section 3.3.1. Thus, the integration of the structure information into TMIS relevant documents causes a large overhead of meta-information stored together with the data. Concerning topographic data which consists of numerous individual geometry objects with identical meta-information (e.g. object type, acquisition method, standard deviation, ...), the amount of metadata to be handled is very high. Nevertheless, section 3.3.5 describes an approach to map two different data formats for topographic data representation onto GML.

### 3.3.3 Scalable Vector Graphics

*Scalable Vector Graphics* (SVG), standardized by the W3C since September 2001 is an XML application for storage, exchange and especially for web presentation of geodata. The currently released version 1.1 can be found on the web (Ferraiolo et al., 2003). Since May 2004, a working draft version of SVG 1.2 is available.

The term *Scalable Vector Graphics* is misleading: SVG is in no way limited to vector graphics; on the contrary, it is surprisingly universal. SVG supports interactivity and animation and it is compatible to other XML standards such as DOM (Document Object Model – supports access of the objects entities), XSL (XML Stylesheet Language), SMIL (Synchronized Multimedia Integration Language) and many others. Therefore, a GML document, for example the result of a database request, can easily be transformed into an SVG document using XSLT.

There are three different groups of object types which can be represented using SVG:

- *Vector Data*
- *Raster Images*
- *Text*

The following basic *vector geometry types* are defined: *rectangle*, *circle*, *ellipse*, *line*, *polyline*, *polygon*, *symbol* and *path*. Path is the most complex one, because it has the capability to represent line segments, square and cubic Bezier curves and arc segments. Various style attributes may be defined such as line-style, weight, color and so on. Using *raster overlays*, raster images can be combined with vector data. They can be treated like any other geometry object using the same methods. *Text objects* have the same status as any other basic geometry type and the same attributes may be assigned to them.

SVG provides numerous methods to visualize and render spatial objects. Besides line-style and color definitions, sophisticated filter methods are realized which can be applied to raster overlays as well as to vector type elements. Another important feature is the capability of SVG to store georeferencing information and to define transformations between different reference frames. Mathematically, all transformations can be represented as 3x3 transformation matrices. Nesting of transformations is allowed.

### SVG and 3D data

A major shortcoming SVG is its sole support of 2D geometry. The SVG schema might be extended, but the additional properties can only be used for internal data representation, because the commercially available software solutions do not support non standardized properties. For example, the coordinates of linear objects are stored as a stream of separated x and y coordinates. Thus, there is no possibility to define a stream consisting of x, y and z coordinates, because no rendering engine will support such a geometry. The following example of a simple DTM analysis tool based on three vector and two raster layers, shows an effort to support 2.5D geometries using SVG. The five data layers are shown in Fig. 3.5.

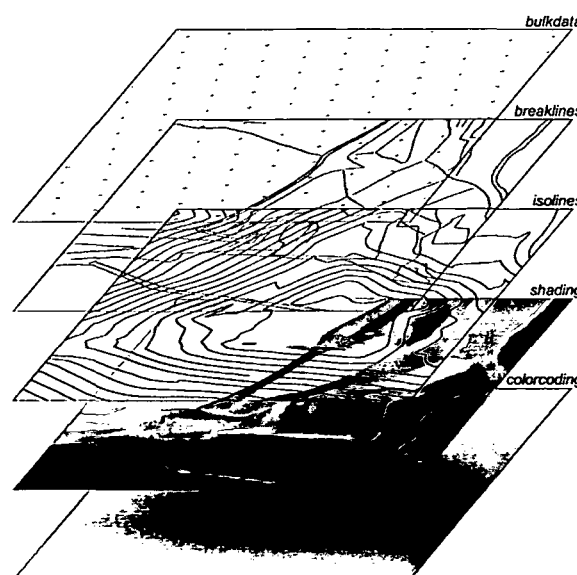


Fig. 3.5: Three vector and two raster layers used to create an SVG-based DTM analysis tool.

The height value of every vector object is stored together with the object-id using the following syntax:

```
<use id='300152_274.45' x='57133.50' y='64938.44' xlink:href='#symbolBulk' />
```

The given example shows the code for positioning the cross-symbol (`symbolBulk`) which is used to represent point objects. The identifier (`id`) is 300152 (this value is equal to the original WINPUT<sup>2</sup> code) followed by an underline '\_'. The following number represents the height value of the object. This information can be interpreted by a client-side JavaScript providing it to the SVG rendering engine. Unfortunately, this method is restricted to associate only one height value to one object. This is correct for single points (e.g. bulk-data) or complex objects with a constant height (e.g. iso-lines). The height of path (polyline) objects with different height values in each point (e.g. break-lines) can not be represented correctly. Therefore, an extension to the SVG standard, supporting coordinate triples ( $x, y, z$ ) would be necessary. Fig. 3.6 shows a rendering of the DTM analysis tool.

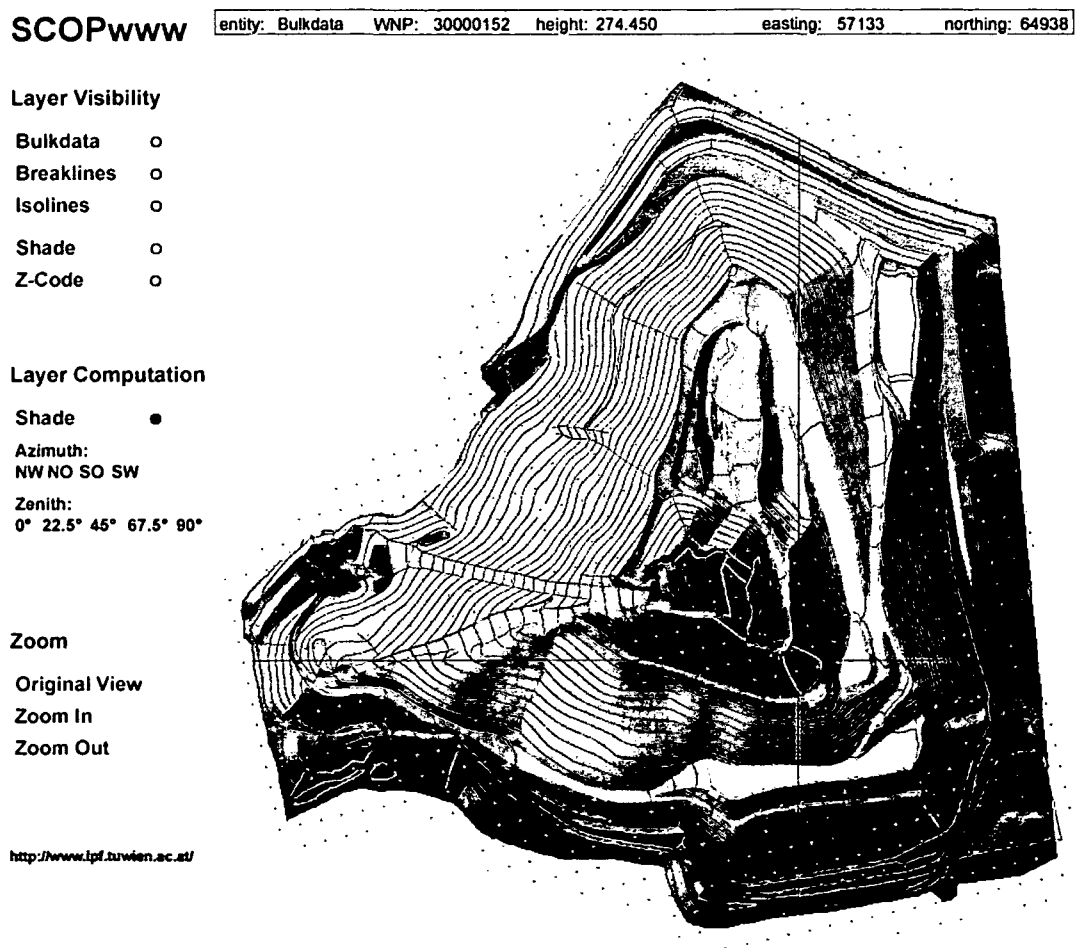


Fig. 3.6: Screenshot of a "DTM analysis tool" based on SVG supporting 3D geometry representation.

The rendered raster images are a shaded relief and a color-coding (from green=bottom to brown=top) derived from the original DTM. The extension of the DTM is 800 by 846 m. The derived raster images

<sup>2</sup> WINPUT is the standard ASCII format used by the software application SCOP++ for topographic data representation. The first two digits represent the so-called feature code (30 = bulk-data). The following digits are a running number (see section 3.3.5 further on).



are provided in PNG format with a resolution of 1 m/pixel. For performance reasons, the whole region was divided into three by three tiles. The color-coding as well as the shaded relief can be rendered individually, or they can be combined, using SVG's filter options. *feComposite*, a predefined filter rule, can be used to combine two source images in the following way:

---


$$result = k_1 \cdot i_1 \cdot i_2 + k_2 \cdot i_1 + k_3 \cdot i_2 + k_4$$


---

$i_1$  is the intensity of image 1 and  $i_2$  the intensity of image 2. The parameters  $k_i$  can be defined individually. The following SVG code snippet shows the application of the *feComposite* filter to combine two images:

---

```
<filter id="filter" filterUnits="objectBoundingBox" x="0" y="0" width="100%"
  height="100%">
  <feImage xlink:href="shd.png" result="shd" />
  <feComposite in="SourceGraphic" in2="shd" operator="arithmetic" k1="0.0" k2="0.75"
    k3="0.75" k4="0.0" result="compIMG"/>
</filter>
```

---

### On the fly Generation of SVG

There are different methods for efficient access and manipulation of SVG documents. In the following, several Java technologies which can be used for on-the-fly (OTF) generation of SVG are introduced.

*JavaServerPages (JSP)* allow to create dynamic and interactive HTML pages. Conventional HTML pages are static. Some rather restricted methods to apply interactivity and dynamic processes to a web page are supported by scripting languages like JavaScript which is a subset of core Java. For example, it can be used to define simple functions, to evaluate input parameters or for visualization purposes. JSP allow to include pure Java code with all its capabilities into a conventional HTML source. To compile and interpret this functionality, a *JSP and Servlet Container* is necessary. For example, the Tomcat Servlet Container, which is part of Apaches Jakarta Project, is an open source Java implementation of such a tool (JAKARTA, 2004). Servlets are Java classes which can be requested by an HTTP request. The given input parameters can be processed and the result is provided as HTML document which can be displayed using standard web browsers. In the same way, SVG documents can be created dynamically. Every JSP is translated and subsequently compiled into a Servlet at the first request. From then on, every request is directly sent to the corresponding Servlet class. Servlets provide full Java functionality and therefore, can call native methods of other classes, thus supporting reuse of already implemented methods that have been used and tested within other applications so far.

There are two shortcomings concerning the dynamical creation of SVG using JSP:

- Embedding into another JSP is not supported by all web browsers, and
- the resulting document cannot be compressed.

A possible solution is the embedding of static SVG into JSP, which are generated and subsequently compressed on demand. Several tests and considerations concerning SVG compression are given in section 3.3.4.

*Java Database Connectivity (JDBC)* is an API (Application Programming Interface) that allows to access tabular data sources such as relational databases. It is based on a driver management enabling the integration of core SQL commands into the Java code. Most vendors of relational database systems provide an JDBC-API.

### ***Current Status of SVG Development***

In the early conceptual phase of the TMIS, in 2001, SVG seemed to become the standard for geodata representation and visualization on the web. They provide many useful features to handle vector data and to render them together with raster images. But the acceptance of SVG did not develop as expected. Microsoft left the SVG standardization group. Adobe, Corel and other members do support import and export interfaces which are not completely compatible to the standard. Exporting a document using an Adobe software application is rendered slightly different within an Corel environment. Especially formatting information is interpreted in different ways. Besides, the automatically generated SVG code is quite unstructured and therefore hard to read. But, the main bottleneck for web presentation is the missing of a standard, platform-independent rendering container for web browsers. A plug-in version provided by Adobe (current version 3.01, ADOBE, 2004) does exist for MS Internet Explorer. It was implemented in 2001. The Mozilla foundation (MOZILLA, 2004) provides a native implementation of the SVG specification for the open Source browser Mozilla. Although this implementation is currently improved, it still does not implement the whole SVG standard and it is not integrated in the browser's kernel. This causes two major problems:

- As long as SVG rendering engines are not integrated into the kernel of web browsers, there will emerge performance shortcomings due to the interaction of plug-in or native implementations with the browser software.
- SVG is not available to everyone, considering the problems of installing an additional software on a computer without administrator's privileges.

A plug-in solution can be successful as well. For example, the Macromedia Flash (MACROMEDIA, 2004) plug-in is provided by a commercial vendor and available in current versions for almost any platform. Thus, it is widely accepted and available to a broad community. In March 2004, NPD Research conducted a study to determine the percentage of Web browsers with Macromedia Flash preinstalled. The result shows, that 98 % of Web users can experience Macromedia Flash content without having to download and install a player, whereas only 17 % have access to an SVG rendering engine (from MACROMEDIA, 2004).

Within the community of web cartographers, there is a large acceptance for the SVG standard. Especially the Swiss Federal Institute of Technology in Zurich, Switzerland, forces its development and application. They established a yearly conference, the SVGOpen (SVGOPEN, 2004), which had about 150 participants for the first time in 2002, and the audience is increasing from year to year. But

as long as there are no outstanding software solutions that force the vendors of web browsers to include SVG viewers into their standard systems, it will not be done. And as long as this viewing functionality is not available to everyone, most software developers hesitate to invest lots of implementation efforts, as they cannot rely on the acceptance of the standard. This is a vicious circle which might have the capability to ruin the impressive capabilities of a standard like SVG. Therefore, further work and development has to be done to bring this standard to the public.

SVG applications are always available in readable ASCII format. For this reason, several commercial vendors are aware to use them, as they are not willing to publish parts of their business logic as implemented within the SVG source code. From this point of view, it would be meaningful to think of a binary coding of SVG. Maybe this could be combined with an appropriate data compression algorithm in order to decrease the filesize of SVG and subsequently improve their performance.

### 3.3.4 Improving XML Performance

XML is stored as readable ASCII-Format and every dataset is described using tags. Therefore a large overhead occurs within the datasets. Considering several Gigabytes of data which might occur within one single laser scanning project, this fact will cause problems as the following example demonstrates:

<i>number of irregularly distributed points:</i>	~ 600 Mio.
<i>latitude / longitude precision:</i>	5 digits
<i>height precision:</i>	3 digits
<i>ASCII list (without XML tags):</i>	16.8 GB
<i>XML document (e.g. GML):</i>	at least 32 GB
<i>binary data stream (regular grid):</i>	about 2 GB (16 bit)

The dataset consists of some 600 Mio. points, sampled by the MOLA instrument. They are available as ASCII list, representing one point per line in latitude, longitude (5 digits of precision) and height (3 digits). This ASCII file requires 16.8 GB of disk space. Assigning XML tags (e.g. according to the GML specification) increases the filesize at least by a factor of two. A regular grid array, derived from the randomly distributed original points, may be stored efficiently as binary data, thus decreasing the amount of data. But the high detailed information, which is provided by the original points, is no longer available. Therefore, in many cases, this is not a sufficient solution.

### Compressing XML Documents

*Data compression* is an attempt to overcome this problem, at least partially. As data compression is a rather time consuming process, this will only be suitable for non time critical problems. Although, with lossless compression algorithms (e.g. *Huffman Encoding* or *Lempel-Ziv*), an acceptable reduction of filesize can be achieved, compressed XML documents are still larger than compressed original files without XML tags by almost 20 %. Thus, further pre-processing makes sense as pointed out by Mertz (2001). He suggests to sort the elements of a document according to their tag names. Then, the original tag names have to be substituted by identifiers in a sophisticated way. After this pre-

processing, a compression algorithm is applied. A detailed description and test results are given by Mertz (2001).

An example of an XML compressor is *XMill*. It is a free and open source software, available on the Internet (XMILL, 2004). According to the vendor's description, the compressed result of an XML document might have only half the size of the compressed original text file without XML tags. Tab. 3.3 compares the results of XMill to other common, lossless file compressor implementations with XML documents as data sources. *Bzip2* (BZIP2, 2004) is used within the TMIS environment for different purposes. *Gzip* (GNU-ZIP, 2004) is supported by many SVG rendering engines<sup>3</sup>.

tool	filesize (bytes)		compression ratio (%)		compression duration (ms)	
	file 1 (SVG)	file 2 (XML)	file 1	file 2	file 1	file 2
original	1,200,389	6,275,197				
XMill	130,223	205,085	89	97	177	401
Bzip2	115,525	186,258	90	97	1,348	11,386
Gzip	146,866	304,769	88	95	154	758

Tab. 3.3: Results of Bzip2 and Gzip implementations compared to the XML compressor XMill.

File 1 is an SVG document consisting of numerous path objects and including objects to realize a navigation menu. Considering compression duration and compression ratio, XMill is the best decision. Bzip2 provides a slightly better compression at the cost of significant longer time. Gzip is slightly faster than XMill while providing the worst compression. File 2 has been derived from a relational table and, therefore, represents structured data according to the rules given in section 3.3.1. In this case, XMill is even faster than Gzip and delivers a similar compression ratio than Bzip2. The tests were performed on an AMD 1700+ with 528 MB RAM under Windows 2000 operating system.

### Binary Data and XML

A further possibility to decrease the filesize of XML-based documents is to combine the advantages of XML data description and binary data storage. Such XML applications are called *Binary XML*. Common image formats (e.g. TIFF or JPEG) store descriptive information (e.g. extension, color-table, ...) in a binary header as prefix of the actual dataset which is provided as binary data stream. This meta-information can be stored using an XML envelope. For instance, the JPEG2000 (2004) standard supports the storage of GML conform rectification information.

Several currently emerging internet protocols (e.g. Simple Object Access Protocol (SOAP, 2004), see section 3.4.1) are realized in a similar way. Parameters for client/server communication are transmitted according to standardized XML schemas. The data itself is transferred in its original format, for instance as a binary data stream representing an image.

The current GML 3 specification supports different ways to represent a location property. One of them is to link another service or an external data source (e.g. in binary format). The external storage of a

<sup>3</sup> A standard SVG document can be compressed using Gzip. The resulting file extension has to be changed to 'svgz'. For performance reasons, Adobe recommends to compress SVG documents, if they shall be rendered using their browser plug-in.

dataset provides an additional advantage, as the data might be accessed through external routines without the necessity of an XML parser.

### 3.3.5 XML and Topographic Data

TopDM and SCOP++ (IPF-SCOP, 2004) are software applications for computation, management, analysis and visualization of topographic data. They distinguish between two groups of topographic data:

- *Original data* as provided by data acquisition and
- *Digital terrain models (DTMs)* derived from original datasets.

For both groups, proprietary data formats are supported:

- The *WINPUT-format* is used to store original data. It supports several object types such as randomly distributed points (bulk-data), single points of interest (spot-heights), linear structures (break-lines, form-lines), borderlines (omit left, omit right, ...) and many more (see Tab. 3.4).
- The *RDH-format* is used to store hybrid DTMs. Hybrid means describing a surface by a regular point grid and additionally by structure information (e.g. structure-lines, spot-heights).

The WINPUT format describes the data as a structured list of points. It supports ASCII and binary data storage. The RDH-format uses binary data storage. In the following, an attempt is described to map these two formats to GML.

#### *WINPUT-format*

Tab. 3.4 lists object types supported by WINPUT and the corresponding GML types. `gml:Point`, `gml:Polygon`, `gml:LinearRing` (closed polygon) and `gml:PointArray` (representing the topology of points of a profile) are used for this mapping.

<i>WINPUT type</i>	<i>WINPUT sub-type</i>	<i>code</i>	<i>GML type</i>
<i>points disregarded by the program</i>		0	<code>gml:Point</code>
<i>profiles</i>	<code>x=const., y=const.</code>	10, 11	<code>gml:PointArray</code>
<i>contour-lines</i>	<code>certain, uncertain</code>	20, 21	<code>gml:Polygon</code>
<i>points distributed at random</i>		30	<code>gml:Point</code>
<i>spot-heights</i>		31	<code>gml:Point</code>
<i>form-lines</i>	<code>open, closed</code>	40, 41	<code>gml:Polygon / gml:LinearRing</code>
<i>break-lines</i>	<code>open, closed</code>	50, 51	<code>gml:Polygon / gml:LinearRing</code>
<i>break-lines, which are also used as borderlines</i>	<code>omit left, right; open, closed</code>	52 - 55	<code>gml:Polygon / gml:LinearRing</code>
<i>border-lines</i>	<code>omit left, right; open, closed, with, without heights</code>	60 - 67	<code>gml:Polygon / gml:LinearRing</code>
<i>special points</i>	<code>off-terrain points</code>	70	<code>gml:Point</code>
<i>elements of the situation</i>		80 - 89	<code>gml:Polygon</code>
<i>control codes</i>	<code>deletion, delimiter code</code>	90, 99	

Tab. 3.4: Mapping of WINPUT types to GML types.

In the following example, these mapping constraints were applied to a dataset consisting of 55,801 points acquired by analytical photogrammetry. 16,140 points belong to compound topological objects such as form-, break- or borderlines. The others are randomly distributed points (mean point distance of some 50 m) and spot-heights. Tab. 3.5 compares the filesize of the original ASCII file in WINPUT-format to that of the GML mapping. The files were compressed using Bzip2 and XMill (see section 3.3.4).

format	filesize (bytes)		
	ASCII	Bzip2-compressed	XMill-compressed
WINPUT	2,567,260	346,363	
GML	4,744,025	335,141	440,327

Tab. 3.5: Comparison of WINPUT and GML documents.

As expected, the XML tags increase the filesize by a factor of two. Similar results were achieved with other datasets. Compressing the WINPUT and the GML document results in almost similar file sizes. This can be explained, as some redundancy of the WINPUT format (e.g. the WINPUT code is stored together with every point of a compound element) is no longer stored within the GML document. Further on, the XML-tags, of the GML document have a high degree of similarity, and allow a high compression rate. Similar to the results of section 3.3.4, the performance of XMill is much better than those of Bzip2 (500 ms vs. 6,800 ms) while providing slightly less compression ratio. The following conclusions can be drawn:

- Due to the significantly greater filesize of GML documents compared to WINPUT files (both in ASCII format), a GML application may suffer from storage problems.
- Although a GML document contains additional information, it can be compressed almost as highly as a WINPUT file. Therefore, GML might be a good choice for non-time-critical applications (e.g. data archiving).

### **RDH-format**

The base structure within the RDH-format is a regular grid of points, derived from the original data. If the original data is provided in WINPUT-format, the groups of objects described in Tab. 3.4 are treated as follows: *points*, *contour-lines* and *points distributed at random* (referred to as bulk or “raster-type” data) are replaced by an interpolated regular grid of points within the RDH structure, carrying just the height values. On the contrary, *spot-heights*, *form-lines*, *break-lines* and *border-lines* (referred to as “vector-type” data) are integrated in the RDH structure. Every spot-height and the vertices of segments of linear structures are stored as 2.5D points (x, y, z-values). Also the height values of the points obtained by intersecting the linear structures with the virtual mesh-lines of the grid are stored. For addressing the integrated “vector-type” data, an optimized system of assignments is stored with them. For performance reasons, the RDH-format is organized in computing units (CU). Fig. 3.7 shows a schematic example of the RDH-data-structure.

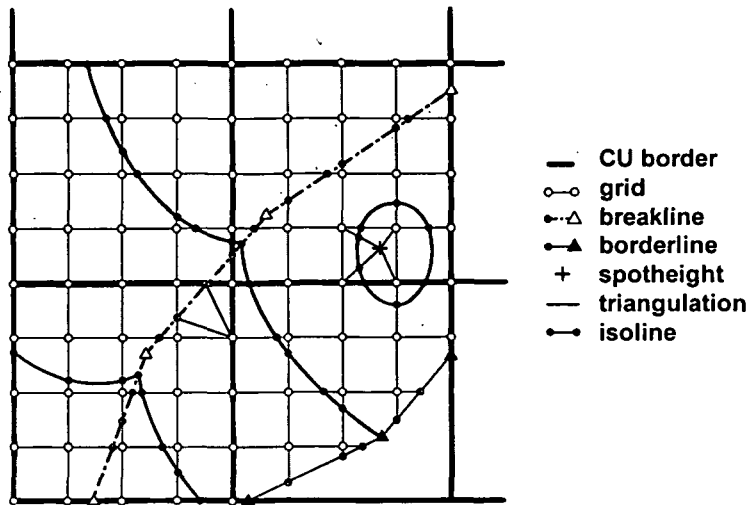


Fig. 3.7: The hybrid data-structure used by the RDH-format for DTM representation (from Kraus, 2000, p 182).

GML mapping has been tested with a hybrid DTM, based on a 25 m grid and derived from the original dataset which was used for the WINPUT mapping test. The resulting binary RDH document was exported to the ASCII WINPUT format and then converted into GML code, using the coverage data type `gml:rectifiedGrid` to represent the grid content. As an example, the following code fragment demonstrates the structure of this type:

---

```

<gml:domainSet>
  <gml:RectifiedGrid gml:id="30" dimension="2">
    <gml:limits>
      <gml:GridEnvelope>
        <gml:low>0 0</gml:low>
        <gml:high>413 351</gml:high>
      </gml:GridEnvelope>
    </gml:limits>
    <gml:axisName>x</gml:axisName>
    <gml:axisName>y</gml:axisName>
    <gml:origin>
      <gml:Point>
        <gml:coordinates>-58400.00,290068.79,0.00</gml:coordinates>
      </gml:Point>
    </gml:origin>
    <gml:offsetVector gml:id="p1">25.0,0.0,0.0</gml:offsetVector>
    <gml:offsetVector gml:id="p2">0.0,-25.0,0.0</gml:offsetVector>
  </gml:RectifiedGrid>
</gml:domainSet>
<gml:DataBlock>
  <gml:doubleList>
    <!-- value information -->
  </gml:doubleList>
</gml:DataBlock>

```

---

(defines the area of interest within the grid)

(shift of origin)

(scale and rotation)

(scale and rotation)

(height values)

The referencing of the grid according to a reference system is stored within the `<domainSet>`. It is accomplished by the 3D origin and two transformation vectors, describing the scale and rotation of the grid. In this example, the individual height values of the grid points are stored as a list of values within the `<DataBlock>`. The `gml:tupelList` property could be used instead of a conventional list. This

would allow to assign value tuples to every grid point, to store several layers (e.g. height, slope, curvature, ...) within one single document.

The same grid object in WINPUT-format requires, besides the WINPUT-code, the three coordinate values (x, y, z) for every grid point. This explains the large filesize compared to the GML representation (Tab. 3.6).

	<i>filesize (bytes)</i>				
	<i>uncompressed</i>		<i>Bzip2-compressed</i>		<i>XMill-compressed</i>
	<i>ASCII</i>	<i>BINARY</i>	<i>ASCII</i>	<i>BINARY</i>	<i>ASCII</i>
<b>RDH</b>	6.014.086	680,744	731,686	556,998	---
<b>GML</b>	2.046.373	---	439,641	---	619,146

Tab. 3.6: Comparison of RDH and GML documents.

Although GML and the binary RDH file have been compared, one must keep in mind that their information content is different: First, tiling is not realized in this example, and second, structure lines have been stored as polylines in GML without the before mentioned mesh intersections contained in RDH. Nevertheless, mapping the indigenous RDH data to standardized GML might be a good choice for data exchange or archiving, as the compressed files have similar size.

### 3.3.6 Integration of XML Documents in Databases

XML-based formats are emerging as the universal standards for publishing and exchanging data on the Internet, while RDBMS are dominating the commercial database market. This section introduces concepts for mapping XML documents to relational schemas and for applying XQuery queries to such databases.

The application of SQL queries using the JDBC-API (section 3.3.3) to access an RDBMS, returns a set of results. A cursor is a mechanism to move within such a set in one single dimension, forward or backward, and to fetch one row of it. An XML document can be represented as a tree using the DOM (Document Object Model) (W3C-DOM, 2004). The adequate query mechanism, XQuery, provides capabilities to move within this DOM structure in multi-dimensions and to fetch a whole tree or a branch of a tree.

Li et al. (2003, pp. 52 ff) describe different approaches to realize such multi-dimensional cursors based on mapping XQuery queries to multiple SQL queries. Liu et al. (2003) realized a virtual XML database engine (VXE-R) performing such mapping. The architecture of the system is shown in Fig. 3.8.



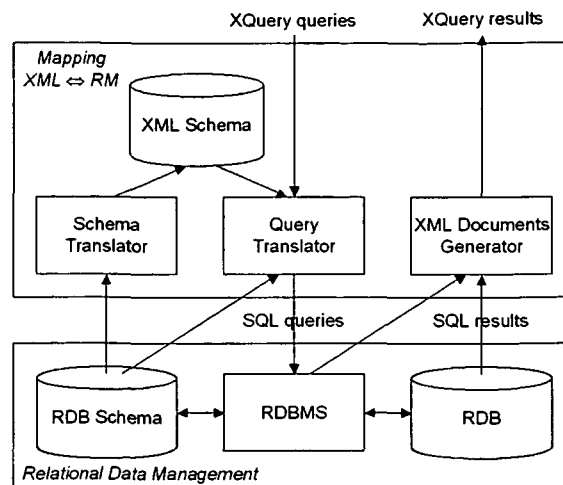


Fig. 3.8: Architecture of the VXE-R system, a virtual XML database engine (from Liu et al. 2003).

The *Schema Translator* maps all integrity constraints of the RDB Schema to the target XML Schema. The *Query Translator* maps the XQuery queries to SQL queries according to the previously determined XML schema. In this case, the mapping can be performed easily, because the XML Schemas are available in a normalized form, as they were derived from RDB Schemas. The *XML Document Generator* restructures the flat result relations by a grouping operator or a nest operator for NF<sup>2</sup> relations (see section 3.2.3) and subsequently converts them into XML documents.

This example was introduced, as such a concept of XML to SQL mapping is realized by most applications supporting XQuery on RDBMS. In the beginning, we tried to use Oracle's XDK (XML Development Kit), a package of Java classes for XML mapping to Oracle Schemas, for the TMIS update routines. But two shortcomings emerged:

- The available structured data had to be transformed into XML documents, which increased the amount of data, and
- the data import performance was bad compared to a traditional insert operation applied to the original datasets.

Therefore, XML is no longer used for most updating routines of the TMIS. Only one table is still updated using the XDK. This table has one attribute which contains formatted text information and is stored within Oracle using a CLOB (Character Large Object) data type. Further information is given in section 4.2.

### 3.3.7 XPath Performance Considerations

XPath is used by several other XML-related technologies such as XSLT, XQuery and Xpointer to address nodes in XML documents. Therefore, efficient XPath processor implementations are necessary for fast XML data processing with respect to data complexity (D) on the one hand and query complexity (Q) on the other hand.

Gottlob et al. (2002) proved, that contemporary implementations of XPath query engines evaluate queries in time exponential in the size of input queries and in the size of data, a very inadequate

behaviour considering comprehensive XML schemas. Thus, they proposed the first algorithm for XPath 1.0 with polynomial time combined complexity. In Gottlob et al. (2003) they improved this algorithm, resulting in the following time combined complexity with  $|D|$  as the size of the data and  $|Q|$  the size of the query:

---

$O( D ^4 *  Q ^2)$	time complexity
$O( D ^2 *  Q ^2)$	space complexity

---

This behavior is much better than the exponential time complexity of current implementations. Therefore, there is still a high potential to increase the performance of currently available XPath processors in order to increase the performance of XML data processing, making the integration of XML documents for exchange of time critical processes more attractive.

### 3.4 Concepts for Web Applications

Conventional applications (e.g. GIS systems, DTM manipulation software, ...) are realized as stand-alone systems providing all capabilities within one integrated software package. Using the Internet as a communication platform between applications allows to combine functionalities of different, distributed applications in order to generate more complex software solutions. *Web Services* are intended to realize such systems. The following sections introduce the characteristics of *Web Services* and their application to spatial data distribution and management.

#### 3.4.1 Web Services

Kreger (2001, p. 6) defines a *Web Service* as follows:

---

*A Web Service is an interface that describes a collection of operations that are network-accessible through standardized XML messaging. A Web Service is described using a standard, formal XML notion, called its service description. It covers all the details necessary to interact with the service, including message formats (that detail the operations), transport protocols and location. The interface hides the implementation details of the service, allowing it to be used independently of the hardware or software platform on which it is implemented and also independently of the programming language in which it is written. This allows and encourages Web Services-based applications to be loosely coupled, component-oriented, cross-technology implementations. Web Services fulfill a specific task or a set of tasks. They can be used alone or with other Web Services to carry out a complex aggregation or a business transaction.*

---

A *Web Service* architecture is based upon the interaction of three roles: *Service Requestor*, *Service Provider*, and *Service Registry*. Fig. 3.9 shows a concept of a *Web Service*. The *Service Requestor* is an application looking for a certain service which provides the necessary functionality (e.g. a user

driven browser, a program without a user interface, ...). It requests the descriptive information of available services from the *Service Registry*. The *Service Registry* is a searchable registration of service descriptions, provided by *Service Providers*. The *Service Provider* hosts access to a certain service which can be based on several other *Web Services* or is provided by an individual application. After having found the necessary service, the *Service Requestor* invokes it using the binding details provided by the service description.

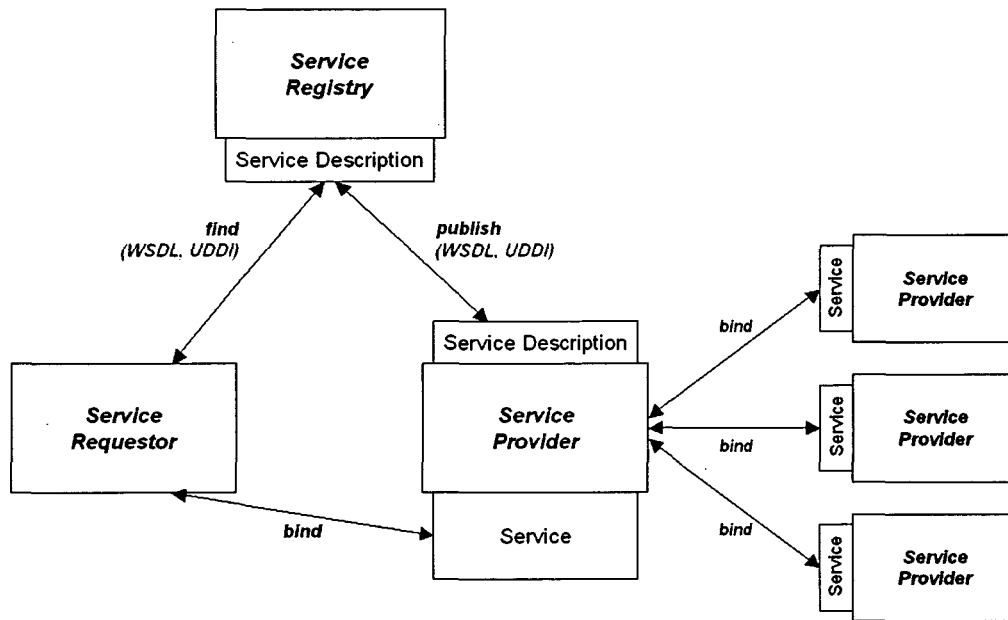


Fig. 3.9: Web Services Architecture (modified from Kreger, 2001).

The XML-based *Web Service Description Language (WSDL)* is the de facto standard for publishing and finding of *Web Services*. The *Universal Description, Discovery and Integration (UDDI)* allows to describe higher level aspects of a service. Both are based on the *Simple Object Access Protocol (SOAP, 2004)*, an XML-based messaging protocol, which is basically an HTTP POST with an XML envelope.

### 3.4.2 Web Services and Spatial Data

As already mentioned in section 3.3.1, a shortcoming of HTML-based data storage is the combination of content and layout within one document. XML-based data structures are intended to overcome this. Similar to the 3-Tier-Architecture of DBMSs (internal schema, conceptual schema and external schema; see section 3.2.1), a 3-Tier-Architecture shall be supported by a “well designed” software application in order to separate the *stored data*, the *access and manipulation logic* used and the *layout and rendering* rules. If data is provided using a *Web Service*, this concept is essential, as the *Data Provider* does not know the final presentation format.

Doyle and Cuthbert (1998) defined an “*essential model of interactive portrayal*”. A slightly modified visualization of this concept is shown in Fig. 3.10.

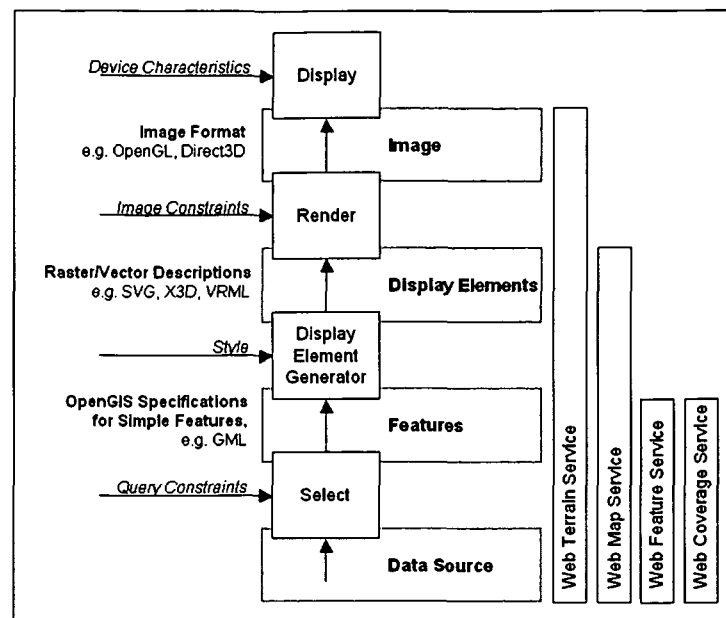


Fig. 3.10: Portrayal Model for presentation of spatial data (modified from Doyle and Cuthbert, 1998).

The portrayal model separates storage (data source), access (features) and manipulation (display elements) and presentation (image). Fig. 3.10 shows this separation and the corresponding communication between the different tiers. Possible formats for data representation at the individual tiers are given as well. The bars at the right side represent several OGC *Web Services* (OGC, 2004) and their integration in this model. The *Web Map Services (WMS)* to create map-based visualizations of spatial data will be discussed in more detail in the following section.

### 3.4.3 Spatial Data Presentation using Web Map Services

The current OGC standard for *Web Map Services (WMS)* was released in November 2001 (version 1.1.1, Beaujardiere, 2001). Since January 2004, a draft of WMS 1.3.0 is available, but it has not been standardized yet. According to the specification, a WMS dynamically creates maps of spatially referenced data from geographic information. This standard defines a "map" to be a portrayal of geographic information as a digital image file suitable for display on a computer screen (Beaujardiere, 2004, p. vii). The resulting maps are generally rendered in a pictorial format (GIF, PNG, JPEG and TIFF are supported), i.e. in a rectangular pixel array of fixed size. Occasionally, vector-based graphical elements (SVG, WebCGM<sup>4</sup>) can be generated. Vector-based formats support a scale-independent description of the graphic elements to be displayed (including point, lines, curves, text and images), such that the size of the display may be changed while preserving the relative arrangement of the graphic elements.

A WMS may support the following three operations:

<sup>4</sup> WebCGM is a web-based profile of CGM (Computer Graphics Metafile – ISO/IEC 8632:1999) for representation of 2D vector data together with images within electronic web documents (CGM, 2004, <http://www.cgmpopen.org>).

- *GetCapabilities* (mandatory): Returns *metadata* on the service using a standardized XML Schema.
- *GetMap* (mandatory): Returns a *map* (or a service exception) according to the given parameters.
- *GetFeatureInfo* (optional): Returns *further information* on a selected feature.

The *GetCapabilities*-operation provides the service description according to the *Web Service* definition. The *GetMap*-operation supports the binding of the service. The implementation of a WMS is presented in section 4.3.

## 4 Realizing the Topographic Mars Information System

The previous chapter introduced concepts for spatial data modeling and XML-based data exchange and visualization formats. The application of *Web Services* for spatial data manipulation and distribution has been described as well. This chapter presents the realization of the *Topographic Mars Information System (TMIS)*, implementing these concepts as far as possible. First, the general architecture of the application framework is outlined. Afterwards, according to the concept of a 3-Tier-Architecture, the realization of data storage, data access and manipulation and data presentation is described. Advantages and shortcomings of the previously described concepts for the application within the TMIS environment are discussed.

### 4.1 System Architecture

Fig. 4.1 shows the system architecture of TMIS. It can be separated into three components:

- *Data Management* using an RDBMS with object-oriented extensions (section 4.2),
- *Data Access and Manipulation* realized in Java (section 4.3) and
- *User Presentation* supporting map-based data access and presentation (section 4.4).

The arrows between the individual components represent different request scenarios. They are labeled with the used communication channels (http, sftp, jdbc, ...). In order to demonstrate the functionality, three types of users, called *User 1*, *User 2* and *User 3* are shown in the example. *User 1* requests meta-information of images using the WMS interface, *User 2* requests HRSC image files and *User 3* requests topographic data from the *Topographic Data Server*. These request scenarios are presented in detail in section 4.3.

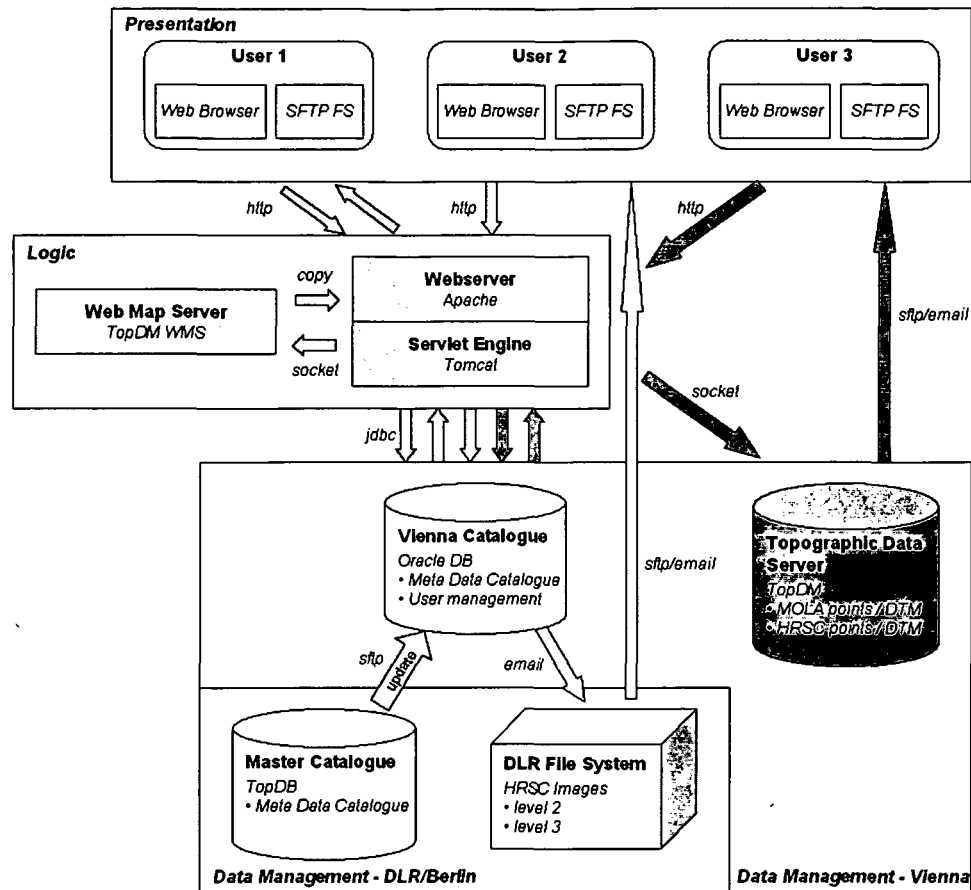


Fig. 4.1: Architecture of TMIS according to its components.

## 4.2 Data Management

Within TMIS, two separate groups of datasets are to be handled:

- The *Meta Data Catalogue (MDC)* which is used to manage and request HRSC images from a separate data repository, and
- the *Topographic Data Server (TDS)* providing topographic datasets as original points and as derived products (e.g. DTMs).

The following sections describe the main characteristics of the MDC and the TDS. The application of previously described concepts is presented, considering the 'phase model' for realizing a database application (proposed by Heuer and Saake, 2000, pp. 171). This model consists of the following steps: *Requirement analysis, conceptual design, distribution design, logical design, data definition, physical design and implementation.*

### 4.2.1 Meta Data Catalogue

The *Meta Data Catalogue (MDC)* contains a set of meta-information describing the HRSC images managed by TMIS. The information is originally available as a set of parameters provided as header

information with each image file<sup>5</sup>. During the *requirement analysis* a list of parameters to be managed within the MDC has been defined. During the *conceptual design*, those parameters were assigned to different groups named entities in the following.

The central entity of the MDC is *Image*. All parameters describing an image (e.g. location, extension, objective, ...) are assigned to this entity. TMIS manages 5 processing levels of an image lifecycle; from planned images to map projected images and other derived products. The polygon defining the borderline of an image on the Mars surface is called footprint. This attribute is stored using Oracle's SDO\_GEOMETRY type (section 3.2.4). The coordinates are assigned to a planimetric reference system based on the Simple Cylindrical map projection (x-axis = longitude, y-axis = latitude). The coordinate values are given in degree, thus, the mapping area has an extension of 360° by 180°.

The entities *Exposure* and *Geometry* contain properties describing the exposure configuration and the geometric constellation of spacecraft, target body (Mars) and illumination source (Sun). Thus, images of different processing levels have the same exposure and geometry attributes. Other descriptive meta-information is provided by individual entities for consistency reasons, according to the normal forms for relational databases. Fig. 4.2 shows a graphical representation of the conceptual model. Within the *logical design*, each conceptual entity has been mapped to a relational table and subsequently realized in the database (*data definition*).

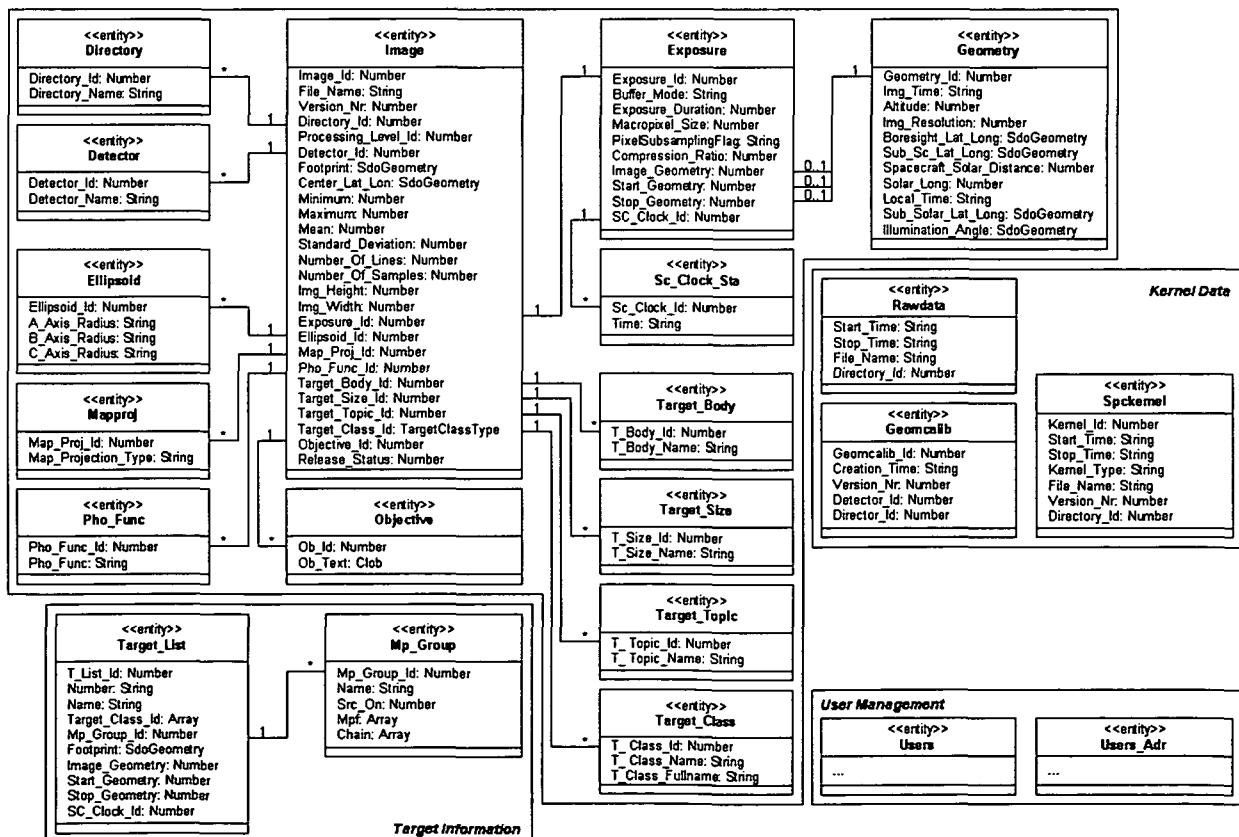


Fig. 4.2: Conceptual database design of the Meta Data Catalogue.

<sup>5</sup> The HRSC images are stored in VICAR format. Roatsch (2001) defines and describes the content of the image ASCII label and the image binary prefix for VICAR-formatted HRSC data. A general overview on VICAR is given in section 5.1.



For security and responsibility reasons, the MDC is managed in two, locally separated, catalogues, physically located on different machines. The so-called *Master Catalogue*, based on *TopDB*, is situated at the *Institute for Planetary Research (Data Processing Working Group)* at the *German Aerospace Center (DLR)* in Berlin, Germany. This catalogue is used for data input of planned and real image metadata. The filling software application is implemented in IDL (Interactive Data Language, 2004). Therefore, an interface between the filling software and *TopDB* has been realized. The *Master Catalogue* is only available for members of the Data Processing Working Group.

The *Vienna Catalogue*, based on an *Oracle Spatial* database kernel, is available to all TMIS users and accessible through the Internet. This catalogue is automatically updated using data unloads from the *Master Catalogue*. The regularly updated tables are *Image*, *Exposure*, *Geometry*, *SC\_Clock\_Sta*, *Objective*, *Kernel* and *Target\_List*. Unfortunately, not only insert operations occur; updates of existing datasets are necessary as well (e.g. planning has been changed, new versions of already existing images have been derived and released, ...). Therefore, it would be complicated to compare the current status of the *Vienna Catalogue* with that of the data, unloaded from the *Master Catalogue*, in order to select the modified datasets. Thus, it is simpler to delete the whole *Vienna Catalogue* and fill it again within every update process. In order to provide system availability during and data consistency after this process, extensive update routines have been implemented. First, an XML-based exchange format was tested. As the data has a structured nature (compare section 3.3.1), the XML overhead turned out to be not necessary (increasing filesize, decreasing performance, ...). Therefore, a simple, ordered ASCII list is used. Only the *OBJECTIVE* table is still updated using an XML exchange format, as it contains an attribute containing formatted text which is mapped to a Character Large Object (CLOB) type within the database.

The HRSC image files are stored in a filesystem at the DLR for two reasons: On the one hand, the Terabytes of available images would increase the size of physical database storage to a great extent, if they were managed within the DBMS (e.g. as Binary Large Objects – BLOBs); on the other hand, many TMIS users employed at the DLR in Berlin and the Principal Investigator have direct access to this filesystem.

#### 4.2.2 Topographic Data Server

Besides the MDC, TMIS provides planet-wide topographic datasets as original data and as derived DTMs, sampled by MOLA or derived from HRSC images. Requests for these datasets are time and CPU intensive transactions. Therefore, the *Topographic Data Server (TDS)* is a physically separate machine. *TopDB* is used for data management. Since data access is provided by *TopDM*, reference system transformation and resampling capabilities are supported.

First tests were performed using the planet-wide MOLA dataset. Two different versions of MOLA surface points are available: The *randomly distributed original measurements* and *derived grid DTMs* with a resolution of  $1/128^\circ$ . The following Tab. 4.1 shows the amount of data if these datasets are managed using *TopDB* and *Oracle Spatial*.

<i>MOLA data format</i>	<i>nr. of points</i>	<i>TopDB</i>	<i>Oracle Spatial</i>
<i>original points</i>	~ 600 Mio.	~6.4 GB	~10.0 GB
<i>DTM grid (1/128°)</i>	~1,000 Mio.	~4.6 GB	~17.7 GB

Tab. 4.1: Database filesize for management of MOLA data using different RDBMS.

In TopDM, the original points are managed in the *Topographic Data Market* whereas the DTM grid is stored in the *Derived Products Market* using the proprietary RDH format (section 3.3.5). In Oracle Spatial, the spatial data type SDO\_GEOMETRY is used to manage the MOLA data. Although Oracle recommends to use the SDO\_POINT attribute for randomly distributed points (section 3.2.4), it is absolutely inconvenient, if millions of points are involved, because every geometry object is stored together with meta-information. Grouping 500 points to one geometry object decreases the necessary filesize to the values given above.

Topographic datasets are managed in the same reference frame as footprint information of HRSC images. To achieve similar scale in plane coordinates and height values (heights are stored in meter), the latitude and longitude values, originally given in decimal degree, were transformed to metric values. The definition of the applied transformation rules will be given in section 5.1.2.

For a better request performance, the original and the derived topographic datasets are divided in tiles. Therefore, if only a regionally limited area is requested, first the corresponding tiles are selected and second a distinct clipping is performed. The performance of requests for low resolution data on the grid-based datasets is improved by using data pyramids in addition to the tiled structure. According to the requested resolution, the corresponding data pyramid level is selected and the final DTM is derived from this dataset.

### 4.3 Data Access and Manipulation

The middle tier of TMIS is based on the *Apache HTTP Server* and the *Jakarta Tomcat JSP and Servlet container* (APACHE, 2004) and implemented in Java (JAVA, 2004). The TMIS environment integrates functionalities from existing applications according to the specifications for *Web Services*. These functionalities are provided by SCOP++ (IPF-SCOP, 2004) and TopDM. Both applications can be started and controlled in batch-mode using a command file. In order to trigger them from remote terminals or processes, a multi-threading server was implemented based on the Java2SE 1.4.2 platform. The *java.net* package provides a bundle of classes to realize client-server communications using a pair of client/server sockets. The input parameters are sent to the server which creates the corresponding batch-file on-the-fly and subsequently starts the application. After successful computation, the client is informed about the location of the result.

### 4.3.1 Requesting Footprint Maps

Fig. 4.3 shows the workflow of a *Web Map Service (WMS)* request (User 1 in Fig. 4.1). According to the WMS specification, a *GetCapabilities* and a *GetMap* function are implemented. *GetMap* supports the mandatory parameters (*WMSversion*, *WMSrequest*, *WMSlayers*, *WMSstyles*, *WMSsrs*, *WMSbbox*, *WMSwidth*, *WMSheight*, *WMSformat*), additional parameters to define database query conditions (e.g. processing level, detector, ...) and style information (e.g. opacity, color, ...).

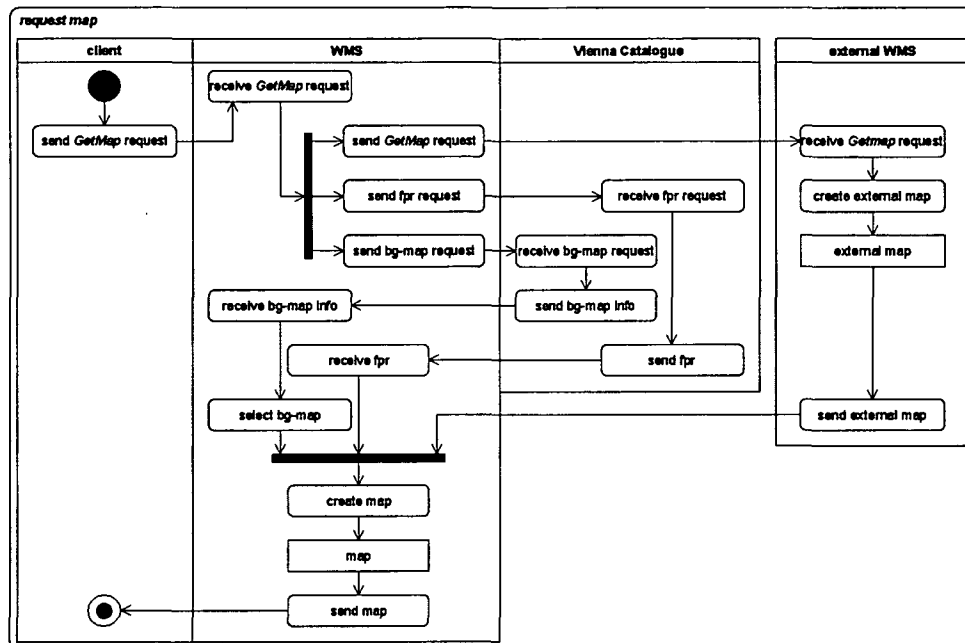


Fig. 4.3: Request for a map visualization of available images using a WMS.

The given workflow shows four components interacting with each other: *client*, *WMS-Server*, *Vienna Catalogue* and an *external WMS*. The core map is composed of two individually requested images, both provided by the *Vienna Catalogue*. A visualization consisting of a combination of height-coding and shaded relief (derived from the MOLA DTM) is used to represent the Mars topography (bg-map). The requested footprint map (fpr-map) consists of individual polylines requested from the *image.footprint* attribute of the MDC. A transparent alpha-channel is used for empty regions in the footprint map and rendered by a vector/raster conversion. This allows to overlay the topographic and the footprint map. Finally, a map-grid is used as third overlay. The map composition is shown in Fig. 4.4.

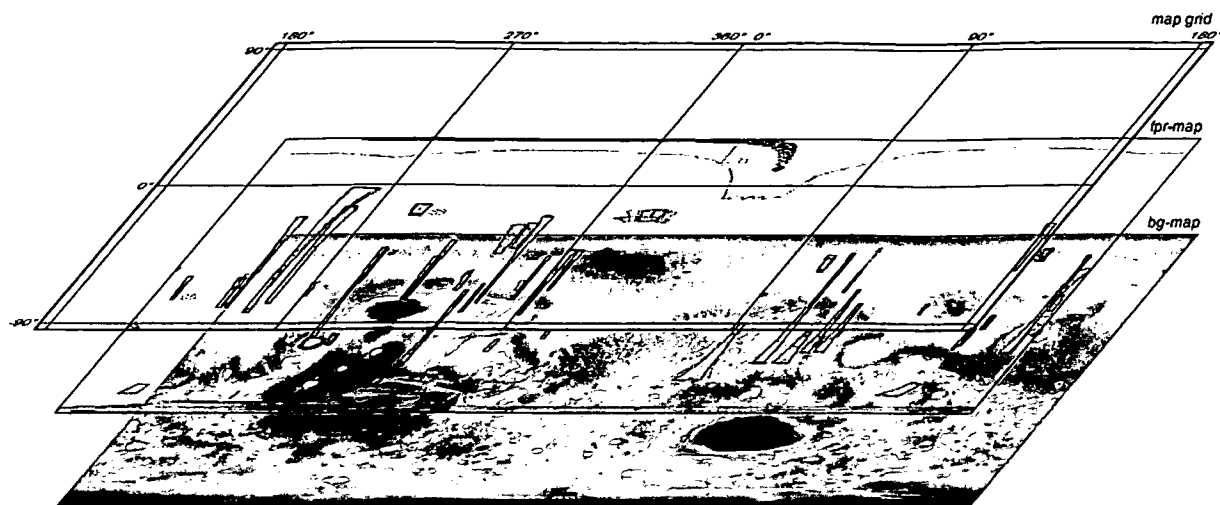


Fig. 4.4: The layer structure of an image created by the WMS.

To increase the performance of standard requests, predefined footprint maps of different resolutions and different contents are created during the MDC update process and stored as image pyramid. Descriptive information about the pyramid structure is stored within the *Vienna Catalogue*. The Mars topography map (bg-map) is provided as image pyramid as well. As the bg-map files are static, they remain in the cache memory of the rendering browser. Thus, only the fpr-maps have to be requested from the server reducing the amount of download data while increasing the response time of the WMS. Of course, this method restricts the flexibility of the WMS for two reasons: First, the final map (a combination of topographic map, footprint map and grid) is not available as one combined image file; second, only predefined scenarios can be requested.

As already pointed out in section 3.4.1, a *Web Service* should support the integration of other *Web Services*. This would allow, for example, to integrate the contents of other Mars related WMSs into the TMIS environment and render them within the final map creation. This ability is indicated by the *external WMS* in Fig. 4.3.

### 4.3.2 Requesting HRSC Images

Fig. 4.5 shows a request for HRSC image data (User 2 in Fig. 4.1). According to a list of input parameters, a list of available image files is selected from the *Vienna Catalogue* and presented to the user as an HTML document. After having sent the request for image data, the user receives a notification about the request status. Furthermore, a list of the requested images together with user verification information is sent to the *Master Catalogue* via email. This mail is evaluated automatically and the requested datasets are copied to the client's filesystem using an encrypted Secure File Transfer Protocol (SFTP) for security reasons. After finishing this job (successfully or not), the user is notified via email.

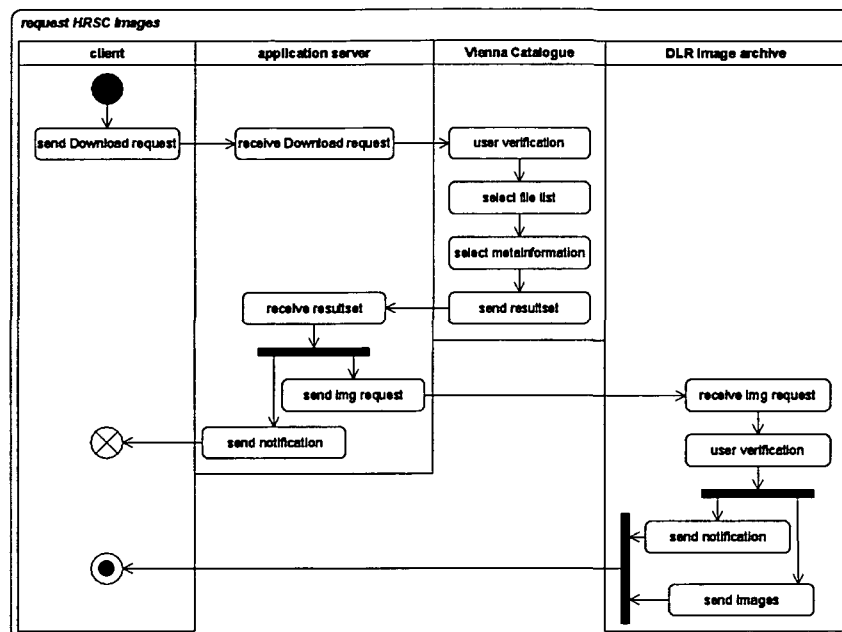


Fig. 4.5: Request for HRSC image data.

This implementation supports a very high level of data security. The catalogue users have no direct access to the real data. They are allowed to login and search within the *Vienna Catalogue* using their personal accounts. In order to receive images, all users had initially to define and disclose to the manager of the DLR archive a destination filesystem, where all requested data will be transferred to. If the *Vienna Catalogue* were hacked, the worst case scenario would be a file copy from the archive to a well-known filesystem of a user and never to one of a hacker.

### 4.3.3 Requesting Topographic Data

The request scenario shown in Fig. 4.6 describes a request for topographic data provided by the *Topographic Data Server (TDS)* (User 3 in Fig. 4.1). From a conceptual point of view, this request is similar to the HRSC image request. But while the HRSC images are static files, the topographic datasets are managed using TopDB (section 4.2) which provides reference system transformation and resampling capabilities. Therefore, every requested file is created on demand and transferred to the client afterwards.

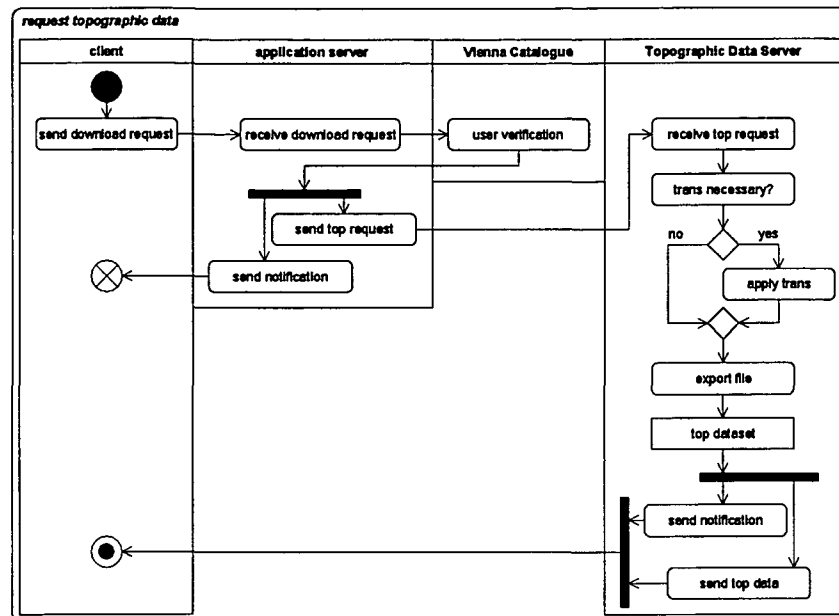


Fig. 4.6: Request for topographic data (DTMs or original points)

The request for topographic data is triggered as described in the introduction of section 4.3 using a multi-threading server which creates a TopDM command file on demand. Thus, the full functionality of TopDM is available.

#### 4.3.4 Integration of DTM Analysis and Visualization Tools

Similar to the TDS request, the functionality of SCOP++ (or any other application supporting batch) can be integrated in the TMIS framework. The scenario shown in Fig. 4.7 describes the workflow of a request for products, derived from DTMs (or original datasets) provided by the TDS and subsequently computed by an application for topographic data manipulation.

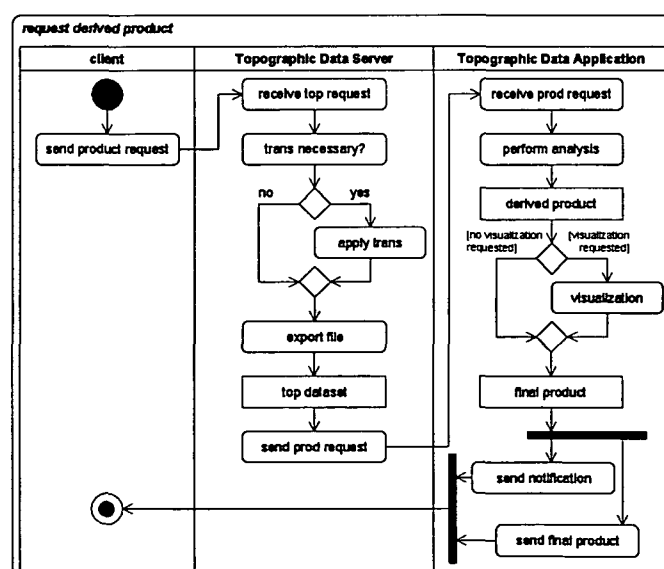


Fig. 4.7: Request for derived products using a topographic data analysis tool.

For reasons of simplicity, a direct communication of the client and the TDS is assumed. First, a topographic dataset is exported from the TDS. This dataset is provided to the Topographic Data Application afterwards. In the case of TMIS, this application is SCOP++, driven in batch-mode. Similar to the TDS request, the SCOP++ request requires a command file which is created on demand. Afterwards, the SCOP++ computation is triggered and the final product (e.g. a DTM derived from original points, a shaded relief, a result of hydrological analysis, a perspective view, ...) is derived and eventually sent to the client.

#### 4.4 Data Presentation

Data presentation is based on web browser environments. Three different access interfaces are available: A *form-based parameter selection* as commonly used by web-based database interfaces and two *map-based interfaces*, one realized as a WMS with pictorial output and the other based on SVG. Fig. 4.8 shows one tab of the form-based parameter selection interface and Fig. 4.9 the presentation of a result list generated according to a set of given input parameter.

HRSC Data Selection

8817 datasets are currently selected deactivate count

Geometry Instrument SpaceCraft Map

min max

Latitude ( $\pm 90^\circ$ ):

Longitude ( $0^\circ - 360^\circ$ ):

min max

Image Time

\* Time Format: YYYY-MM-DDThh:mm:ss.fff or a substring

Image Resolution  m  m

Solar Longitude

Local Time  h  h

File Name (Orbit)

Target Body Target Size Target Topic Target Class

SELECT ALL SELECT ALL SELECT ALL SELECT ALL

mars local mapping volcanic  
phobos regional stereo tectonic  
deimos global color impact

Longitude Input Processing Level ID

eastern ☐ -3 ☐ -2 ☐ 2 ☐ 3 ☐ 4

Map Selection Request Resultlist Apply Parameters  
create FPR map from DB min/max Par Values

Close this window Start Download Reset Parameters  
Personal Settings

Fig. 4.8: Form-based TMIS interface.

HRSC Data Selection - Result List

p/s HTML list p/s ASCII list Close Result List

File Name	VER_NR	FILESIZE	IMG_CENTER		Download	
		[MB]	Lat	Lon	IMG	MOLA
h0205_0000.s23	3	162	-7.2	187.9	<input type="checkbox"/>	<input type="checkbox"/>
h0228_0000.s23	5	60	-30.4	157.2	<input type="checkbox"/>	<input type="checkbox"/>
h0232_0000.s23	5	38	8.5	74.5	<input type="checkbox"/>	<input type="checkbox"/>
h0241_0000.s23	7	56	-30.7	156.4	<input type="checkbox"/>	<input type="checkbox"/>
h0243_0000.s23	4	41	-7.3	297.6	<input type="checkbox"/>	<input type="checkbox"/>
h0248_0000.s23	1	31	-37.4	102.8	<input type="checkbox"/>	<input type="checkbox"/>

6 images found (2004-06-07 / 17:04:48 - GMT+01:00)

Select Data for Download View additional information

Select all ☐ Image ☐ MOLA

Deselect all

Start Download

none  
ALTITUDE  
BUFFER\_MODE  
DETECTOR  
EVENT\_NOTE

Apply

p/s HTML list p/s ASCII list Close Result List

Fig. 4.9: Result of image metadata request.

In the following sections, the map-based interfaces are introduced and finally, image and object-based visualization formats for spatial data presentation on the web are compared.

#### 4.4.1 Object-Based Visualization Methods

SVG can be used to present cartographic information on the Internet. The integration of JavaScript functionality supports interactivity. Unfortunately, the Document Object Model (DOM) of these JavaScripts is not interpreted in the same way by different browsers. Thus, it is better to integrate the functionality in the SVG in order to use the DOM interpreter of the SVG rendering engine.



Fig. 4.10: SVG-based map user interface of TMIS.



Fig. 4.11: High-resolution rendering of footprints with the SVG interface.

Fig. 4.10 shows the SVG-based user interface of TMIS rendered by the MS Internet Explorer. The SVG is embedded in a JSP. To connect to the TMIS data catalogue from the SVG, the user verification information is taken into account using cookies. If cookies are disabled at the client-side, it is necessary to re-enter the user verification information to connect to the database. To support multiple browser environments, the navigation menu is integrated in the SVG. The SVG rendering engine supports scalability to a certain degree. Fig. 4.10 shows a representation of the whole Mars surface using a raster image map with a resolution of  $1/4^\circ$  in Simple Cylindrical map projection. To support further zooming to a higher resolution (Fig. 4.11), different levels of detail are provided in a pyramid structure. If a certain zoom level is reached, the corresponding SVG level is requested from the server and replaces the former one.

Every HRSC footprint is stored in the TMIS MDC with 100 points. As it is often the case, thousands of images have to be displayed within one SVG. This results in requesting large amounts of data from



the server, and thus in comprising the performance of the rendering (e.g. 16 bytes per point \* 100 points \* 10,000 objects = 16 MB). Therefore, the polylines, representing the footprints, are thinned out, taking into consideration the curvature of the represented lines. A threshold, dependent on the resolution used for the visualization, determines the maximum deviation of the rendered SVG object from the original footprints. In this way, the number of points can be reduced and consequently the filesizes of SVG of low resolution pyramid levels decrease by up to a factor of 10. The small footprints of SRC images (originally stored with 34 points) can be even represented sufficiently by the four corner points. The footprints are grouped according to two parameters: *Detector* and *Processing Level ID (PID)*. This allows to change the visibility status of the visualized polygons according to these parameters.

Requests for meta-information of images at a certain location are initiated by clicking into the mapping area on the point of interest. All footprints containing this point will be selected as possible candidates. Another option for requests is defining a rectangular area of interest by two diagonally opposite corner points. All image footprints intersecting this area are selected as candidates, the respective request is initiated and the result list is displayed (Fig. 4.9).

As mentioned in section 3.3.3, SVG rendering engines are faster if zipped documents are used. Therefore, the TMIS map GUI employs static zipped files instead of dynamically created documents, accepting the drawback that user verification information cannot be provided to the SVG. Still, a certain flexibility is given by the possibility to create the files on demand. Zoom levels and panning is realized by providing different background maps and by appropriate adaptation of the geometric reference information. Hence, a WMS request is also possible.

#### 4.4.2 Image-Based Visualization Methods

Most of the current WMS implementations only support static image map presentation, although object-based output formats are considered in the WMS specification (Beaujardiere, 2004). Since the SVG approach described above requires the installation of a rendering container, which was finally not available to all potentially users of TMIS, the following approach is based on a static-at-client-side WMS. Fig. 4.12 shows the currently implemented interface.

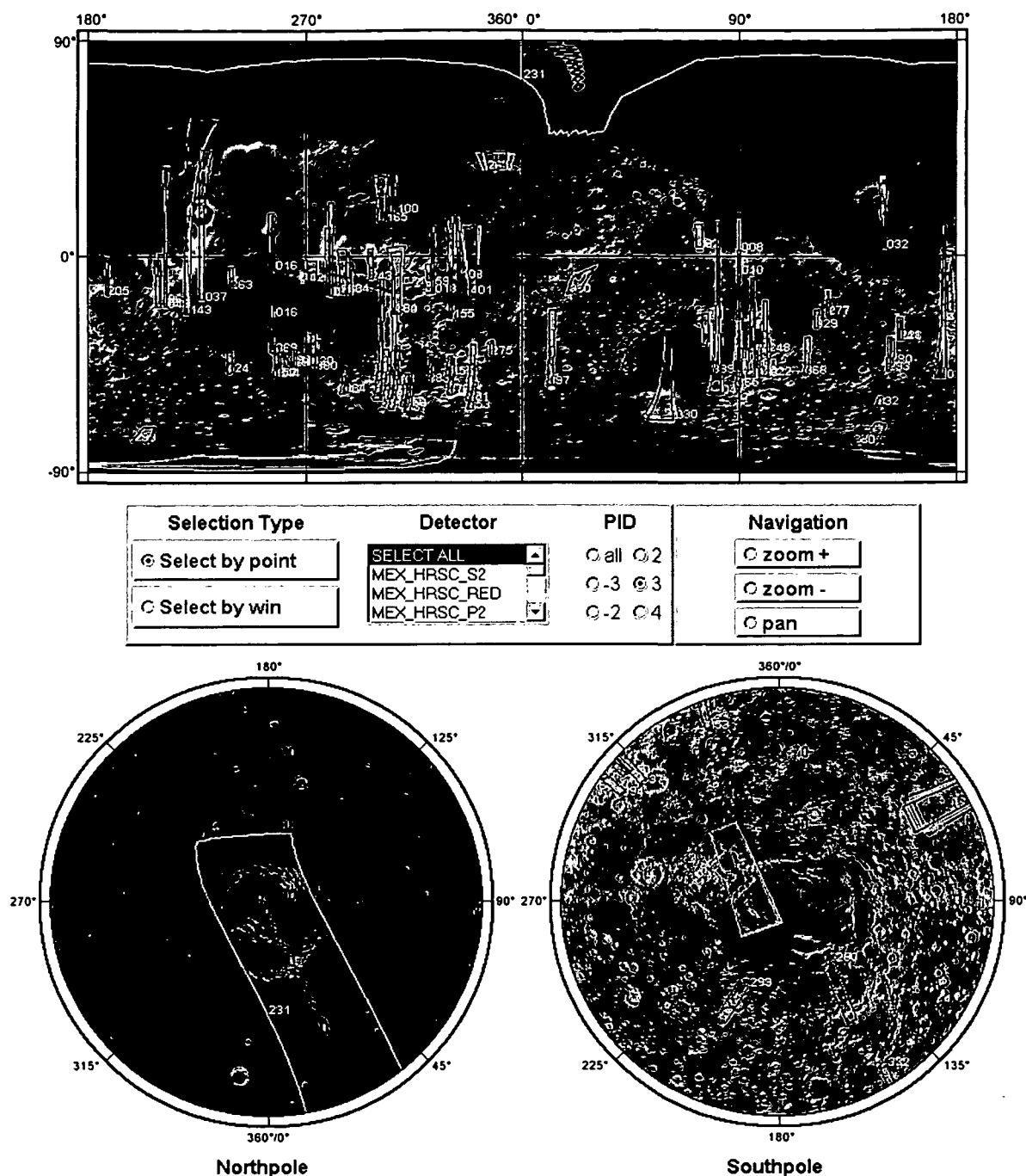


Fig. 4.12: TMIS-interface using an image-based WMS.

Two different map projections are currently supported: A Simple Cylindrical map projection, representing the whole Mars surface and an Azimuthal Equidistant map projection, representing the polar regions in an appropriate way. The Simple Cylindrical representation supports point- and rectangle-based requests for images; the Azimuthal projections supports only point-based requests. Zooming and Panning are possible only using the Simple Cylindrical representation and restricted to a predefined pyramid structure (section 4.3).

#### 4.4.3 Object- vs. Image-Based Visualization Methods

Section 3.4 described concepts for realizing WMSs. Several times it has been pointed out, that, from a conceptual point of view, WMSs support object-based output formats such as SVG or WebCGM and image-based map presentations, which most of the current realizations are based on. The previous sections also described realizations supporting both formats. This section summarizes the characteristics of these different implementations and tries to find pros and cons for both realizations.

Object-based methods support client-side interactivity, because they provide every represented feature as an individual object. Therefore, every object can be fetched at the client-side and handled interactively. For instance, an object's visibility status can be changed, further information can be displayed, and so forth. Contrarily, image-based map presentations (e.g. GIF, PNG, JPEG, ...) behave static, as no client-side interaction is allowed. Every user interaction has to be sent to the server which starts a transaction and finally transfers a new map to the client. At a first glance, the object-based methods seem to require a higher transfer volume than the image-based, as the individually requested files are bigger. But as they are providing client-side scalability and interactivity, far less requests should be necessary, thus decreasing the total amount of requested data. A great advantage of image-based maps is the fact, that no further software is required for rendering purposes, whereas the named object-based formats require rendering engines, which have to be available at the client-side. The following table summarizes the characteristics of both methods.

	<i>object-based</i>	<i>image-based</i>
<i>interactivity</i>	client- and server-side	server-side
<i>scalability</i>	client-side (for large zoom ranges, a server-side pyramid structure should be provided)	server-side
<i>server requests</i>	few (interaction at client-side)	many
<i>filesize</i>	dependent on nr. of objects (vector) if a complex background map is used: dependent on image resolution as well	dependent on image resolution (raster)
<i>software requirements (client)</i>	plug-in	none
<i>hardware requirements (server)</i>	probably smaller than image-based server	fat server fast response time to support interactivity
<i>integration of extern WMS</i>	client- and server-side: difficulties due to possibly complex document structures; integration as raster map would be possible	client-side: using overlays server-side: integration into final map creation

Tab. 4.2: Characteristics of object- and image-based WMS.

Tab. 4.2 shows the advantages and shortcomings of both methods. Thus, the adequate choice depends on the application. For implementations providing a high degree of interactivity, object-based methods are recommended. If a broad group of users should be reached by a service with few interactivity, image-based methods are a good solution. As already pointed out in section 3.3.3 the integration of rendering engines for object-based formats such as SVG or WebCGM into the kernel of commonly used web browsers would be necessary to increase the importance of object-based web presentation methods. As long as this requirement is not fulfilled, such methods will not emerge.

## 5 Modeling the Topography of Mars

Information systems dealing with spatial data are often named *Geographic Information Systems (GIS)*. Per definition, a GIS is a computer based system, consisting of hardware, software, data and applications. It is dedicated to acquisition, editing, storage, and reorganization, to modeling and analysis and to alphanumeric and graphical presentation of spatial data. Although TMIS fulfills those requirements, it cannot be compared to commercial GIS systems such as ArcInfo (ESRI, 2004) or to the open source project GRASS (GRASS, 2004), as the provided functionality has been separated into two different groups:

- data management and distribution and
- analysis and visualization.

Chapter 3 presented concepts and methods for data management and distribution and chapter 4 their application to realize the TMIS. The integration of topographic data processing and analysis tools into the TMIS environment is discussed in this chapter (topographic data processing) and chapter 6 (application and results). The tools and methods providing these capabilities are named *TMIS Extended Functionality (TMIS-EF)*. Most of these tools are directly integrated into the TMIS and available through the TMIS-Col-Interface. Some are part of the software application SCOP++ (IPF-SCOP, 2004), which is – as part of the TMIS usage contract – available to the entire HRSC Co-Investigator project group.

The following sections describe the initial state of the available methods (most of them originally developed for application on Earth) and the necessary modifications and extensions for application to Mars DTMs. The investigation and implementation of methods and algorithms for manipulation, analysis and visualization of topographic data is of general interest. But in order to evaluate their usability, it is essential to apply them within an appropriate context and to modify them if necessary. Therefore, topographic and image datasets from the NASA mission *Mars Global Surveyor (MGS)* were investigated in detail.

This chapter and the following chapter 6 deals present whole workflow as applied to the available data – from data pre-processing to the computation of DTMs – and the analysis and appropriate visualizations of both, the data and the results. After an overview of the initial situation, chapter 5 deals with the task of deriving a homogeneous DTM from the available MOLA original points which contain erroneous measurements. Thus, the data pre-processing consists of error elimination and data homogenization. An automated method for error detection and subsequent elimination of erroneous points from the original MOLA point cloud is described in detail and different possibilities to derive a grid-based DTM from the inhomogeneously distributed original points are discussed.

In chapter 6, the application of raster-based methods for analyzing those DTMs is described. Especially hydrological analysis seems to have a high potential to derive models to reconstruct the behavior of possible former surface water on Mars in a plausible manner. The results of the analysis of

three selected regions on Mars, which are very likely to have been formed by surface water, are discussed in detail:

- hydrological mapping of the *Tharsis Highlands* and *Valles Marineris* (section 6.1.1);
- outflow channel detection in the *Elysium Region* (section 6.1.2);
- simulated outflow behavior in *Ma'adim Vallis* and *Gusev Crater* (section 6.1.3).

Finally different methods for 3D visualization of DTMs and corresponding raster image overlays are described and exemplary results are presented.

## 5.1 Initial Situation

Most of the widely used methods and applications for DTM analysis and visualization are based on a *raster data structure*. A discrete quadratic area, often named pixel, is associated to one single value containing the mean height of the area to be represented. A regular raster of adjacent cells covers the whole area of interest (Kraus, 2000, p. 181). A commonly used software application applied to topographic Mars data is *VICAR*. It is a set of computer programs and procedures designed to facilitate the acquisition, processing and handling of digital image data. The *VICAR* image processing language was defined and implemented in 1966 at the *Jet Propulsion Laboratory* (JPL) to process image data produced by the planetary exploration program (Duxbury and Jensen, 1994). Since then, it has been continuously improved.

A raster-based DTM is a simple matrix structure, organized in lines and samples and stored as a binary stream of values, e.g. representing the heights. The meta-information (extension, geo-referencing, data acquisition, ...) can be provided by a so-called header included in the dataset. The *VICAR* format may include two separate parts of meta-information: A plain text label provided as a header containing general information on the dataset (e.g. number of lines, number of samples, referencing, origin, purpose, ...) and an optional label information for each individual line, containing descriptive information on this line (e.g. erroneous pixel, ...). Such formats are simple to read and write and thus provide a high performance as no redundant information is necessary. Contrary to randomly distributed points, in a regular raster it is not necessary to store the individual coordinates of the points. The location can be derived from the associated line and sample number using the header information. The great advantage of the possibility to use fast raster-based operations is combined with the disadvantage that derived products depend on the given raster width. Thus, data manipulation involving resampling (e.g. a datum transformation) can cause a loss of information.

The data format used in the following considerations describes the terrain using a hybrid DTM structure (section 3.3.5). As a matter of principle, it is also based on the storage of regular, grid-wise distributed points, derived from the original measured points. But the data access algorithm supports the computation of any point within this grid using a high level function to interpolate the area between the given points. This allows to derive products (iso-lines, shaded relief, ...) at a higher resolution as provided by the given grid.

### 5.1.1 Topographic and Image Data from the Mars Surface

#### **Mars Orbiter Laser Altimeter**

The laser profiling altimeter *Mars Orbiter Laser Altimeter (MOLA)* aboard MGS acquired more than 600 million single points along the ground track of the orbiter, as the measurements were performed in nadir direction. Tab. 5.1 provides an overview of the specification of the instrument. Detailed information is provided by Smith et al. (1999) and at the MOLA website (NASA-MOLA 2004).

<b>transmitter</b>	
<i>laser:</i>	diode pumped, Q-switched Nd:YAG
<i>wavelength:</i>	1064 nm
<i>pulse rate:</i>	10 Hz
<i>energy:</i>	48 mJ/Puls
<i>laser spot:</i>	0.4 mrad
<b>receiver</b>	
<i>mirror:</i>	50 cm parabolic
<i>detector:</i>	silicon-avalanche photodiode
<i>field-of-view:</i>	0.85 mrad
<b>resolution</b>	
<i>vertical precision (shot-by-shot):</i>	37.5 cm
<i>absolute vertical accuracy:</i>	< 10 m (depends on accuracy of reconstruction of radial spacecraft orbit)
<i>surface spot size:</i>	130 m
<i>along track shot spacing:</i>	330 m
<i>across track shot spacing:</i>	depends on mapping orbit and will vary with latitude; up to several km

Tab. 5.1: The instrument specifications of the Mars Orbiter Laser Altimeter (MOLA)

Since the original MOLA dataset contained gross errors due to incorrect referencing of the sensor platform, a method to detect and subsequently eliminate those erroneous points had to be developed. It is based on semi-automatic robust interpolation methods as described in section 5.2.

#### **Mars Orbiter Camera**

The *Mars Orbiter Camera (MOC)* aboard the MGS consists of a narrow-angle camera which provides high-resolution images at a resolution of about 1.4 meter/pixel of selected areas and a wide-angle camera mapped almost the whole surface of the planet at a resolution of about 280 meter/pixel (NASA-MOC 2004). In the following, an image mosaic derived from MOC wide-angle images is used for different visualization purposes. The mosaicking of the original MOC images was performed by Wählisch et al. (2002). The original ortho-image map has a resolution of 256 pixel/degree which corresponds to 231.5 meter/pixel at the Mars equator.

### 5.1.2 Referencing Considerations

Most DTM datasets available from Mars are provided in VICAR format. VICAR DTM files contain an ASCII (plain text) header with meta-information, also referred to as label information, followed by a binary data stream representing the height values of the DTM pixels. This data format is used for the storage of image data as well.

#### **MOLA Grid Data**

The *MOLA grid data* is released by the Washington University in St. Louis (NASA-MOLA, 2004). The following table Tab. 5.2 provides parts of the label information:

<i>reference system:</i>	IAU 2000
<i>map projection type :</i>	simple cylindrical
<i>a = b = c-axis:</i>	3,396.0 km
<i>map resolution:</i>	1/128°
<i>map scale:</i>	0.463 km/pixel (at the equator)
<i>coordinate system name:</i>	planetocentric

Tab. 5.2: Referencing information of the MOLA grid datasets.

The *International Astronomical Union (IAU)* released a reference system for Mars in the year 2000 (IAU 2000) considering the state of the art information about the body of the planet and defining a standardized datum. A sphere as well as a biaxial ellipsoid are defined as reference bodies. The reference system shown in Tab. 5.2 is defined according to the IAU 2000 system, using a sphere as reference body. Unfortunately, the specifications for map resolution and map scale are contradictory as the following calculation demonstrates:

$$P = 2 \cdot 3,396 \cdot \pi = 21,337.697 \text{ km} \quad (5.1)$$

$$m = \frac{P}{\text{map resolution}} = \frac{21,337.697}{360 \cdot 128} = 0.463058 \text{ km} \quad (5.2)$$

$$0.463058 \text{ km} - 0.463 \text{ km} = 5.8 \text{ cm} \cdot 128 \cdot 360 = 2.657 \text{ km} \approx 6 \text{ pixel} \quad (5.3)$$

$P$  in Eq. (5.1) is the perimeter of the sphere considering the radius of the IAU 2000 sphere. Eq. (5.2) computes the map scale  $m$  using perimeter  $P$  and a resolution of 1/128°. The discrepancy between the given map scale (0.463 km) and the derived scale (0.463058 km) is 5.8 cm/pixel resulting in a total difference of 2.657 km at the equator corresponding to about 6 pixel at a resolution of 463 m/pixel. Though not indicated, the map scale value of the header is obviously rounded to  $m$ , as the above calculations demonstrate. Therefore, the given metric pixel size must not be used for geometric computations over larger regions. Thus, for further processing of MOLA data, the following convention was defined:

As the following methods used for DTM computation and analysis require map projected topographic datasets with equivalent scale in location (latitude / longitude) and height, a grid width of 463 m was considered to be equivalent to  $1/128^\circ$ . All datasets used for processing and analysis were scaled according to this definition. Final products are defined using parts of degrees (e.g.  $1/128^\circ$ ,  $1/64^\circ$ , ...) for the definition of the scale. Therefore, the previously applied scaling factor has no influence and the reference system is the same as those of the original data.

The following figure Fig. 5.1 gives an overview of referencing the MOLA grid datasets available as tiles in Simple Cylindrical map projection.

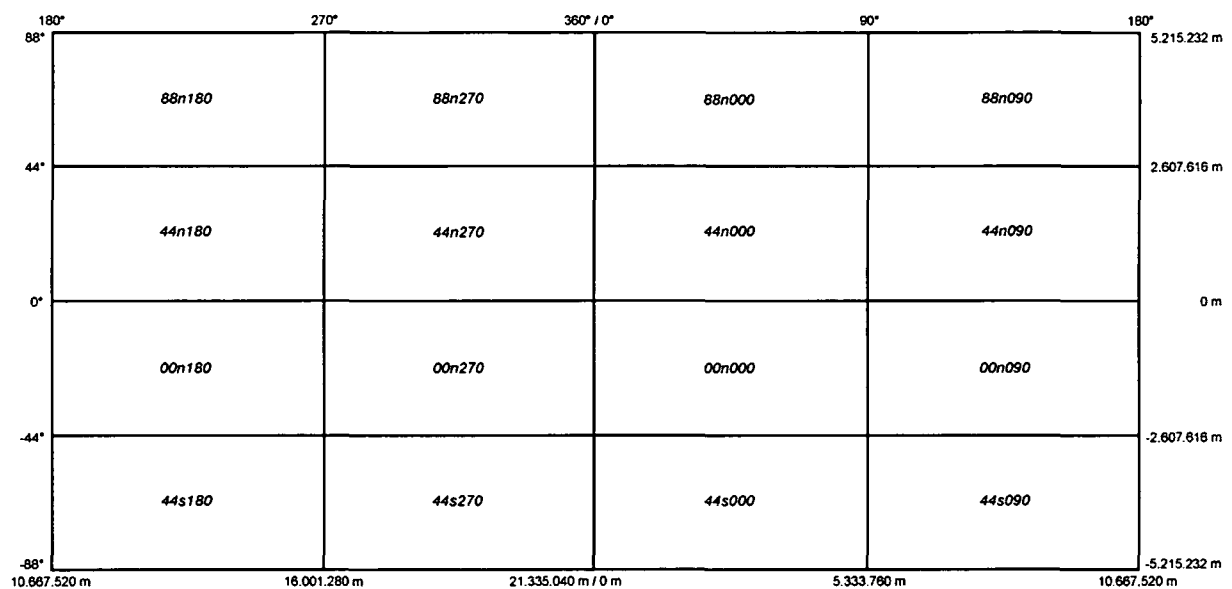


Fig. 5.1: Referencing of the available MOLA grid tiles available in Simple Cylindrical map projection. The nomenclature of each tile consists of latitude and longitude in degree of the upper left corner (n = northern latitude, s = southern latitude). The grid width is  $1/128^\circ$ . The referencing in meter assumes that this grid width corresponds to 463 m.

### MOC Image Mosaic

The following table Tab. 5.3 provides the referencing information of the used MOC image mosaic data:

map projection type :	sinusoidal
a = b axis:	3396.19 km
c axis:	3376.2 km
map resolution:	$1/256^\circ$
map scale:	0.231529 km/pixel
coordinate system name:	planetographic <sup>6</sup>

Tab. 5.3: Referencing information of the MOC image mosaic.

<sup>6</sup> The latitudes of the MOLA dataset (Tab. 5.2) are provided using geocentric notation. In contrary, the latitudes of the MOC images are given as geographic angles.



The discrepancy of the given map scale (0.231529 km/pixel) to that derived using Eq. (5.1) to Eq. (5.3) (0.231541 km/pix) is 1.178 km (almost 3 pixel at a grid width of 1/128°) at the equator. For the elliptical latitudes, this value is completely senseless.

The MOC image mosaic, which was available in tiles as well, was transformed into the MOLA grid reference system using the TMIS functionality. The original image tiles in Sinusoidal Projection were imported into the Topographic Data Market (section 3.2.4). The transformation into Simple Cylindrical map projection was performed using the implemented coordinate transformation algorithms. Finally, a new grid was interpolated and prepared as VICAR image format.

## 5.2 DTM Computation from Original Mars Surface Points

In the following, methods to derive homogeneous DTMs from the original MOLA point cloud are described. First, a short introduction into linear prediction is given. This method is used for DTM approximation and simultaneous elimination of random distributed errors in order to compute a regular grid representation from original point clouds. Afterwards, a method for detection and elimination of gross erroneous points within the original MOLA point cloud is presented and illustrated by visualizations of exemplary results. As the error elimination method provides a point cloud consisting of original measurements – it performs a classification of the given points into error free and erroneous points – the inhomogeneity in spatial distribution is still a problem to be solved. Several methods to increase the homogeneity have been tested and are discussed finally.

During this work, the MOLA science team released a raster-based dataset derived from the original points. This dataset was obviously pre-processed as the influence of the erroneous spacecraft referencing is reduced.

### 5.2.1 Method for DTM Interpolation

The approach used in this work for the determination of a smooth and homogeneous surface from a given irregular point cloud (e.g. MOLA or HRSC matched points) is *linear prediction* described by Kraus (2000, pp. 154 – 180). It is equivalent to the widely used Kriging estimator (Kraus, 1998).

Given are  $n$  points  $P_i$  with the heights  $z_i$ , which have been reduced by subtracting a trend surface (e.g. a plane). After this reduction the expectancy of the observed heights is zero. The height  $z$  at a position  $P$  is determined by Eq. (5.4):

$$z = c^T C^{-1} z \quad (5.4)$$

with:

$$c = (C_{(PP_1)}, C_{(PP_2)}, \dots, C_{(PP_n)})^T \quad (5.5)$$

$$z = (z_1, z_2, \dots, z_n)^T \quad (5.6)$$

$$C = \begin{pmatrix} V_{zzp_1} & C_{(P_1P_2)} & \cdots & C_{(P_1P_n)} \\ & V_{zzp_2} & & C_{(P_2P_n)} \\ & & \ddots & \vdots \\ & & & V_{zzp_n} \end{pmatrix} \quad (5.7)$$

The values  $C(p_i p_k)$  describe the covariance between two points on the surface in the following way (Gaussian model):

$$C_{(P_i P_k)} = C_{(0)} e^{-\left(\frac{P_i P_k}{c}\right)^2} \quad (5.8)$$

with:

- $C_{(0)}$  = covariance for a distance of zero,
- $P_i P_k$  = horizontal Euclidian distance between the two surface points  $P_i$  and  $P_k$ ,
- $c$  = factor (estimated from the given points) for controlling the steepness of the covariance function.

$V_{zzp_i}$  in Matrix  $C$  of Eq. (5.7) is the variance of the given points, which is the sum of  $C(0)$  and the variance of the measurements  $\sigma_i^2$ . The points are considered to have the same  $\sigma_0^2$  (a priori accuracy), but different weights  $p_i$ . The accuracy  $\sigma_i^2$  of a point  $P_i$  is obtained from:

$$\sigma_i^2 = \frac{\sigma_0^2}{p_i} \quad (5.9)$$

The variance of each point  $P_i$  can be computed by:

$$V_{zzp_i} = C_{(0)} + \sigma_i^2 \quad (5.10)$$

(Kraus, 2000). It can be proved, that a high point density (high redundancy) allows for the computation of a DTM with a better inner accuracy of the interpolated points than those of the individual given points. Furthermore, it should be mentioned, that Eq. (5.4) can be derived in another way by minimizing the sum of the squares of the interpolation errors. So the *linear prediction* approach is also known as *least squares interpolation* as described by Moritz and Sünkel (1978).

### 5.2.2 Error Elimination

A prerequisite for deriving high-quality DTMs is a correct and accurate dataset of measurements. Initially, the free available dataset of MOLA original points, released by the MOLA science team and

distributed on the web (NASA-MOLA, 2004), contained errors due to incorrect referencing of the spacecraft, as already mentioned. Since October 2002, an improved dataset is available. The predefined grid spacing of this dataset is  $1/128^\circ$  which corresponds to about 463 m at the Mars equator (see section 5.1.2). The original points have been released in October 2003 using an improved reference system. Within this “final” release, several erroneous tracks have been removed, while some are still remaining within the dataset. Publications about the applied error elimination methods are not available.

The following approach is an automated method for detection and subsequent elimination of erroneous points, based on robust interpolation methods. It allows to do this without having information about the orbit data and thus, without the possibility to correct them. This approach, therefore, would work within other similarly deteriorated data as well as it does not require detailed a priori knowledge about the dataset and about reasons for incorrectness of the data.

Because of the inhomogeneous distribution of the given points, the use of a hierarchical robust interpolation seemed to be appropriate. This method was originally developed to classify airborne laser scanner (ALS) data in Earth applications into terrain points for DTM interpolation, and off-terrain points, such as vegetation or buildings. A detailed description of this method and its capabilities is provided by Briese et al. (2002a, pp. 55 – 61). Unexpectedly, when applied to the MOLA points, the results were not satisfying. Due to the roughness of the Mars surface, points in regions without scan errors were eliminated as well. The rugged terrain did not fit the functional model of linear prediction, which was originally designed to generate very smooth surfaces as they usually occur in Earth applications. Several tests of applying the hierarchical robust interpolation for classification of ALS data in mountain regions at the Earth show similar effects in rocky alpine areas with their peaks, rims, ridges and other rough structures. In that cases, a smoothing effect eliminates the typical roughness of the terrain.

Currently no satisfying solution is available for the application of ALS data. In order to improve the results on MOLA points, the approach was modified as follows. Instead of analyzing each individual point, scan line segments were investigated, assuming that the errors to be detected are always effecting a series of successive points rather than single points. The average filter value of a segment, the RMS (root mean square error of the residuals of the points belonging to this segment), turned out to provide an appropriate measure for detecting segments with gross errors. The separation in segments was enabled due to the fact that the original points are available track-wise in the order of measurement. This circumstance allowed for considering a series of points (e.g. 500) as one segment. Unfortunately, erroneous segments cause a deformation of the interpolated DTM and increase the RMS of correct line segments in their neighborhood with respect to the (incorrect) DTM. The profile of a DTM as shown in Fig. 5.2 sketches the behavior of a predicted surface (a horizontal plane) near to a gross error. The light gray band represents the threshold for acceptance of points. This threshold would obviously eliminate correct line segments due to the strong deformation of the model in that area caused by one gross erroneous track. In order to solve this problem, the method has to be applied iteratively, starting with a large threshold value and reducing it from one iteration to the next. This procedure corresponds to a robust interpolation using a box weight function to yield decreasing

values in consecutive iteration steps. Fig. 5.3 shows this function with three different thresholds of 200, 75 and 20 m.

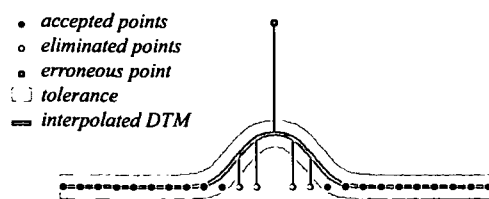


Fig. 5.2: Profile of an interpolated DTM representing its behavior near a gross error. The light gray band represents a threshold for acceptance of points.

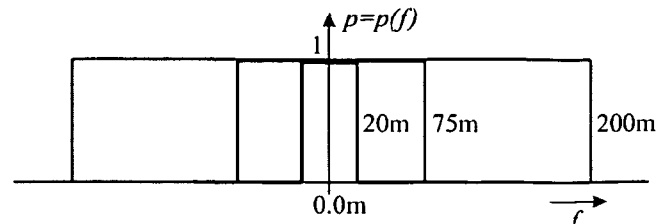


Fig. 5.3: Box weight function with different tolerances (200, 75 and 20 m) as used iteratively to detect and subsequently eliminate erroneous points.

In addition, not all points along an erroneous scan line segment need be affected by gross errors. In the first step of classification, all possibly erroneous points according to a detected segment are separated from the correct points. Afterwards, the discrepancy of every eliminated point is analyzed with respect to a DTM computed without these potential gross erroneous segments, and all previously eliminated points within a certain threshold value are accepted again. The five steps of the iterative procedure are the following:

1. computing a DTM with all points;
2. computing the RMS per scan line segment and eliminating segments with an RMS higher than the defined threshold;
3. computing a DTM with the accepted scan line segments;
4. accepting formerly eliminated points, if they are within a certain tolerance to the DTM derived in step 3;
5. computing a new DTM.

Steps 2 to 5 are repeated with decreasing tolerance values, until the tolerance of the RMS per scan line segment reaches a user-defined threshold value (Briese et al., 2002a, pp. 55 – 61). The following two figures demonstrate the influence of step 2 and 4 (elimination and re-acceptance of points according to thresholds) when applying the final step of four iterations (200 m, 75 m, 20 m, 15 m). The red dots in Fig. 5.4 show the positions of all those points eliminated in step 2. The black dots in Fig. 5.5 show the points which are restored in step 4. Only those points still represented by red dots are classified to be erroneous. Green dots represent all sampled points not influenced by this procedure and regions appearing gray are areas void of points which had to be extrapolated from the given points. The test area has an extension of about  $10^\circ \times 10^\circ$  (600 km x 600 km) and represents *Arsia Mons*, the most southern one of the three large shield volcanoes on the *Tharsis Highlands*. The diameter of its caldera is about 120 km (Heuseler et al., 1997, p. 113).

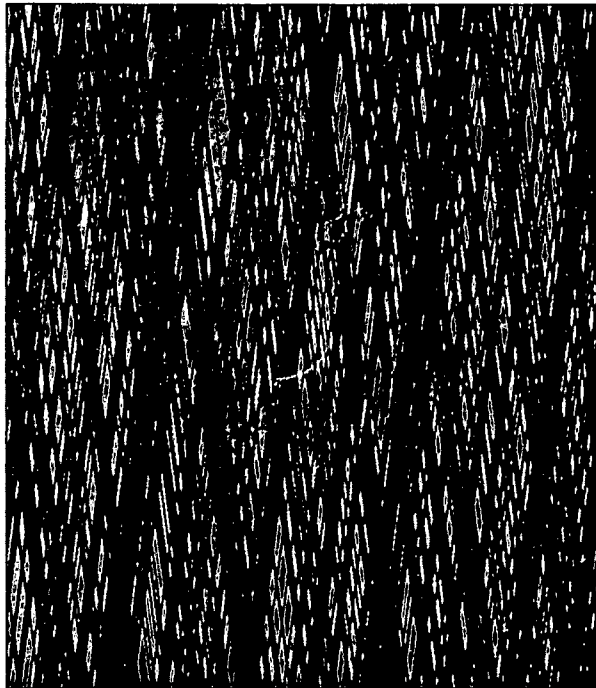


Fig. 5.4: The effect of step 2 (elimination of all points according to line segments with an RMS higher than the threshold). Red dots represent all points classified as possibly erroneous; green dots are the given points; gray areas are void of points.



Fig. 5.5: The effect of step 4 (re-acceptance of single points previously classified as erroneous, if their RMS is smaller than the threshold). Black dots represent points accepted again. Red dots are classified as erroneous and are not taken into account for further processing.

While the first two iteration steps with thresholds of 200 m and 75 m seem to be appropriate for almost every region on the Mars surface (they are dependent on the expected range of errors to be detected, which is a priori known or, at least, may easily be estimated from the data acquisition method), the final threshold has to be adapted by the user according to the roughness within the area of investigation. The following example demonstrates the influence of the final threshold.

The lava flow, which covers the surrounding of the caldera by hundreds of meters, generates a very inhomogeneous roughness as the lava itself (north and south of the caldera) appears very smooth at the resolution of the derived DTM (463 m grid width), while the areas without lava (northwestern area) appear very rough. Fig. 5.6 shows the result after three iterations (200 m, 75 m, 20 m; referred to as DTM20). It is obvious that a final threshold of 20 m is not small enough to eliminate all erroneous points within the smooth areas (southern partial enlargement). Fig. 5.7 was achieved using a final threshold of 15 m instead of 20 m (DTM15d). This enabled the elimination of the erroneous points in the southern regions, but some detailed structures north of the caldera were eliminated as well. Thus, four iterations (200 m, 75 m, 20 m, 15 m) were applied to derive Fig. 5.8 (DTM15). The aim of eliminating the erroneous points in the South has been reached, while the accepted points are able to describe the high level of detail of the northern region of the caldera. A final threshold of 10 m (this value corresponds to the absolute vertical measurement accuracy of the MOLA instrument) is obviously too small, as too many points within the rough areas are eliminated (Fig. 5.9).



Fig. 5.6: Shaded relief of the DTM derived with a final threshold of 20 m (DTM20). Erroneous points remain within the smooth areas (see partial enlargement of the southern area).



Fig. 5.7: Applying a final threshold of 15 m instead of 20 m (DTM15d). The erroneous points in the southern area are eliminated, but the rough topography north of the caldera is distorted.



Fig. 5.8: Applying four iteration steps (200 m, 75 m, 20 m, 15 m) instead of three achieves the best result (DTM15). The erroneous points within the smooth areas are eliminated and the rich details within the rough areas remain.



Fig. 5.9: Applying a final threshold of 10 m obviously eliminates too many points within rough areas (black regions).

The following two figures show color-coded visualizations of the discrepancies between the different models. Fig. 5.10 shows the height differences of DTM20 and DTM15. The two erroneous tracks (south of the caldera and inside the caldera) are eliminated in DTM15. The mean occurring discrepancies are between  $\pm 100$  m. Fig. 5.11 shows the differences between DTM15d and DTM15.

The erroneous tracks are eliminated in both models, but especially the rough areas north and south of the caldera are deformed to a great extent.

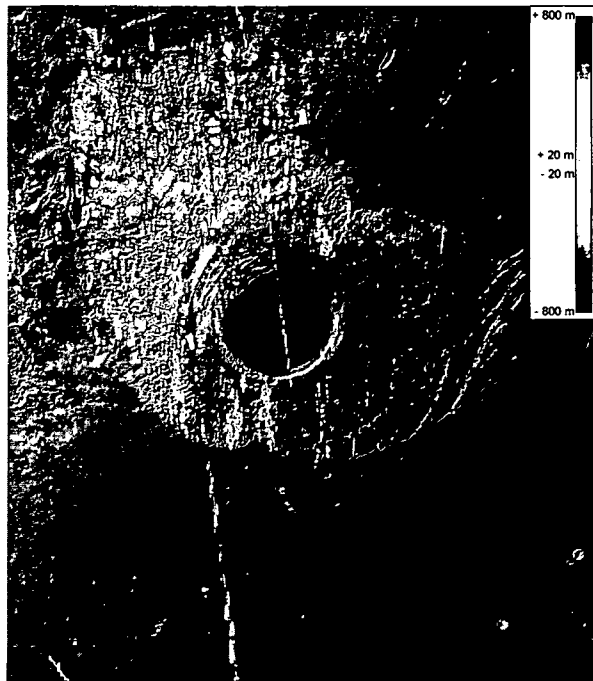


Fig. 5.10: Discrepancies between DTM20 (Fig. 5.6) and DTM15 (Fig. 5.8).

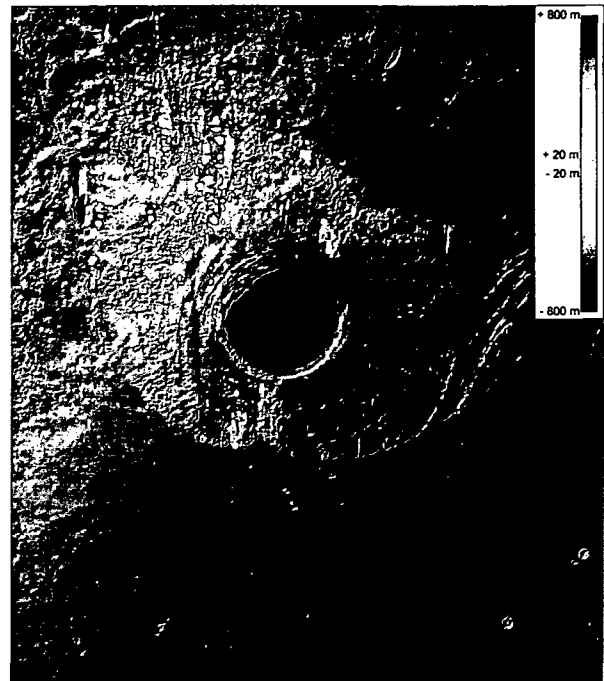


Fig. 5.11: Discrepancies between DTM15d (Fig. 5.7) and DTM15 (Fig. 5.8).

The automatic determination of the final threshold value will be subject to further investigation and has not been thoroughly tested yet. Already existing roughness maps might be useful (Kreslavsky and Head, 2000), but they were not available in an appropriate resolution during this work.

Fig. 5.12 to Fig. 5.15 show shaded relief of an area of  $10^\circ$  by  $10^\circ$  within the central part of the *Valles Marineris*, the largest rift system on Mars with a total length of more than 4000 km. The average height difference from the rim to the bottom is about 8 km. The first figure was derived from all available MOLA points. The following three figures show the DTM during the error elimination process using three iterations with thresholds of 200 m, 75 m and 25 m.



*Fig. 5.12: Shaded relief of a DTM derived from the original point cloud containing erroneous points. The white areas appear in regions without given points.*



*Fig. 5.13: Result after the first iteration (threshold = 200 m). The RMS of the erroneous track, crossing the model in north/south direction (Fig. 5.12), was almost 2,000 m.*



*Fig. 5.14: Result after second iteration (threshold = 75 m).*



*Fig. 5.15: Final result after third (final) iteration (threshold = 25 m).*



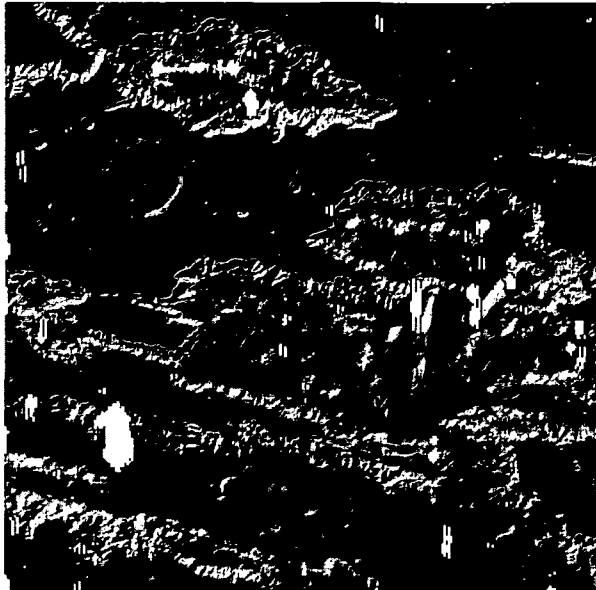


Fig. 5.16: If the final threshold is too small (20 m), error free points are likely to be eliminated especially in rough regions.



Fig. 5.17: Improved visualization of the final result (Fig. 5.15) using different DTM computation parameters (section 5.2.4).

A final threshold of 20 m (Fig. 5.16) is obviously too small to be applied in this area due to the high roughness, especially within the rift system. It causes error free points to be eliminated as well (white regions).

Fig. 5.15 and Fig. 5.17 are derived from the same points, determined using a final threshold of 25 m. To bridge the void areas, initially, a coarse raster was computed and merged with the original points. This method is described in section 5.2.4 in more detail. Afterwards a grid-based DTM is derived, which enables a visualization without gaps as shown in Fig. 5.17.

<i>description</i>	<i>iteration</i>	<i>threshold</i>	<i>nr. of points</i>
number of given MOLA points for DTM computation (including erroneous)	1 - step 1		902,564
points classified as erroneous (only line segments are considered)	1 - step 2	200 m	- 9,629
points reaccepted (every single point is considered)	1 - step 4	200 m	+ 6,633
number of points classified as error free after first iteration	1 - step 5		899,568
points classified as erroneous	2 - step 2	75 m	- 5,938
points reaccepted	2 - step 4	75 m	+ 4,087
number of points classified as error free after second iteration	2 - step 5		897,717
points classified as erroneous	3 - step 2	25 m	- 82,143
points reaccepted	3 - step 4	25 m	+ 39,865
number of points classified as error free after third iteration	3 - step 5		855,439

Tab. 5.4: Overview of the error elimination as applied to a 10° by 10° area described by MOLA points within the central part of the Valles Marineris. A total amount of 902564 MOLA points is reduced to 855439 points applying a classification into erroneous and error free points.

Tab. 5.4 provides an overview of the applied classification as used to derive the final DTM visualized in Fig. 5.17. The number of points is listed according to the iteration step applied during the error elimination. Step 1 derives a first DTM from all given MOLA points (902,564 points). Step 2 applies a

classification using the given thresholds of 200 m, 75 m and 25 m to find possibly erroneous track segments and step 4 uses the same thresholds for re-acceptance of individual points having a smaller RMS compared to a DTM derived without those segments. Step 5 derives a DTM as final step of each iteration. Finally 855,439 points remain to derive an improved, "error free" DTM.

Within this test area, about 5 % of the original MOLA points were classified as erroneous. This percentage is dependent to a high degree on the roughness of the surface and on the final threshold, which depends on the roughness as well.

### 5.2.3 Comparison of Error Elimination Methods

Compared to manual methods, an automated method for error elimination provides a more objective result, as it is not dependent on subjective selection criteria as applied by an operator. Furthermore, no a priori knowledge on the given data such as orbit information or known errors due to spacecraft orbit correction maneuvers is necessary. Every point is compared to its neighborhood according to predefined rules. The advantages can be characterized as follows:

- if referencing errors of the satellite are not known, the resulting erroneous points can be detected and eliminated without any manual interaction;
- if the satellite track has been corrected in advance, the resulting points will be accepted anyway for the following DTM generation;
- if, for some reason, other erroneous measurements (of either individual points or series of points) do occur, they will also be treated in an appropriate way;
- the method treats the whole dataset following the same, predefined rules.

Fig. 5.18 shows the influence of one single track, which seems to be erroneous in the northern part, but improving in quality (as compared to its surroundings) in the southern part. This example demonstrates the robustness of the method against the possibly changing state of consecutive points.

Fig. 5.19 shows the influence of the last iteration step (threshold = 20 m) as applied to a DTM within the central part of *Valles Marineris*. It might be a challenge for an operator to select erroneous tracks according to the same criteria as the automated method. It is obvious, that not all tracks containing points which appear erroneous in the left image, should be eliminated in advance. Furthermore, performing this manually would cause a large effort.

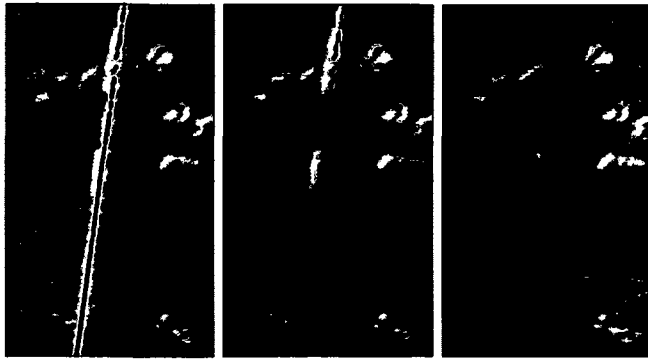


Fig. 5.18: The left image shows the locations of the points as measured within one track which was obviously corrupt in the northern part but it fits to its surroundings in the south. The center image shows the same shaded relief without the footprints of this track. The right image shows a shaded relief derived after the error elimination process.

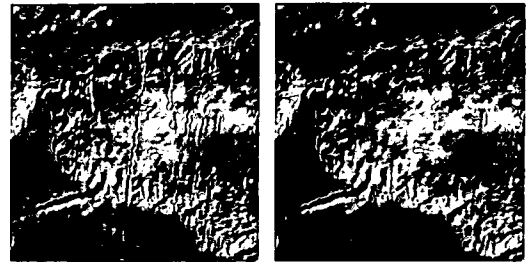


Fig. 5.19: Influence of the last iteration step (threshold = 20 m) as applied to a small region within the Valles Marineris. The left image shows a shaded relief after applying a threshold of 75 m. The right image shows the same region after the final iteration step.

#### 5.2.4 DTM Computation

The error elimination, as described above, detects and eliminates most systematic errors within the given dataset. Nevertheless, random errors caused by the inherent inaccuracies of the measuring system are also a disturbing factor. Therefore, the interpolation algorithm used for DTM generation has to cope with them in order to deliver the most likely surface representation of a given point cloud.

The linear prediction, as described in section 5.2.1, offers the appropriate means, although it needs a homogeneous distribution of the given points for optimum results. Different approaches to homogenize the MOLA dataset are described in the following.

A terrain model should represent the original surface in a homogeneous way. It is rather difficult to fulfill this condition, if the original dataset has an inhomogeneous distribution like the MOLA dataset with its high along-track ( $\sim 300$  m) and low across-track (up to several kilometers) point density. To derive a homogeneous DTM from the MOLA original points, it is necessary to find a compromise for the highly anisotropic point distribution. It is obvious, that gaps (areas void of points) between the tracks represent missing information which cannot be replaced by any interpolation algorithm. The primary task, therefore, is to find an interpolation procedure that delivers the most plausible surface representation with as few disturbing artifacts as possible. Several solutions have been tested as follows:

- *scaling* in the east-west direction (normal to the tracks) to minimize the inter-track gaps;
- applying *morphological operators* normal to the tracks to interpolate the heights in these gaps;
- using *triangulation* methods (Delauney) to bridge the space between given tracks;
- using a *coarse raster* to fill the gaps.

Visualizations of the first two methods showed deformation effects in the east-west direction as they introduce a systematic modeling effect which is dependent on the direction. The third method, the *Delauney Triangulation* (Kraus, 2000, pp. 72 – 81), approximates the area between the given points

using plane triangles. The quality of a triangulation depends on the homogeneity of the given point distribution. The more homogeneous the points are, the better is the quality of the triangulation. Because of the distribution of the given MOLA points, many small triangles were built along the tracks as well as extremely long ones were built between them. The resulting DTM appears very inhomogeneous and includes east-west artifacts, similar to the results of the previously described methods, as a triangulation performs a linear interpolation between the given points of each triangle without considering other neighboring points.

The fourth method provides the most plausible representation of the original surface. The steps applied are visualized in Fig. 5.20 as a block diagram. First, a coarse grid is computed for the whole area of interest. Afterwards, using distance transformation (chamfering), the gaps within the original dataset are determined. Borgefors (1986, pp. 334 – 371) describes this method. A visualization of the resulting distance model is shown in Fig. 5.21. The gaps found are closed using the formerly computed coarse raster. The computation of the final DTM is carried out using the combination of the original points and the selected points from the coarse raster. This method was used to derive the model visualized in Fig. 5.17. In addition, the distance model can serve as a *quality description* of the resulting DTM, too, as the distance of each (computed) raster point to the closest measured point provides a cue for the interpolation quality. This and other measures for the quality of DTM describe in Kraus et al. (2004).

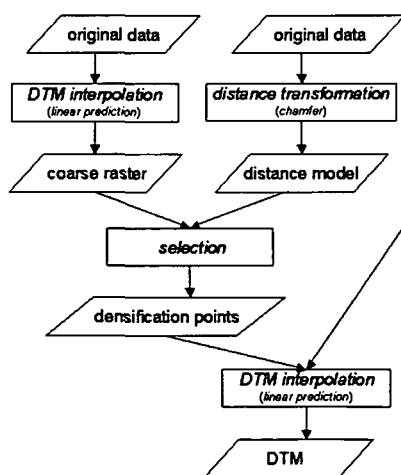


Fig. 5.20: Workflow of the homogenization method as used to close the across-track gaps within the MOLA dataset.

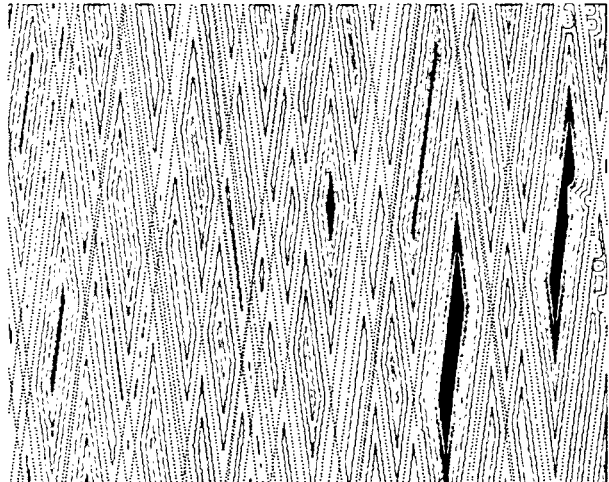


Fig. 5.21: Visualization of the result of a distance transformation (chamfering) as applied to the MOLA points (black dots). White areas represent regions with less than 500 m point distance; black areas with more than 2500 m.

After closing the gaps with points of the coarse raster, the method of linear prediction is used to derive a regular grid-based DTM. As mentioned in section 5.2.1, this method reduces the influence of random errors, often referred to as measurement noise, caused by the data acquisition method. The influence of the given points depends on their distance to the derived grid point. Shifting the peak of the covariance function (Eq. (5.8)), enables, that the interpolated surface is not forced to include the given points; the resulting surface approximates the measured surface as described by the points, instead. This behavior of the approximation can be influenced by a so-called *filter value*. This value should

correspond to the average measurement error of the instrument used for data acquisition (absolute vertical positioning accuracy of MOLA = 10 m, (NASA-MOLA, 2004)). Too small filter values increase the influence of the individual measurements on the approximated surface, resulting in a rough surface model. Greater filter values provide a smoothing effect on the surface of the model. This eliminates the influence of gross errors, but it tends to eliminate real details as well. Fig. 5.22 to Fig. 5.25 show the influence of different filter values (2 m, 10 m, 20 m, 40 m) applied to an area of approximately  $1^\circ$  by  $1^\circ$ .



*Fig. 5.22: Filter value = 2 m. The very high level of detail in track direction is caused by measurement noise rather than by real Mars surface features.*

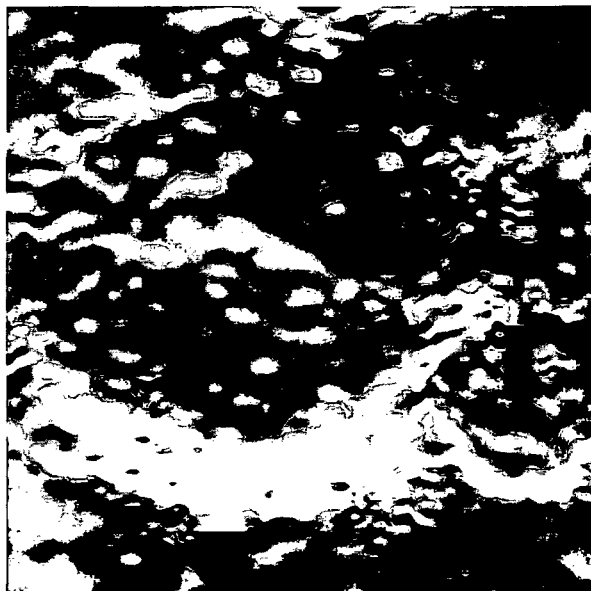


*Fig. 5.23: Filter value = 10 m (absolute vertical positioning accuracy of the MOLA instrument). Within some regions of the crater rim, the influence of the measurement noise is still noticeable.*

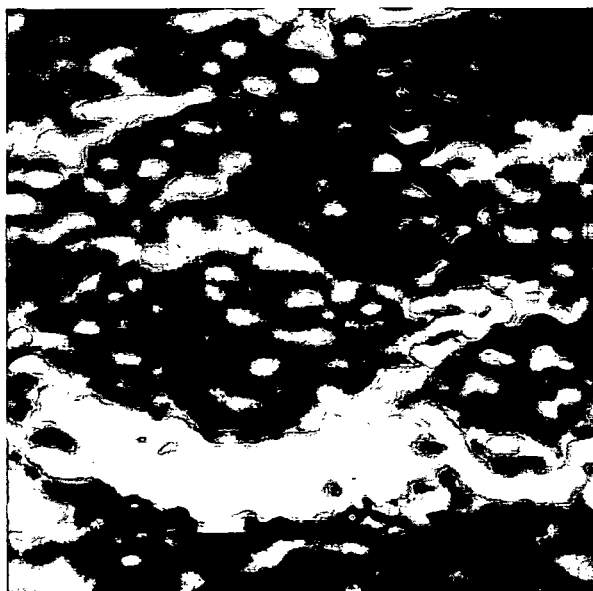


*Fig. 5.24: Filter value = 20 m. The derived DTM appears very homogeneous. Most artifacts, caused by random measurement errors, are eliminated.*



*Fig. 5.25: Filter value = 40 m. All artifacts are eliminated without eliminating details compared to the results shown in Fig. 5.24.*

The discrepancy of the MOLA instrument accuracy (10 m) and the filter value providing the best results (40 m) is caused by the erroneous positioning information of the spacecraft. If two different tracks have a very small across track distance but a slightly positioning shift, peaks occur within the derived models as the surface is dependent on the influence of the individual points of both tracks. Such small referencing errors are very likely, as the time of acquisition of two adjacent tracks can be very different. Fig. 5.26 and Fig. 5.27 show this effect on a DTM as shaded relief and as a profile.

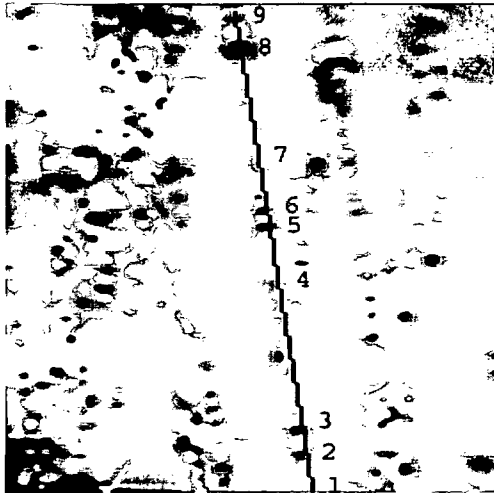


Fig. 5.26: Derived surface using a very small filter value (2 m). The black line shows the position of the profile which is shown in Fig. 5.27. The peaks along two parallel, small distanced tracks are visible.

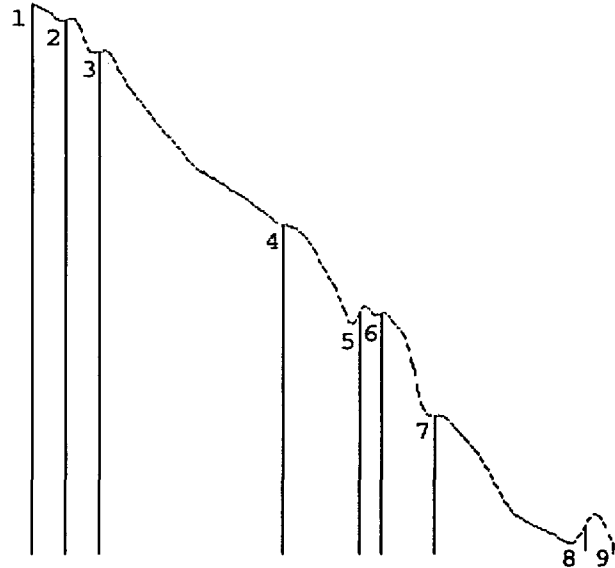


Fig. 5.27: Height profile as measured in the model shown in Fig. 5.26.

The *inner accuracy* of the interpolated points is between  $\pm 15$  m and  $\pm 25$  m with respect to the original points. This estimation was derived from the mean a posteriori filter values (the irregular part of the reduced z-value) of all interpolated points. The variation of the accuracy value depends on the roughness of the interpolated surface. The rougher the interpolated surface is, the worse is the inner accuracy.

### 5.2.5 Results

There is a great demand for error free DTMs derived from original MOLA points for different reasons. Until October 2002, only the erroneous track-wise data was available. Wählisch et al. (2002) created 'A new digital orthoimage map of the Martian western hemisphere using data obtained from the Mars Orbiter Camera at a resolution of 256 pixel per deg' which was presented at the 33<sup>rd</sup> Lunar and Planetary Science Conference in Houston, Texas in March 2002. In order to create this map in a proper way and to derive homogeneous iso-lines, an error free DTM was essential. The area to be modelled had an extension of  $45^\circ$  by  $30^\circ$  at a resolution of 330 m/pixel. The error elimination was applied after subdividing the whole area into 12 rectangular tiles which were processed as described above. Fig. 5.17 shows one of those tiles.

Fig. 5.28 and Fig. 5.29 show *Ceraunius Fossae*, a volcanic field south of *Alba Patera* at the *Tharsis Highland*. It consists of a series of overlapping lava flows whose surfaces are relatively smooth. The topography of this region is characterized by linear features which are almost exactly aligned with the tracks of the spacecraft orbit. Nevertheless, the algorithm behaves robustly against these structures and eliminates the linear features caused by the erroneous points, without influencing the real topography of the modeled surface.

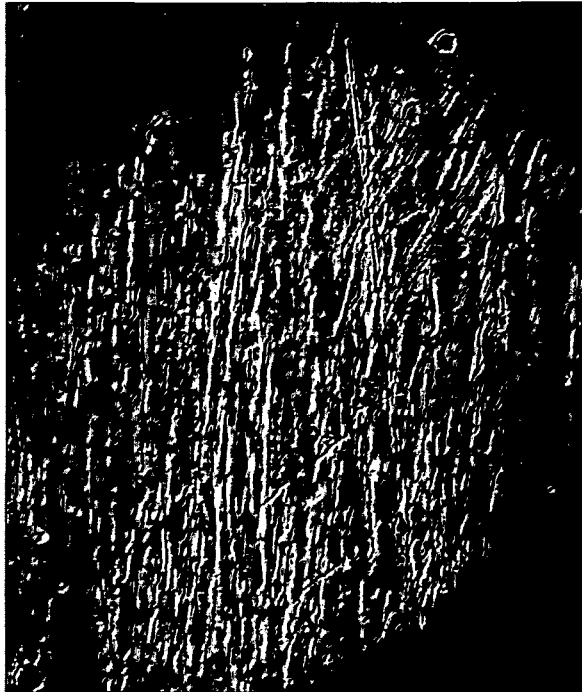


Fig. 5.28: Shaded relief of *Ceraunius Fossae* including erroneous points. The alignment of tracks and topographic features is almost identical.

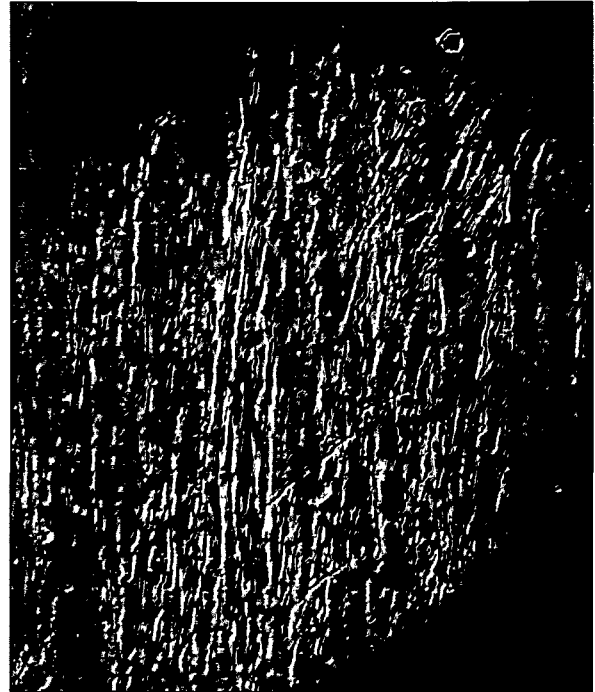


Fig. 5.29: Visualization of a DTM derived after the error elimination. The algorithm did not effect the structure, but the obviously erroneous points were eliminated correctly.

## 6 Hydrological Analysis of the Mars Surface

This chapter describes raster-based methods for surface exploration. Detailed information on the algorithms used are given by Kraus (2000, pp. 398 – 400) and by Rieger (1992b). Fig. 6.1 presents an overview of the methods applied to the MOLA dataset in the area of *Valles Marineris*. The DTM used was derived from the original, track-wise available MOLA point cloud after error elimination as described in chapter 5. The grid width is about  $1/64^\circ$ .

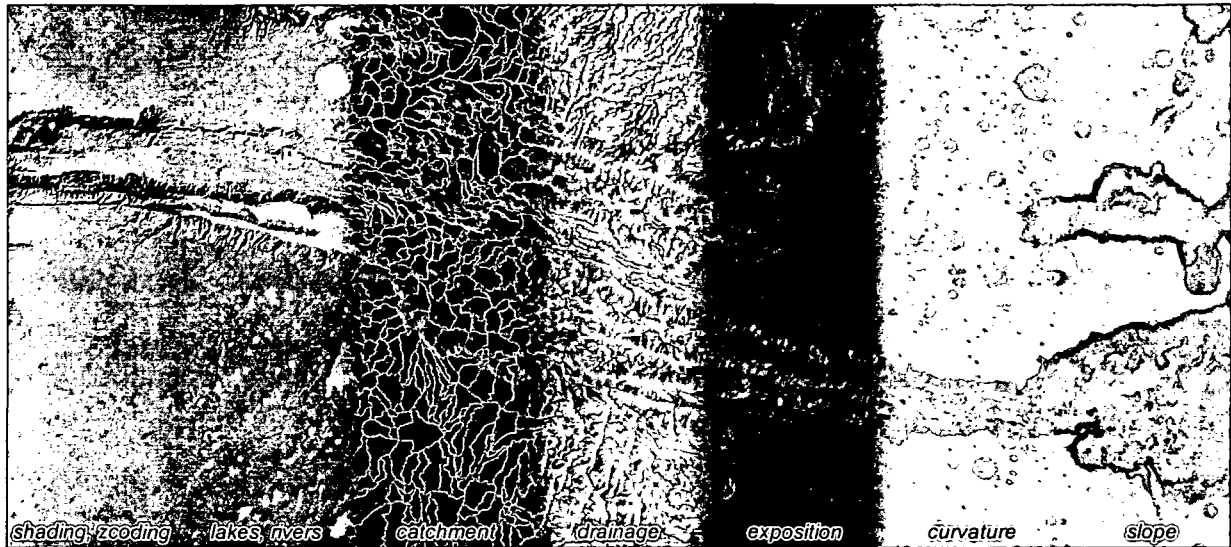


Fig. 6.1: Overview of raster-based analysis methods in the area of *Valles Marineris*. The given area is  $3,192,399 \text{ km}^2$ . The analysis was applied to a DTM with a grid width of  $1/64^\circ$  ( $1 \text{ km}$ ) per pixel in Simple Cylindrical projection.

The methods visualized in Fig. 6.1 can be classified in two groups:

Exposition, curvature and slope computation belong to *mathematical analysis* involving the neighbors of each pixel. They will not be further investigated hereafter, although curvature analysis is useful for estimating roughness values which are needed for finding the final threshold in the error elimination process automatically (as described in 5.2.2) or for setting an initial value for structure line detection (to be discussed in section 0).

On the contrary, methods for *hydrological analysis* were investigated extensively. At the first sight, it might seem that hydrological analysis cannot make much sense for studying the topography of a planet without any current surface water. Yet methods of that sort support the structural analysis of the surface and furthermore they presumably bear a high potential for answering questions concerning the existence of liquid surface water in the past. The following section discusses the methods as well as achieved results in detail.

Finally different methods for *3D visualization* of the results together with exemplary visualizations are presented.



## 6.1 Hydrological Analysis

The methods used for hydrological analysis were implemented as *systolic processes*, where the conditions of the cells in a rectangular grid array are derived synchronously by taking only their neighbors into consideration. The visualization of the results is prepared with the help of special *filtering operations*. The rain simulation, for instance, can be described as follows:

---

*Per definition, the same amount of water is brought onto each grid element of the given (impermeable) surface, thus simulating a permanent, homogeneous rainfall. Depending on the height of the neighborhood, the water drains in a certain direction; the steeper the area, the faster the drainage (only the full neighbors (4-environment) are considered). The amount of water is permitted to be split up to several neighbor cells. After having left the surface element, a new amount of water is brought in. These two steps are repeated until a condition of equilibrium is reached. During this process, rivers will emerge as soon as there is enough water available flowing from the adjacent slopes to the riverbed. These rivers start to make their way downwards following gravity (assuming orthometric heights). If a river flows into a local minimum, as it occurs, for instance, in a crater, it starts to flood this minimum, until its lowest border point (at the crater rim) is reached. The resulting flooded area defines a local minimum with no way out other than the outflow point. It can be interpreted as a lake. From then on, the river follows gravity again, until it reaches the border of the defined area of interest where the water flows out.*

---

This abstractly described behavior is realized in two steps: *Depression analysis* to find local minima and *drainage analysis* which represents the amount of water as a 2D array of values after reaching the condition of equilibrium. Hence, further analysis may be appended such as the derivation of river lines (Rieger 1992a).

For further scientific investigation, it is necessary to visualize the results. An overlay of rivers and lakes provides a realistic visualization of water behavior on an impermeable surface during permanent, homogeneous rainfall.

Understanding the history of water on Mars is important for two reasons:

- Water is essential for the evolution and existence of life as we know it from the Earth.
- Water is essential for future manned Mars missions.

The following sections provide exemplary results of the application of the described hydrological analysis to MOLA DTMs to different regions of Mars, which are very likely to have been formed by fluvial processes.

### 6.1.1 Hydrological Map of Tharsis Region and Valles Marineris

The three large shield volcanoes at the *Tharsis Highland* – *Arsia Mons*, *Pavonis Mons* and *Ascäus Mons* (from south to north) – arose along a tectonic break line. Together with the largest shield

volcano *Olympus Mons*, situated northwest of them, they are the largest and longest active volcanoes (billions of years) within our solar system (Heuseler et al., 1997, p. 110). The *Valles Marineris* are situated east of the *Tharsis Region*, just below the equator. Their longitudinal extension in east/west direction is about 4,000 km. Geographically they can be separated into three areas: The *Noctis Labyrinthus* in the West, the *central rims* and the beginning of the *drainage valleys* in the east (Heuseler et al., 1997, p. 90). The regions east of the *Valles Marineris* are characterized by so called *chaotic regions*. These areas are 2 – 5 km below the surrounding, undisturbed terrain and mostly covered with large jumbled blocks of material from the former surface. This indicates that the chaotic terrain have formed by collapse rather than by removal of material from the above, indicating the involvement of groundwater in the channel formation process. They merge westwards with the canyon system and northwards with outflow channels. However, particularly to the north of the *Valles Marineris*, channels tend to emanate from completely enclosed canyons containing chaotic terrain like *Echus*, *Hebes*, *Juventas* and *Ganges Chasma* (Jaumann et al. 2001, p. 91).

The most reliable hypothesis about the evolution of the large outflow channels, starting in these chaotic areas and draining into *Chryse Planitia* (a former 'ocean' northeast of *Valles Marineris*), are catastrophic releases of ground water or drainage of surface lakes. Several processes are discussed that may cause large floods on Mars. For instance, groundwater under high artesian pressure confined below a permafrost zone may break out, triggered by events, which disrupt the permafrost seal, such as impacts or Mars-quakes, either by breaking the surface or sending a large pressure pulse through the aquifer. The dimensions of the outflow channels indicate discharges in the order of  $10^7$ - $10^9$  m<sup>3</sup>s<sup>-1</sup> (Jaumann et al. 2001, p. 101, Carr 1996).

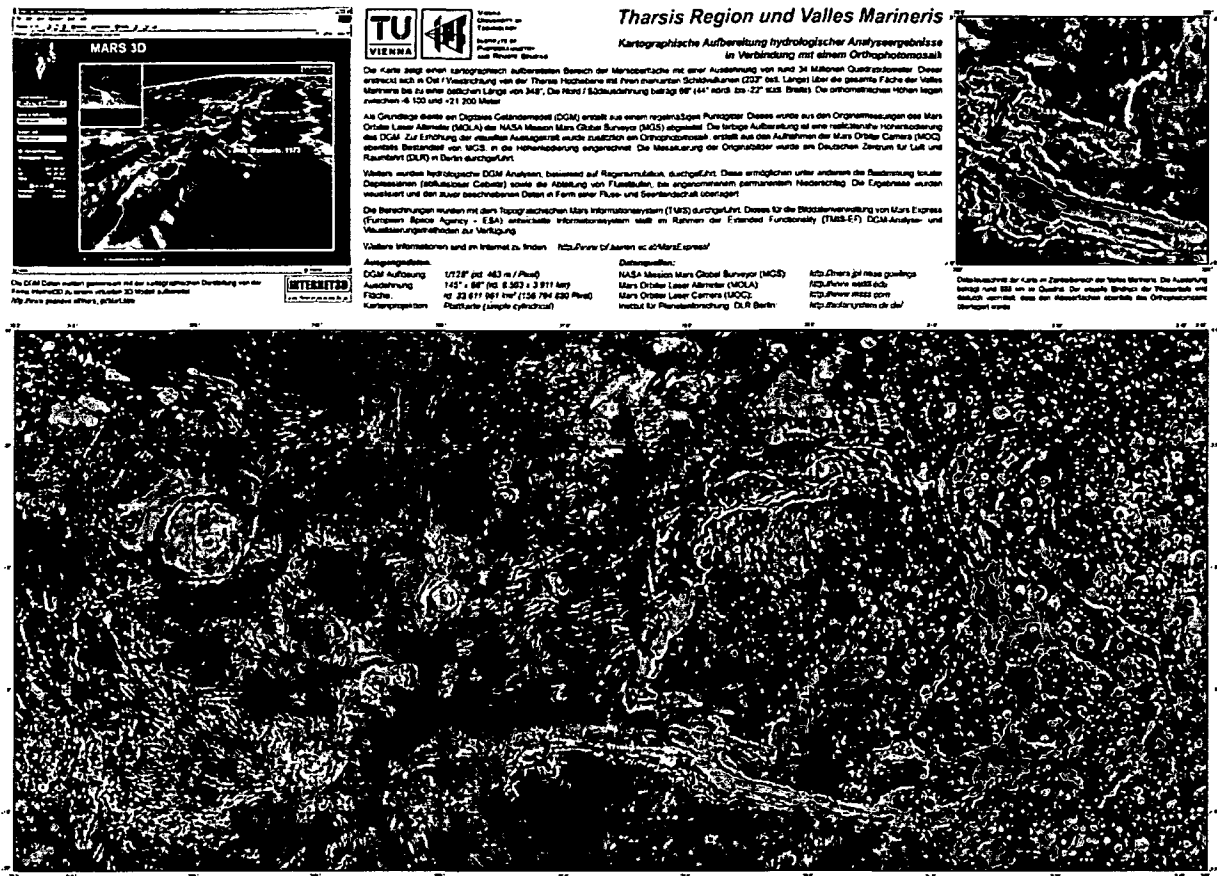


Fig. 6.2: A map projected visualization of hydrological analysis results applied to an area of about 34 Mio. km<sup>2</sup> containing the Tharsis Highlands and the Valles Marineris.

The map presented in Fig. 6.2 was derived from MGS data. It represents a cartographic preparation of the surface of Mars with an extension of about 34 mio. km<sup>2</sup> (~157 mio. regular grid points) in Simple Cylindrical map projection. It spans in east/west direction from the *Tharsis Highlands* (203° eastern longitude) covering the *Valles Marineris* to an eastern longitude of 348°, thus containing the previously described chaotic areas and the adjacent outflow channels into the *Chryse Region*. The extension in north/south direction is 66° (44° northern to -22° southern latitude). The height values given are orthometric and range from -6,100 m to +21,200 m.

The map is based on a DTM derived from the regular MOLA point grid at a resolution of 1/128° (463 m/pix at the equator). The color information is a height-coding of the DTM. The colors used try to represent the real surface color in a way representing lower areas with darker colors and higher areas with brighter colors. In order to improve the expressiveness of the map, an orthophoto mosaic was superimposed on the map representing the albedo information of the surface (section 5.1.1).

The blue colored areas of the map are results of hydrological analysis, applied to a DTM with a resolution of 1/32° (1852 m/pixel). The blue patchy features are local minima resulting from depression analysis. Depressions are local areas which are surrounded by an embankment representing a barrier for the outflowing water. Therefore, the water level will increase until a local minimum of the embankment, the outflow point, is reached. Per definition, the border of the analyzed area enables the water to flow off. As the analyzed area was larger than the presented map, local depressions at the

border of the map are filled. In order to represent the topographic structure of the bottom of the lakes, the albedo map was superimposed on the depression regions in combination with the blue layer. It has to be mentioned, that this result cannot be achieved by a height-coding so far. Each local depression is detected individually and has an individual sea level, dependent on the orthometric height of its outflow point.

The blue, linear features are the result of river line detection based on drainage analysis. The width of the derived rivers is determined by the raster width of the data, i.e. 1,852 m in this example. The value is applied to the whole course of the river, independent of a possibly increasing amount of water along the river-flow.

### 6.1.2 Outflow Channel Detection in the Elysium Region

Most channels on Mars are denoted as outflow channels, even though their occurrence, origin and geological context differ from area to area. By far the largest channels occur around the *Chryse Basin* which covers the eastern part of the map shown in Fig. 6.2.

*Elysium Planitia* is the second largest volcanic region on Mars. It is located on a broad dome that is 1,700 by 2,400 kilometer in size. Several assumptions on the origin of the large outflow channels from the *Cerberus Plain*, located south of the *Elysium Volcanoes* and draining in northeast direction into *Amazonis Planitia*, exist, which differ in some manner. But they all have in common, that the channel forming processes, which characterize the morphology of this region, are the result of volcanic activity followed by water flow. For example, MOC provided images which show pseudo-craters. These morphological structures emerge from explosions due to the interaction of molten lava with a water-rich surface. Possible Martian pseudo-craters are of interest because they mark the locations of shallow water or ice at the time the lava was emplaced (Fuller and Head, 2001).

Images from the MOC instrument show relatively young lava flows in the *Marte Vallis* region. These flows were estimated to be 10 million years old (Hartmann and Berman, 2000), possibly making them the most recent volcanic activity on the planet, and suggesting a more recent volcanically active Mars than earlier believed (Garvin et al., 2000). Scott and Tanaka (1986) associated the appearance of *Marte Vallis*, located between 170° – 190° eastern longitude and 0° – 20° latitude, as a region, characterized primarily by channels of possible fluvial origin. Later volcanic activity, in the form of flood basalts and long lava flows, utilized these channels to transport lava for distances as great as five hundred kilometers or more (Plescia, 1990) on slopes <0,01° (Gregg and Sakimoto, 2000).

It should be emphasized again that the results of this thesis are not aimed at giving distinct answers to geologic or hydrologic processes which formed the surface of the Mars in former times. This work is rather intended to support research by geologists and hydrologists by providing an highly accurate geometric foundation for finding solutions to open questions. It turned out, that the river line detection, as described in the introduction to this section, is not an appropriate method to detect former outflow channels in their whole extend, as those structures on Mars are rather broad and cannot be represented by linear features.

Depression analysis of the area south of the *Elysium Planitia* containing the *Cerberus Plain* and the *Marte Vallis*, delivers numerous small, direction dependent local depressions. Fig. 6.3 shows a shaded relief of this area with an extension of about  $35^\circ$  by  $24^\circ$ . The light blue areas represent the result of the depression analysis. A morphological closing (i.e. a sequence of blowing and shrinking) combines adjacent depressions to continuous areas. The large continuous river area in *Marte Vallis* is superimposed in dark blue. Morphologic features with a high degree of similarity to Earth-like fluvial topography with meanders, islands and well defined river banks can be recognized. The presented results were achieved by analyzing a grid-based DTM of this area derived from MOLA grid data at a resolution of  $1/64^\circ$  (926 m) per pixel.

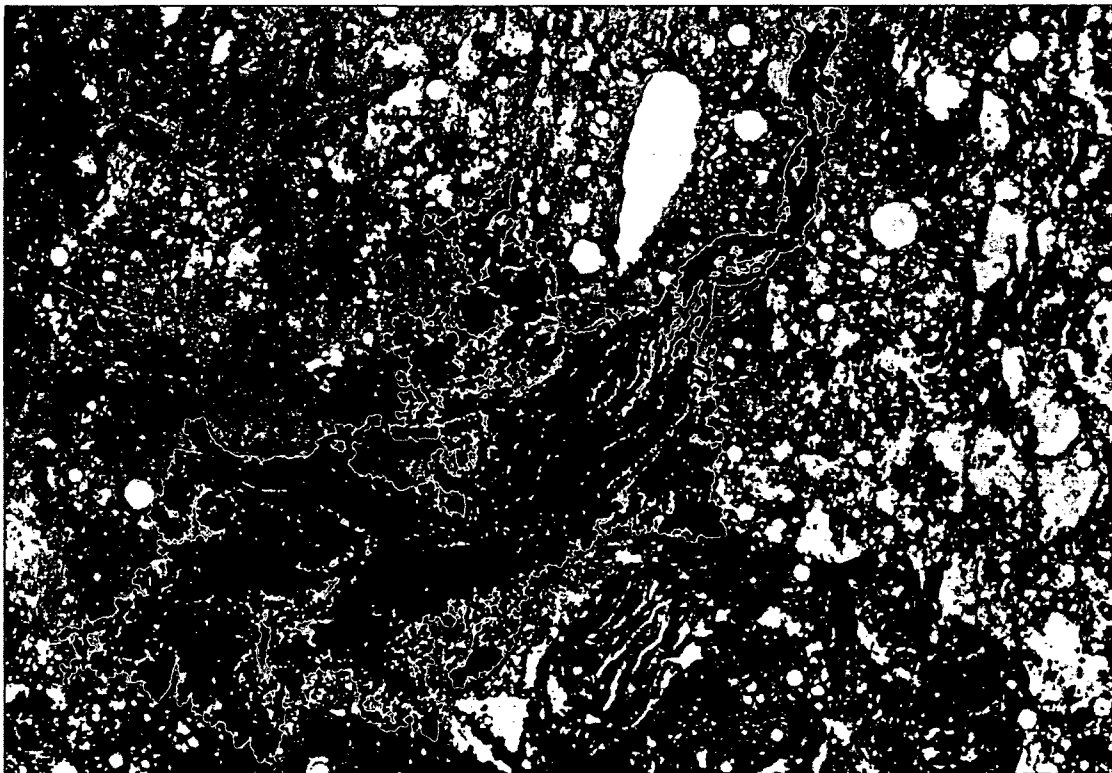


Fig. 6.3: Shaded relief derived from the MOLA grid DTM data representing the area of *Cerberus Plain* and *Marte Vallis*. The light blue areas represent the result of a depression analysis. The dark blue area has been obtained by joining adjacent depressions with the help of a pixel-based closing operation.

Fig. 6.4 to Fig. 6.7 show the *Marte Vallis* region at a higher resolution. The different steps of the semi-automatic boundary extraction of the fluvial area are the following:

- *depression analysis* (Fig. 6.4);
- *morphological blowing* to combine the numerous, adjacent depressions;
- *morphological shrinking* to derive the original outer extend of the river (Fig. 6.5);
- *selection of the continuous river area of Marte Vallis*
- *boundary extraction* (Fig. 6.6).



Fig. 6.4: Result of depression analysis of a DTM of Marte Vallis. The numerous adjacent depressions make the river-like topography visible.



Fig. 6.5: Continuous river area of Marte Vallis.



Fig. 6.6: The extracted boundary derived of the continuous river area (Fig. 6.5).



Fig. 6.7: Color-coding of a simulated river surface level, 15 m above the bottom of the valley.

Since the real topography of the *Marte Vallis* area is supposed to have a continuous decreasing height in flow direction from Cerberus Plain to Amazonis Planitia, the cause of the occurring depressions has

to be further investigated. Fig. 6.8 shows a 600 km long height profile along Marte Vallis. A continuously decreasing height can be observed, as expected.

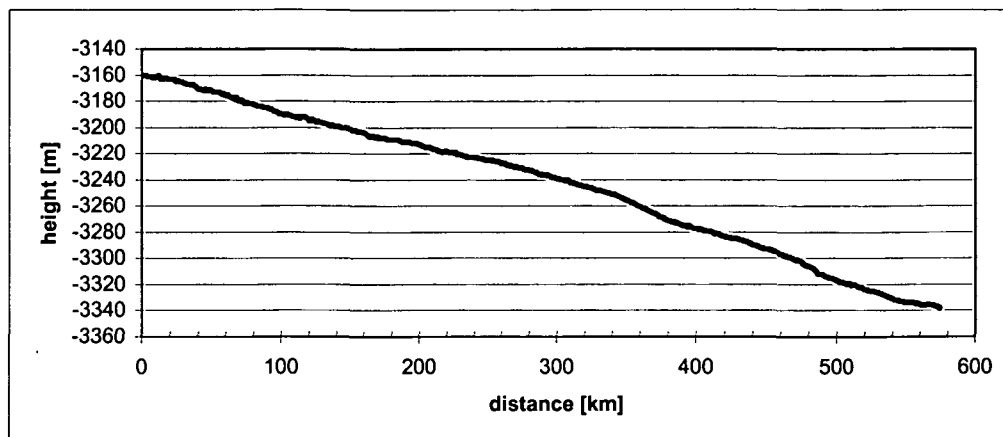


Fig. 6.8: Profile of Marte Vallis measured in flow direction. A continuously decreasing height can be observed.

The MOLA grid dataset is available as binary data using integer numbers to represent the height values. Thus, all height values are rounded to meter precision. Compared to the accuracy of the measurement, which is about 10 m (Tab. 5.1), and considering the data sampling size of about 130 m (surface spot size), a height resolution of 1 meter for the DTM grid seems to be appropriate. As shown in Fig. 6.8, the mean gradient of Marte Vallis is about 0.03 % ( $\Delta H = 180$  m,  $D = 600$  km) leading to a mean height difference of 0.14 meter per DTM grid cell of 463 meter. Therefore, the heights of about 7 grid cells are rounded to the same value, resulting in a terraced surface model as shown in Fig. 6.9 by the black line. The gray line represents an estimation of the real topography derived by smoothing the terraces.

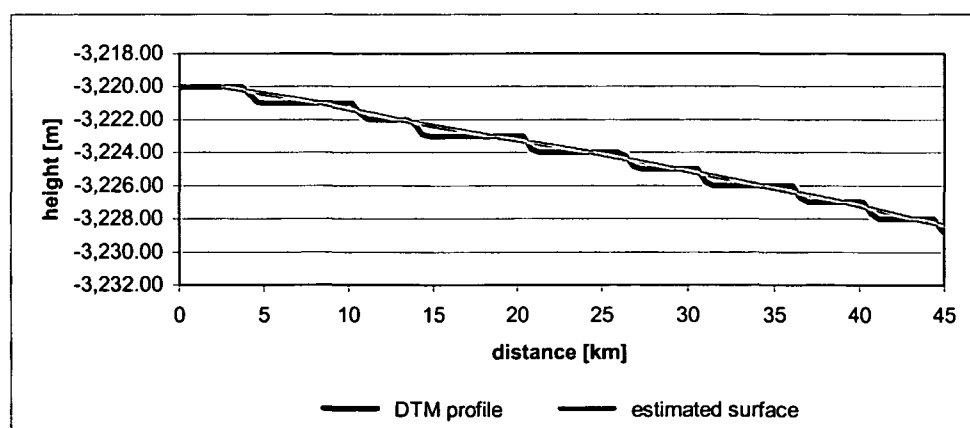


Fig. 6.9: Profile in the area of Marte Vallis measured in flow direction at a length of 45 km.

This effect is responsible for the artifacts after the depression analysis. The algorithm can detect two different types of pits: Those occurring in the real topography and represented by the DTM, and those introduced by data acquisition and modeling, therefore named spurious pits (Rieger, 1992a, p. 16). As for the algorithm the origin of the topographic features is irrelevant, all depressions are treated equally. From a geomorphologic point of view, spurious pits should not occur within a DTM and therefore they

should be avoided by appropriate data acquisition or, if not avoidable, at least eliminated during the DTM generation process. Nevertheless, in this special case, this systematic, geomorphological incorrectness allows to determine the river-like topography of *Cerberus Plain* and *Marte Vallis*! The numerous adjacent depressions are spurious pits resulting from the terrace effect. The small bands, separating the distinct depressions, are representing the height steps from one terrace to the next. Therefore, this algorithm will only be successful for this kind of river detection, as long as the topography is not too steep, because such spurious pits only do occur if the terrace effect occurs.

Fig. 6.7 shows the prediction of a geometrically defined river surface level, 15 meter above the bottom of the valley. A detailed description of the method used is given in the following section.

### 6.1.3 Simulated Outflow Behavior in *Ma'adim Vallis* and *Gusev Crater*

*Ma'adim Vallis* and *Gusev Crater*, are regions which are very likely formed by fluvial surface water (Jaumann et al., 2001, p. 101). This makes hydrological analysis reasonable. The results presented in the following are not interpreted from a geological point of view so far. It is again an approach of using hydrological analysis in order to derive geometrically defined simulations for further scientific interpretation.

*Ma'adim Vallis* is one of the largest valley networks on Mars, stretching 950 km in length and up to 25 km in width. Multiple episodes of flows were envisioned to explain the terraced topography of the valley (Schneeberger, 1989). In the early history of the planet, the valley was dammed due to the formation of *Gusev Crater* which has a diameter of 150 km and a maximum depth of 1600 m. *Gusev* became popular, as the *Mars Exploration Rover (MER)*, which was launched in July 2003, landed there successfully on 4<sup>th</sup> of January 2004 (Grant et al., 2004, pp. 11 – 22).

The following results were achieved by the combination of two different hydrological analysis methods. The approach tries to derive a reasonable water surface of a flooded *Ma'adim Vallis* from its origin down to the *Gusev Crater*. The water level within the crater is defined by the absolute height of the outflow channels situated in the northwestern part of the crater's rim, thus defining the outflow points of a depression. Therefore the water surface level can be found by depression analysis as described in section 6.1. The water level of *Ma'adim Vallis* was defined geometrically just by increasing the amount of water with the distance from the river's origin and by taking into consideration possible tributary rivers.



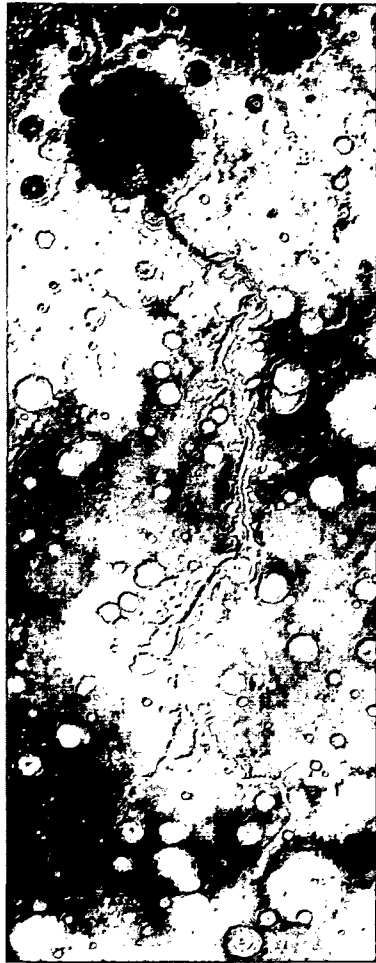


Fig. 6.10: Height-coding combined with a shaded relief of the Ma'adim Vallis and Gusev Crater region. The southern part of Ma'adim is characterized by a network of tributary rivers.



Fig. 6.11: Definition of the height of the predicted river surface level. The blue line following Ma'adim Vallis and crossing Gusev defines the axis of the river. Twelve cross profiles were defined. The gray band represents the positions of densification points derived from the cross profiles.

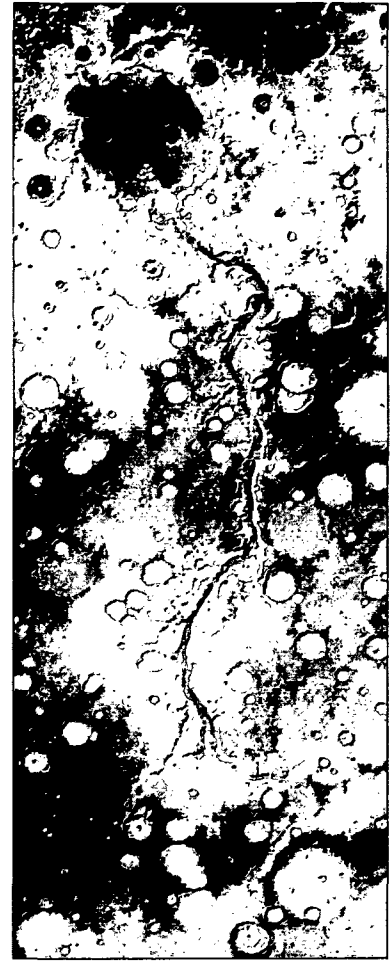


Fig. 6.12: Color coded visualization of the simulated water depth in Ma'adim Vallis, Gusev Crater and after the outflow northwards into the Aeolis region.

Fig. 6.10 shows the region of Ma'adim Vallis and the Gusev Crater as a combination of a height-coding of a DTM and a shaded relief. The image was derived from the MOLA grid dataset at a resolution of  $1/128^\circ$  (463 m) per pixel. The extension of the analyzed region is  $7^\circ$  by  $18^\circ$  (896 x 2304 pixel). The height values range from  $-2,881$  m (dark green) to  $2,913$  m (dark brown). The absolute zero level is represented in yellow.

The following list describes the steps which were applied in order to define a probable water surface within the valley region and the crater:

1. definition of an axis profile along the main valley of Ma'adim Vallis and crossing Gusev Crater (length: 1,170 km);
2. computation of cross profiles in normal direction to the axis in a distance of 117 km;
3. detection of the lowest point of each cross profile, representing the bottom of the valley profile;

4. adding a height difference representing the amount of water available at those levels and assigning these heights to the points defining the cross profiles;
5. densification of the cross profiles to define a continuous surface between the profiles;
6. intersection of the water level surface and the original DTM;
7. color-coding of the difference model according to water depth (0 m = cyan; -1,416 m = dark blue).

Fig. 6.11 shows the defined axis profile along the valley (step 1) and the cross profiles (step 2; numbered from 1 to 12) as blue lines. One additional profile (11) was defined in order to derive a continuously plain water surface within the *Gusev Crater*. The height difference representing the available amount of water was defined in different ways according to their location. As already mentioned, this definition was done geometrically without considering any hydrological models. At profile 1, an absolute water depth of 200 m was defined increasing by 20 % from profile to profile down to profile 6 resulting in an absolute water depth of 498 m at this profile. As no more important inflows exist from profile 6 to profile 8, the amount of water was considered to be constant (498 m). The following profiles 9 to 11 are defining the water level inside the *Gusev Crater*. The absolute height of this level is considered to be constant 200 m above the level of the three outflow channels in the northwest region of the crater (-1,400 m). The gray band between the cross profiles represents the coverage of the surface defined by the densification points as derived by step 5. Below the *Gusev Crater*, at profile 12, the amount of water is about 600 m above the mean height of this cross profile.

The axis profile (gray line) and the geometrically defined water level (black line) derived from 12 discrete values are shown in Fig. 6.13.

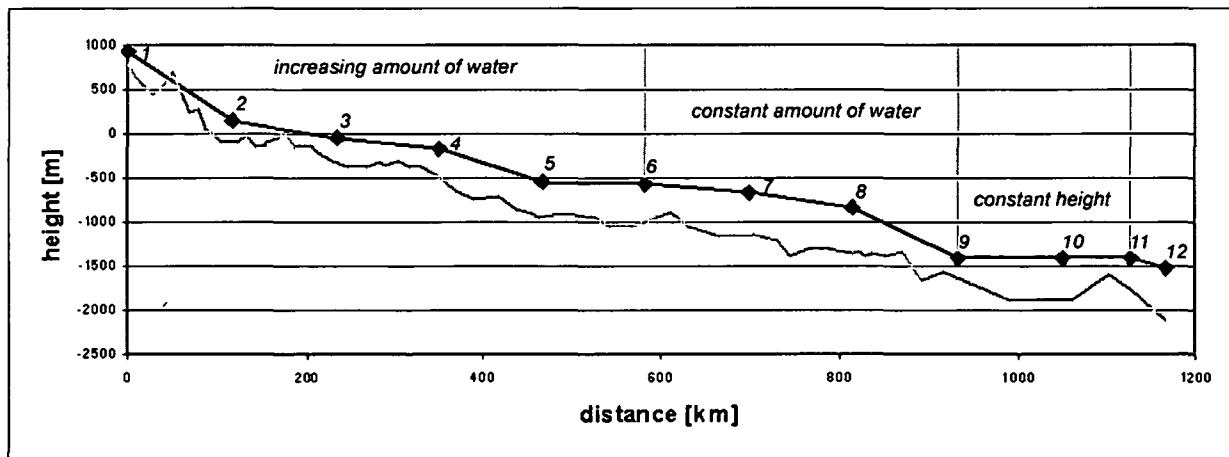


Fig. 6.13: Axis profile of Ma'adim Vallis (gray line) and geometrically defined water level (black line) defined by 12 discrete values simulating an increasing amount of water in the upper regions, a constant amount in the regions without inflow and a constant river surface level in *Gusev Crater*, defined by the height of its outflow channels into the Aeolis region.

Fig. 6.14 to Fig. 6.17 show four cross profiles as they were used to derive the absolute height of the water surface. The depth of the valley changes in flow direction increasing from about 200 m at profile 1 to more than 1,500 m at profile 7. The black lines represent profiles measured within the MOLA grid DTM. The x-axes are labeled in meter (30 km each) and they are located in normal direction to the axis of the valley. 30 points define a profile. The gray horizontal lines define the water levels,

estimated in constant heights above the lowest points of each profile. The height differences were defined geometrically, according to the rules described above<sup>7</sup>.

After defining the water levels of the distinct profiles, *morphological methods* were used to derive points defining the water surface between the profiles. These methods were originally developed to model a riverbed described by several cross profiles, measured, for example, by echo sounding (Mandlburger, 2000). In our case, the riverbed itself did not need to be modeled, as it is already defined by the MOLA grid DTM. But those methods were applied to the previously defined profiles describing the water level. Finally, a regular, grid-based DTM was derived from those points, and an intersection of this water model with the surrounding Mars surface DTM was performed. This difference model represents the water body. The zero level corresponds with the river surface level; regions with negative heights represent watered areas; positive heights represent areas, where the surface of the Mars is above the defined water level. A color-coding of the negative values, e.g. ranging from 0 m (cyan) to -1,416 m (dark blue), allows to derive a visualization of the water body representing the water depth using the color-coding. Such a visualization of the whole area is given in Fig. 6.12. The shaded relief representing the riverbed topography was superimposed to the color-coding.

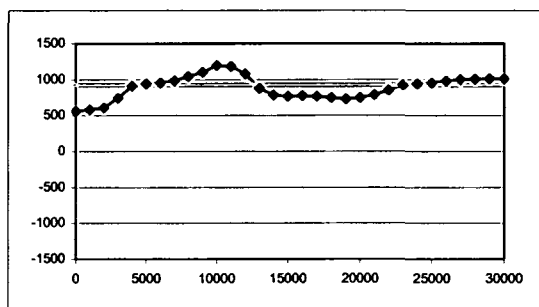


Fig. 6.14: Cross profile 1 (30 points) derived from the MOLA grid DTM (black line). The gray line defines the water level.

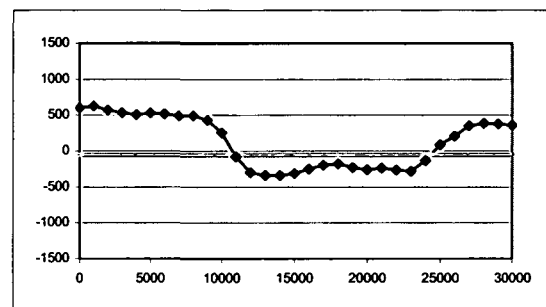


Fig. 6.15: Cross profile 3 and water level.

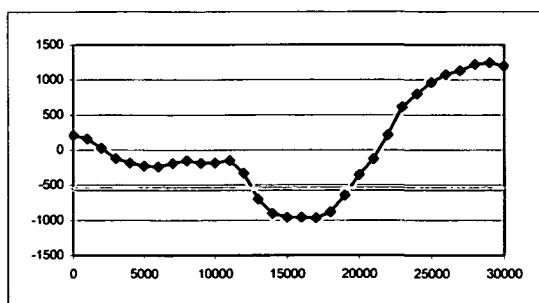


Fig. 6.16: Cross profile 5 showing an asymmetric behavior caused by an impact crater.

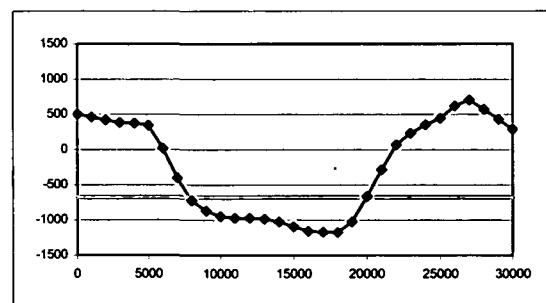


Fig. 6.17: Cross profile 7 and water level.

<sup>7</sup> The method would allow to consider any kind of hydrological model to determine the height differences. For example, Cabrol and Grin (1998) define a model for discharge rate computation in Ma'adim Vallis which might improve the quality of the water surface model.

## 6.2 Deriving Structure Lines from Point Clouds

Laser scanning instruments such as MOLA acquire the topography of an area by sampling many surface points by single point measurement. Therefore, the modeling accuracy of the surface structure can only be influenced by the point density: The higher the point density, the more details can be determined. Since the methods subsequently used for mathematical modeling aim at deriving a homogeneous surface, a smoothing of the modeled topography must be expected. In other words: Even a very high point density is not able to model non-continuous surface structures. Those structures will be smoothed in any case.

To improve the model (DTM) derived directly from the original points, it seems to be important, or even crucial, to detect such non-continuous structures and subsequently model them in an appropriate way together with the derived grid points. Adequate software applications are required for managing and processing of such so-called hybrid DTM structures as well as suitable data formats (section 3.3.5). In the following, a short introduction into the application of the previously described hydrological analysis methods to derive structure lines from point clouds is given. A detailed description and examples presents Dorninger (2004).

River lines, as defined in section 6.1, are likely to occur along linear discontinuities of a topographic surface. Thus, rivers determined from a given point grid can be used to detect possibly structure lines. Fig. 6.18 and Fig. 6.19 show the capability of this method as applied to a DTM of an alpine area in Austria. The left image shows a shaded relief of a DTM derived from a point grid (grid width: 50 m). The right image shows the DTM improved by structure lines, which were derived using hydrological river line detection and subsequently included into the DTM structure.



Fig. 6.18: Shaded relief of a DTM derived from a point grid.



Fig. 6.19: Improved DTM structure by the integration of automatically derived structure lines.

The river-line detection is based on a drainage analysis, which estimates the amount of water in every grid cell of the analyzed DTM (section 6.1). Rivers are defined to occur if the amount of water is big enough. Watersheds are defined by linear structures from which the water flows off. Therefore those lines can be used to derive structure lines as well. Watersheds and rivers are likely to occur at local

maxima and minima of the surface, respectively. Fig. 6.20 and Fig. 6.21 show the result of structure line detection as applied to a second order derivative model (curvature), which enable the detection of line features with significant linear curvature anomalies.

The planimetry (x, y coordinates) of the river-lines is determined by a raster-vector conversion of the drainage analysis. The heights are derived from the original model by interpolation. In order to improve the accuracy of these heights, other methods, probably using those edges as initial values, might be applied. Briese et al. (2002b) describe a method based on the computation of discrete approximation planes on both sides of such an initial edge and their subsequent intersection for an exact modeling of the terrain edge.

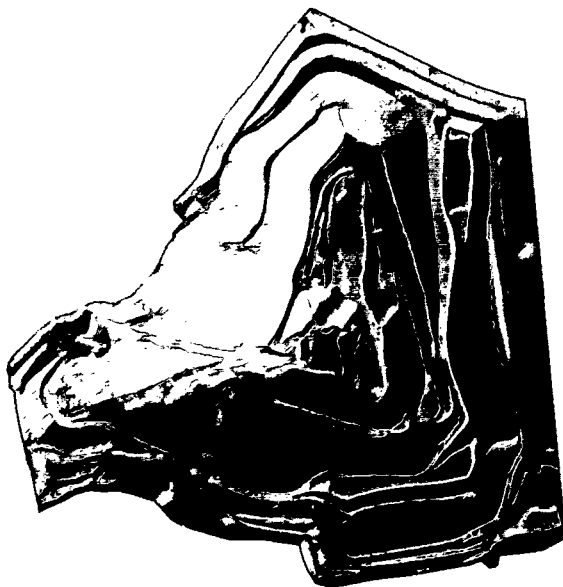


Fig. 6.20: Shaded relief of a DTM with many structure lines, not occurring on local minimum or maximum edges.

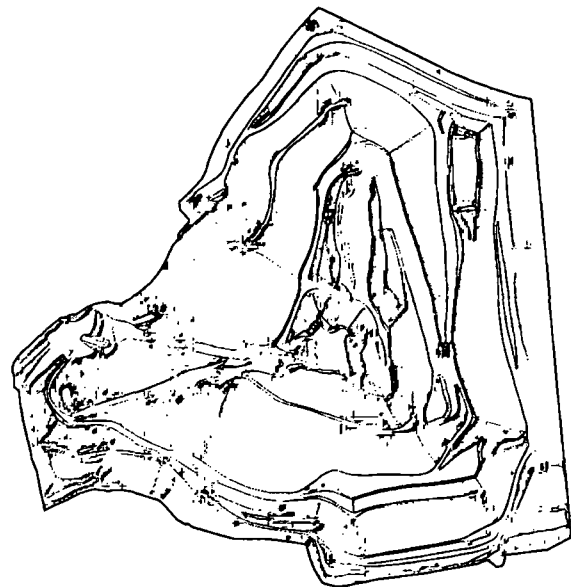


Fig. 6.21: Edges derived from the model of Fig. 6.20. The edges where detected in a second order derivative model (curvature).

All presented results were derived from Earth datasets. These methods have not been applied to Mars DTMs so far, because the currently available topographic datasets from Mars (HRSC and MOLA) still lack homogeneity. As the Mars surface is rougher than those of the Earth, many occurring local minima and maxima, prevent long, continuous rivers to emerge. Most of these disturbing structures seem to be artifacts, caused by the data acquisition. Therefore, they represent spurious pits as described in section 6.1.3. Thus, a detailed pre-processing in order to eliminate those artifacts is essential and will be subject of further investigation.

### 6.3 Visualizations

Attractive presentations of results on modern media like Internet, require adequate visualizations. Especially perspective views as well as 3D models are well suited for that purpose. Required are a DTM, which describes the topography, and a geo-referenced raster overlay for texture mapping. The raster overlay can be a visualization of hydrological analysis (section 6.1), a digital ortho-image, for example a MOC or HRSC image, or any other available raster-based representation of the area

described by the DTM. The combination of different data sources, e.g. MOC and MOLA, may augment the perceivable information content of the visualization. A map projected visualization as shown in Fig. 6.2 provides a high quality instrument for further investigation and analysis. But common maps are 2D visualizations of a 3D reality. In the HRSC project group, Buchroithner and Waelder (2004, pp. 409 – 411) are investigating the generation of 3D hardcopy maps based on lenticular techniques, in order try to overcome those shortcomings.

The following sections present perspective view visualizations and virtual 3D models of MOC and MOLA data.

### 6.3.1 Perspective Views

Parallel-projection perspective views can be used for static 2D presentations of topographic data in combination with raster based texture overlays. Fig. 6.22 shows a 5° by 5° area of *Valles Marineris* as a perspective view. The DTM was derived from original MOLA points with a grid width of 500 m applying the error detection and elimination method described in section 5.2. The height is exaggerated by a factor of 5. The raster image overlay is a combination of a height-coding, derived from the DTM, lakes and rivers, predicted using hydrological analysis (section 6.1) and a high-resolution MOC image mosaic (section 6.1.1).

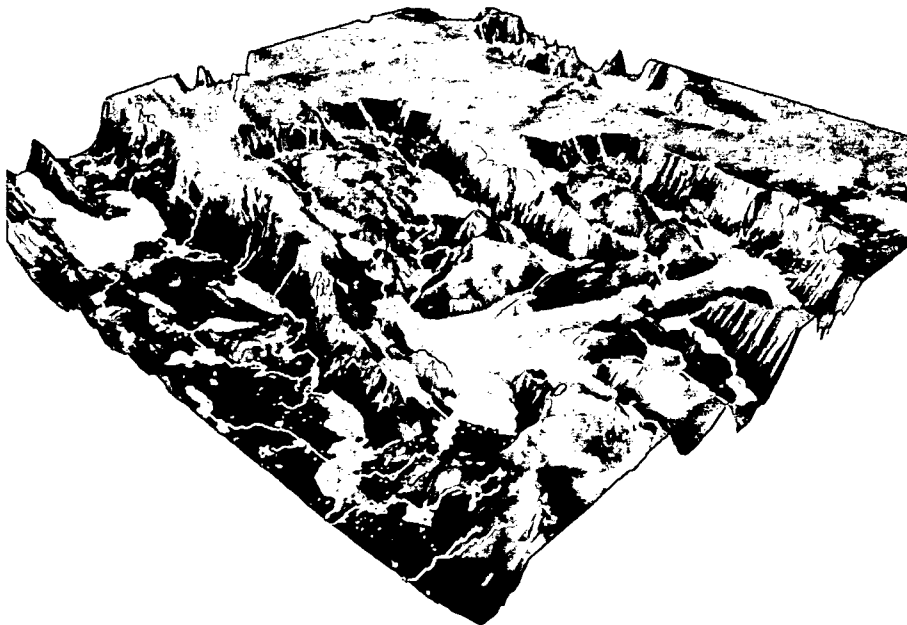


Fig. 6.22: Perspective view of the area of *Valles Marineris* (5° by 5°). The DTM was derived from original MOLA points using the described error elimination method. The raster image overlay is a combination of height-coding, lakes and rivers predicted using hydrological analysis and a MOC mosaic map. The DTM is exaggerated by a factor of 5.

The application of appropriate viewpoint parameters enables to generate 360° panorama views as shown in Fig. 6.23. The visualization shows the same region as Fig. 6.22 with different raster overlays. The overlay of the upper left image consists of a combination of the MOC ortho-image map and a height-coding; the lower left images shows the results of depression analysis and river line detection

additionally. The right image, which has similar viewpoint parameters as Fig. 6.22, additionally shows named Mars features of the region superimposed on it. They were requested by the Gazetteer of Planetary Nomenclature, United States Geological Survey (USGS-NAMES, 2004).

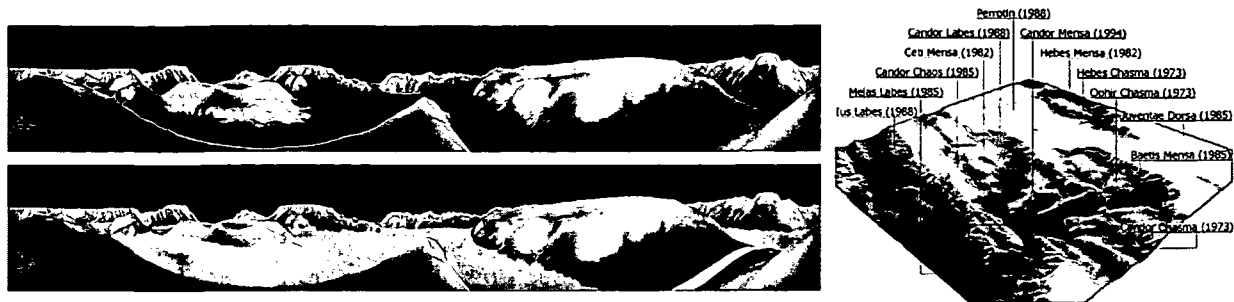


Fig. 6.23: 360° panorama views in the area of Valles Marineris showing the same region as Fig. 6.22. The texture overlay of the upper left visualization is a combination of a height-coding and a MOC images mosaic. The lower left visualization shows the same area with predicted lakes and rivers in addition. The perspective view on the right covers the same area with the nomenclature of named Mars features superimposed on it.

### 6.3.2 Virtual 3D Modeling

The visualizations as presented above are all static without the capability of animation or interactivity. The *Virtual Reality Modeling Language (VRML)* enables interactive 3D visualization of terrain models using raster image overlays as texture. Since its standardization in 1997, VRML has become a standard format for describing interactive virtual 3D models on the World Wide Web. A VRML model can be derived from a given DTM and the corresponding raster image overlay. Using, for example, an internet browser with the appropriate plug-in, it is possible to carry out virtual flights over VRML models. Unfortunately, the capability to display such models has not been integrated into standard web browsers yet. Thus, the web user is forced to install a non standardized add-on, mostly developed by a third-party-vendor. This results in several shortcomings such as lack of performance or interface shortcomings resulting in different visualizations of the same model.

*Extensible 3D (X3D)* is a software standard for defining interactive web- and broadcast-based 3D content integrated with multimedia. The final working draft specification was presented in July 2002 by the Web3D consortium (Web3D-X3D, 2004). X3D is intended for use on a variety of hardware devices and in a broad range of application areas such as engineering and scientific visualization, multimedia presentations, entertainment and educational titles, web pages and shared virtual worlds. X3D is also intended to be a universal interchange format for integrated 3D graphics and multimedia. X3D is the successor to the VRML, the original ISO standard for web-based 3D graphics (ISO/IEC 14772). X3D improves upon VRML with new features, advanced application programmer interfaces, additional data encoding formats, stricter conformance, and a componentized architecture that allows for a modular approach to supporting the standard (Web3D-XML, 2004). X3D supports full separation of data and visualization. Therefore, the data is fully independent of its final visualization format. X3D is also compliant to the Extensible Stylesheet Language-transformations (XSLT), which enables the definition of transformation rules from an XML format into other formats. So it may be easily converted into

formats like VRML, Scalable Vector Graphics (SVG) or Adobe Portable Document Format (PDF) using given XSLT definitions.

However X3D as well as other XML-based standards are widely accepted by industrial vendors which support import interfaces to those formats, a pressing need for suitable data management solutions has become apparent (Nebiker, 2003). Beck (1999, 2003) describes the implementation of such a system and tries to estimate the effort for such a realization.

DILAS<sup>TM</sup> (Digital Landscape Server) is a 3D GIS platform for the integrated management of regional to national 3D landscape and city models and for the generation of web-based geo-information services. DILAS<sup>TM</sup> is a commercial product line of GEONOVA AG (GEONOVA, 2004) (Nebiker, 2003). Fig. 6.24 shows the central part of *Valles Marineris* prepared by the commercial vendor INTERNET3D (Polly-Pazourek-Burtscher GesnB, Neunkirchen, Austria) using DILAS. The same DTM and raster data as used to generate the hydrological map of Fig. 6.2 was prepared with DILAS Modeler which is part of the DILAS system.

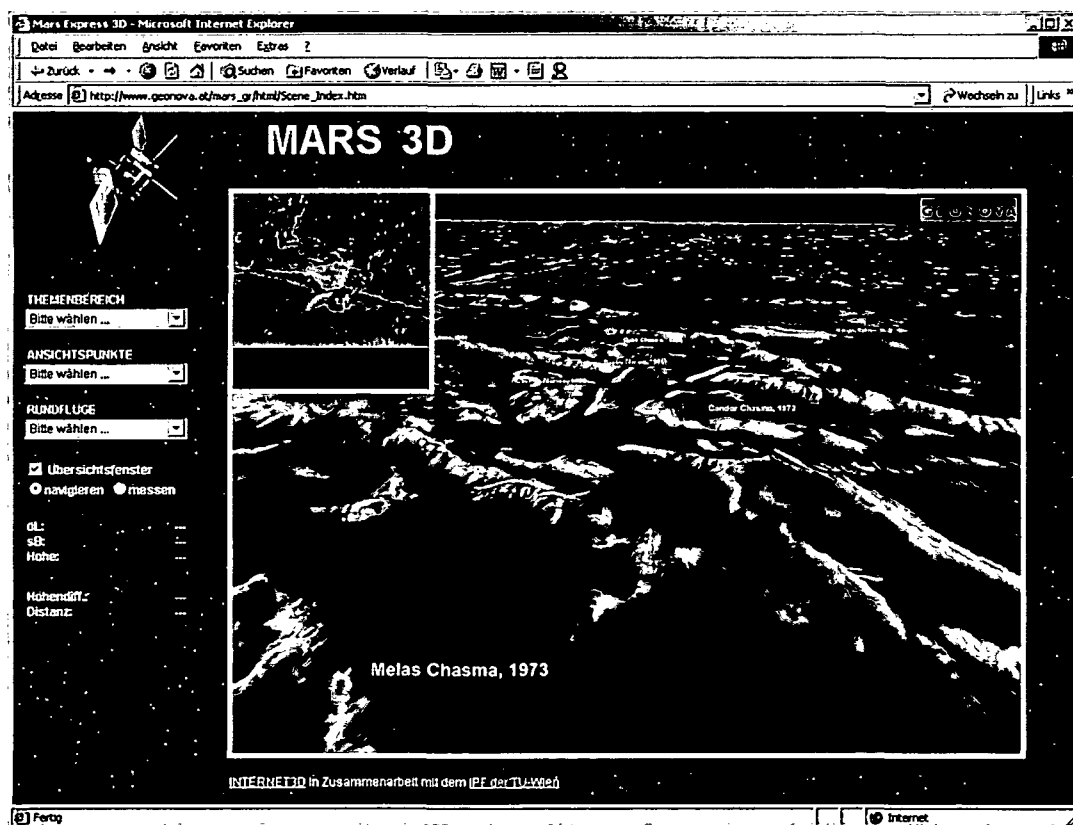


Fig. 6.24: The central part of *Valles Marineris* rendered by the G-Vista plug-in. The resolution of the prepared raster image overlay is  $1/64^\circ$  (926 m). The DTM resolution is  $1/32^\circ$  (1,852 m).

The model is available online (GEONOVA, 2004). The 3D-visualisation software G-VISTA, which is available as plug-in for standard browsers (currently MS Internet Explorer and Netscape are supported), is used to render 3D scenes prepared by DILAS. Apart from common navigation functionality, G-VISTA supports a measurement tool, thus providing a simple form of interactive analysis. The Mars model can be visualized using two raster overlays: The one shown in Fig. 6.24 consisting of the MOC image map and a height-coding, and another one with extracted river lines and



results of depression analysis superimposed on it. The model was presented at the Intergeo 2003 in Hamburg, Germany.

### 6.3.3 3D Hardcopy of Olympus Mons

The above described methods were applied to derive virtual 3D models. An appropriate virtual reality environment is necessary to visualize such models, for instance, on a monitor. This finally described task aims to create a three-dimensional hardcopy of the caldera region of *Olympus Mons*.

The output device used was a Dimension 3D plotter (DIMENSION, 2004). This plotter generates 3D plastics hardcopies of any three-dimensional digital model. The plastics used for modeling is melted and brought onto a platform slice by slice. Every slice has a thickness of 0.25 mm. The digital input model has to be a closed (water proof) surface provided in Stereo Lithography (STL) format. STL describes a surface by the means of triangulation. The closed model of *Olympus Mons* consisted of a bottom plain, the topographical model and four vertical plains connecting the topographic surface with the bottom.

The topography was derived from HRSC stereo images by the DLR applying feature-based image matching. The regular grid DTM describing the caldera region had an extension of 100 km by 80 km. The maximum workspace of the plotter is 20 cm by 20 cm by 30 cm (height). The model grid width was assigned to 0.25 mm, according to the height resolution of the plotter (thickness of the individual slices). Thus, the hardcopy had a planimetric extension of 20 cm by 16 cm representing a scale of 1:500,000. The height values were exaggerated by a factor of 5, resulting in an absolute model height of about 6 cm.

First attempts to derive a triangulation from the grid-based DTM were made using the software package *Geomagic Studio* by *Raindrop Geomagic* (GEOMAGIC, 2004). This software provides two different implementations of a full 3D triangulation algorithm. They are named *Surface* and *Volume*. Unfortunately, the *Surface* method showed a direction dependent behavior, as the triangulation was not performed properly in almost vertical areas. Fig. 6.25 shows a quarter of the caldera to be modeled with missing triangulation surfaces at the steep rim of the crater.

The second implementation, *Volume*, seemed to be more appropriate to model the given body in a correct way. First attempts on a simplified model were promising. But as applied to the full detailed object, the used machine was not able to perform the computation (528 MB RAM).

Therefore a simple 2D triangulation was implemented, thus deriving the edges of the triangles from a regular planimetric grid. The height values of the given points were assigned to the nodes of the triangles afterwards, and the result was converted to STL format. This simple triangulation was only possible because of the 2.5D behavior of the given dataset. A rendered visualization of this object is shown in Fig. 6.26. The plotting process lasted about 16 hours.

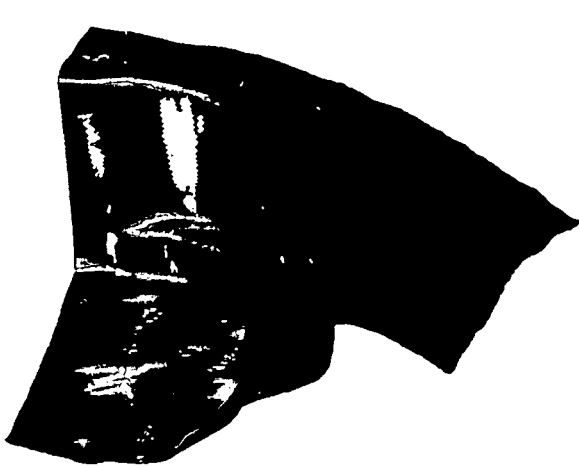


*Fig. 6.25: Incorrectly triangulated model derived from a given grid-based DTM using Raindrop Geomagic Studio (Surface).*

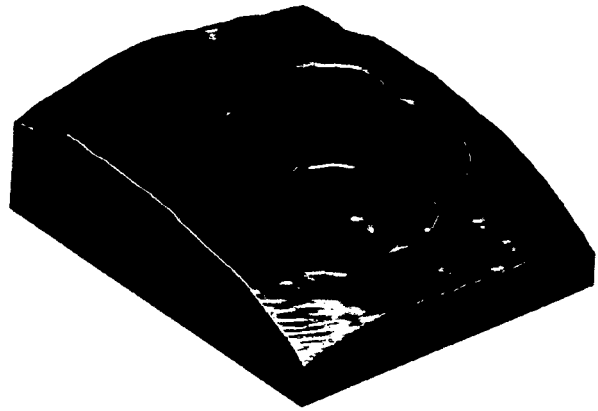


*Fig. 6.26: Correct triangulation of the whole body. The triangulation of the DTM surface was performed applying a 2D triangulation to the regular grid.*

Fig. 6.27 shows a photograph of the hardcopy. The extends of the model are 20 cm by 16 cm by ~6 cm. The terrace effect (Fig. 6.28) is caused by the plotter's height resolution of 0.25 mm, i.e. the minimum thickness of the individual slices.

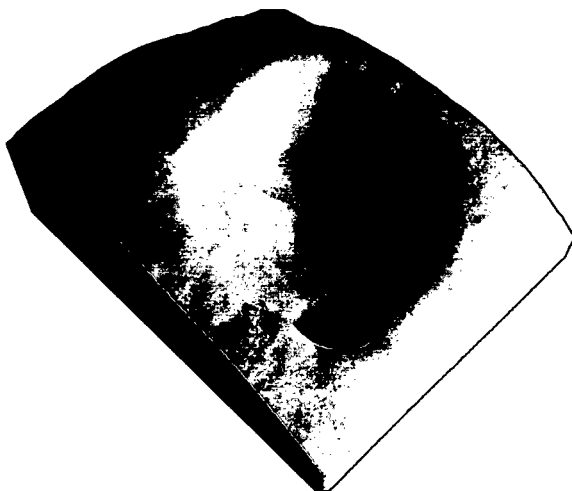


*Fig. 6.27: Photo of the hard copy model of Olympus Mons plotted at a 3D plotter.*

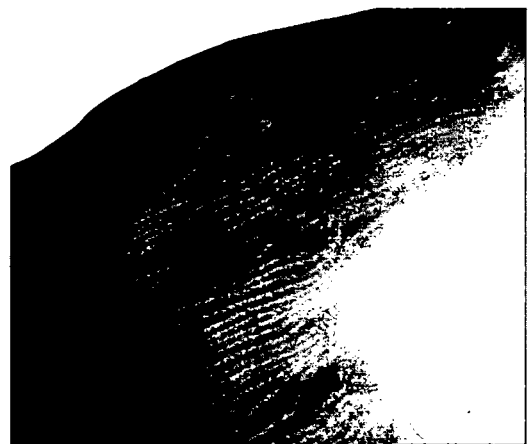


*Fig. 6.28: Detail of the hard copy showing the terrace effect caused by the individually plotted slices.*

## 7 Conclusions

### 7.1 Summary and Achievements

In the recent past, the Internet emerged as platform for interoperable services which can be joined to realize complex software solutions. The concepts for *Web Services* based on appropriate communication protocols and data exchange formats support the realization of inter-vendor applications, thus, they can integrate functionalities from other service providers. In this context, the role of vendor-independent organizations (e.g. OGC, ISO, W3C, ...) for defining applicable standards, which are accepted and supported by software developers, is of crucial importance. As part of this thesis, XML-based data exchange formats have been investigated to evaluate their applicability to spatial data. GML turned out to be appropriate for representation and exchange of topographic datasets, either consisting of randomly distributed points or in grid-based form. SVG, originally restricted to 2D geometry, has been extended to provide height information of the represented vector-based objects. Furthermore, it has been used to realize a map-based user interface for the representation of planet-wide shape information (polygonal boundaries of regions) within a web browser environment. Object-based formats for data presentation support client-side interactivity, scalability and rendering, and thus, they are preferable to static image formats provided by most current WMS.

Common *Web Services* are based upon DBMS. Thus, appropriate data modeling structures supporting efficient data access are indispensable. Most DBMSs providing enhancements for spatial data management are based on relational data models with object-oriented extensions. The supported data types are restricted to objects defined as "Simple Features" by the OGC. Complex objects are rarely supported.

The realization of the *Topographic Mars Information System (TMIS)* illustrates the application of the presented concepts, standards and methods. It is used to manage and distribute planet-wide image and topographic data. Data Access is provided by different form- and map-based interfaces. The internal workflow of the system is described using the standardized Universal Modeling Language (UML).

TMIS integrates DTM processing, analysis and visualization functionality, which has been applied to topographic Mars data. As the test dataset contained gross errors, a method for detection and subsequent elimination of erroneous points has been developed. It is based on iteratively applied robust interpolation methods. Thus, dependent on the roughness of the investigated area, erroneous points down to an RMS of 15 – 20 m compared to their surroundings can be detected. Due to the inhomogeneous planimetric distribution of the original points, different methods to derive the most reliable regular point grid representation have been tested. The method used to derive DTMs for further investigations starts with the computation of a coarse raster to bridge areas not containing any points. Afterwards, the original points and the coarse raster are merged, and a DTM is derived applying least squares interpolation. Based on such DTMs, the topography of three regions

characterized by potentially fluvially formed surface structures has been investigated with hydrological analysis. The results can be used as a basis for further research to find out whether the seemingly fluvially influenced areas really have been formed by former surface water. Finally, visualizations of the results have been prepared for 3D presentation, especially on the Internet.

## 7.2 Further Investigations

Within TMIS, a great amount of "simple structured" data (e.g. grid-based topographical models, polygonal image footprints, ...) has to be managed. Data acquisition methods with a high degree of automation (e.g. feature-based image matching or airborne laser scanning) are emerging technologies for Earth-based topographic data sampling. They provide data suited for modeling objects which have a much more complex structure than those typical for current Mars models. For instance, modeling buildings for subsequent generation of so-called cyber-cities could become essential. These buildings can be integrated in DTMs which should support 3D. To model the topography of urban areas in a consistent way, 3D support is absolutely necessary, considering bridges, underpasses, and so forth. Therefore, more complex data formats than the presented 2.5D format for DTM representation will be necessary.

The capabilities of the XML-based standards GML and SVG have been investigated concentrating on representation and visualization of simple structured data. As SVG support is limited to 2D geometry, they are not applicable for 3D modeling. On the contrary, the current GML specification supports a variety of properties for modeling complex objects including sophisticated line interpolations and surface definitions. Topological relations are supported as well. Thus, the concepts of spatial data modeling realized in GML according to ISO specifications can be taken into account for the definition of data structures for database management of spatial data. The investigation of new methods for topographic data processing and modeling is a central area of investigation within the Christian Doppler Laboratory for "Spatial Data from Laser Scanning and Remote Sensing" which was established at the I.P.F. in December 2003. Furthermore, this laboratory will concentrate on the determination of hydrological models for flood risk management. Thus, the Mars related hydrological investigations will be considered.

Concerning the experiences of modeling and analysis of the Mars topography, there are still open questions. The current method for error detection and elimination is dependent on a user defined final threshold. Therefore, roughness maps have to be integrated and applied for automatic derivation of this threshold. The methods of hydrological analysis applied to define a hypothetical river surface level in *Ma'adim Vallis* are based on overly simple assumptions. For instance, Cabrol and Grin (1998) describe sophisticated methods to estimate the discharge rates of potential Mars rivers. These methods should be taken into account to derive a more reliable river surface level.

A method for automated structure line detection in grid-based topographic models has been introduced. Within this work, it has not yet been applied to Mars data, although this or similar methods might improve the quality of current surface models which are solely based on grid-wise distributed points.

Finally it has to be stated, that none of the described methods had ever been applied to DTMs derived from HRSC image data, although the HRSC project has been the framework for this thesis. First attempts to derive reliable DTMs from currently available point clouds which have been acquired by feature-based image matching methods, have not been satisfying. It will be a great challenge to perform the described hydrological analysis to the high-resolution topographic models of Mars provided by the HRSC in order to to evaluate the presented results using the more detailed information.

The main task of TMIS is management and distribution of planet-wide image and topographic data. Since January 2004 the Mars Express spacecraft is in operational mode and it has already delivered almost 100 Gigabytes of image data which is available to all related scientists via TMIS. The application of the investigated methods for topographic data processing and analysis to HRSC data will be a future challenge!

## Appendix

### A Mars Fact Sheet

An overview of parameters characterizing Mars (NASA-NSSDC, 2004):

#### *Bulk parameters*

	Mars	Earth	Ratio (Mars/Earth)
Mass ( $10^{24}$ kg)	0.64185	5.9736	0.107
Volume ( $10^{10}$ km <sup>3</sup> )	16.318	108.321	0.151
Equatorial radius (km)	3,397	6,378.1	0.533
Polar radius (km)	3,375	6,356.8	0.531
Volumetric mean radius (km)	3,390	6371	0.532
Core radius (km)	1,700	3485	0.488
Ellipticity (Flattening)	0.00648	0.00335	1.93
Mean density (kg/m <sup>3</sup> )	3,933	5515	0.713
Surface gravity (m/s <sup>2</sup> )	3.71	9.8	0.379
Surface acceleration (m/s <sup>2</sup> )	3.69	9.78	0.377
Escape velocity (km/s)	5.03	11.19	0.45
GM ( $\times 10^6$ km <sup>3</sup> /s <sup>2</sup> )	0.04283	0.3986	0.107
Bond albedo	0.25	0.306	0.817
Visual geometric albedo	0.15	0.367	0.409
Visual magnitude V(1,0)	-1.52	-3.86	-
Solar irradiance (W/m <sup>2</sup> )	589.2	1,367.6	0.431
Black-body temperature (K)	210.1	254.3	0.826
Topographic range (km)	30	20	1.5
Moment of inertia (I/MR <sup>2</sup> )	0.366	0.3308	1.106
J <sub>2</sub> ( $\times 10^{-6}$ )	1,960.45	1,082.63	1.811
Number of natural satellites	2	1	
Planetary ring system	No	No	

#### *Orbital parameters*

	Mars	Earth	Ratio (Mars/Earth)
Semimajor axis ( $10^6$ km)	227.92	149.6	1.524
Sidereal orbit period (days)	686.98	365.256	1.881
Tropical orbit period (days)	686.973	365.242	1.881
Perihelion ( $10^6$ km)	206.62	147.09	1.405
Aphelion ( $10^6$ km)	249.23	152.1	1.639
Synodic period (days)	779.94	-	-
Mean orbital velocity (km/s)	24.13	29.78	0.81
Max. orbital velocity (km/s)	26.5	30.29	0.875
Min. orbital velocity (km/s)	21.97	29.29	0.75

Orbit inclination (deg)	1.85	0	-
Orbit eccentricity	0.0935	0.0167	5.599
Sidereal rotation period (hrs)	24.6229	23.9345	1.029

### Mars Observational Parameters

Discoverer	unknown
Discovery Date	prehistoric

	<i>min</i>	<i>max</i>
Distance from Earth ( $10^6$ km)	55.7	401.3
Apparent diameter from Earth (sec of arc)	25.1	3.5

<i>Mean values at opposition from Earth</i>	
Distance from Earth ( $10^6$ km)	78.39
Apparent diameter (sec of arc)	17.9
Apparent visual magnitude	-2
Maximum apparent visual magnitude	-2.91

### Mars Mean Orbital Elements (J2000)

Semimajor axis (AU)	1.52366231
Orbital eccentricity	0.09341233
Orbital inclination (deg)	1.85061
Longitude of ascending node (deg)	49.57854
Longitude of perihelion (deg)	336.04084
Mean Longitude (deg)	355.45332

### North Pole of Rotation

Right Ascension	317.681 - 0.108T
Declination	52.886 - 0.061T
Reference Date	12:00 UT 1 Jan 2000 (JD 2451545.0)
T = Julian centuries from reference date	

### Martian Atmosphere

Surface pressure	6.36 mb at mean radius (variable from 4.0 to 8.7 mb depending on season)
	[6.9 mb to 9 mb (Viking 1 Lander site)]
Surface density	~0.020 kg/m <sup>3</sup>
Scale height	11.1 km
Total mass of atmosphere	~2.5 x 10 <sup>16</sup> kg
Average temperature	~210 K (-63°C)
Diurnal temperature range	184 K to 242 K (-89 to -31°C) (Viking 1 Lander site)
Wind speeds	2-7 m/s (summer), 5-10 m/s (fall), 17-30 m/s (dust storm) (Viking Lander sites)
Mean molecular weight	43.34 g/mole
Atmospheric composition (by volume)	
Major	Carbon Dioxide (CO <sub>2</sub> ) - 95.32% ; Nitrogen (N <sub>2</sub> ) - 2.7%
	Argon (Ar) - 1.6%; Oxygen (O <sub>2</sub> ) - 0.13%; Carbon Monoxide (CO) - 0.08%

Minor (ppm)	Water (H <sub>2</sub> O) - 210; Nitrogen Oxide (NO) - 100; Neon (Ne) - 2.5;
	Hydrogen-Deuterium-Oxygen (HDO) - 0.85; Krypton (Kr) - 0.3; Xenon (Xe) - 0.08

### Satellites of Mars

	Phobos	Deimos
Semi-major axis* (km)	9378	23459
Sidereal orbit period (days)	0.31891	1.26244
Sidereal rotation period (days)	0.31891	1.26244
Orbital inclination (deg)	1.08	1.79
Orbital eccentricity	0.0151	0.0005
Major axis radius (km)	13.4	7.5
Median axis radius (km)	11.2	6.1
Minor axis radius (km)	9.2	5.2
Mass (10 <sup>15</sup> kg)	10.6	2.4
Mean density (kg/m <sup>3</sup> )	1900	1750
Geometric albedo	0.07	0.08
Visual magnitude V(1,0)	11.8	12.89
Apparent visual magnitude (V0)	11.3	12.4

\*Mean orbital distance from the center of Mars.



## B Chronology of Mars Exploration

The following table is a chronological listing of Mars missions. It summarizes information from several data sources (Heuseler et al., 1997, Puttkamer, 1997, NASA-NSSDC, 2004).

Mission name	Country	Mission type	Mass	Start	Arrival	Results
Marsnik 1	USSR	flyby	?	10.10.1960	---	Launch Failure (120 km)
Marsnik 2	USSR	flyby	640	14.10.1960	---	Launch Failure (120 km)
Sputnik 22	USSR	flyby	890	24.10.1962	---	lost in Earth orbit
Mars 1	USSR	flyby	694	01.11.1962	---	contact lost, 21.03.1963 (106 Mio. km)
Sputnik 24	USSR	lander	890	04.11.1962	---	lost in Earth orbit
Mariner 3	USA	flyby	261	05.11.1964	---	Launch Failure (did not reach Earth orbit)
Mariner 4	USA	flyby	261	28.11.1964	14.07.1965	min. distance: 9,846 km, 22 images
Zond 2	USSR	flyby	890	30.11.1964	---	contact lost (April 1965), min. distance: 1,500 km (06.08.1965)
Zond 3	USSR	flyby	890	18.07.1965	---	Lunar flyby, Mars missed - no data
Mariner 6	USA	flyby	413	24.02.1969	31.07.1969	min. distance: 3,360 km, 75 images, analysis of atmosphere (structure and consistency)
Mariner 7	USA	flyby	413	27.03.1969	05.08.1969	min. distance: 3,430 km, 200 images, analysis of atmosphere (structure and consistency)
Mars 1969A	USSR	orbiter/lander	3,190	27.03.1969	---	Launch Failure
Mars 1969B	USSR	orbiter/lander	3,190	02.04.1969	---	Launch Failure
Mariner 8	USA	orbiter	1,031	08.05.1971	---	Launch Failure
Cosmos 419	USSR	orbiter/lander	4,650	10.05.1971	---	lost in Earth orbit
Mars 2	USSR	orbiter/lander	4,650	19.05.1971	27.11.1971	several images; lander crashed
Mars 3	USSR	orbiter/lander	4,650	28.05.1971	03.12.1971	first smooth landing, lost after 20 sec. (27.12.1971)
Mariner 9	USA	orbiter	1,030	30.05.1971	13.11.1971	first artificial satellite of a planet (1,395 km), 6.876 images, max. resolution: 100 m/pix, lost on 27.10.1972
Mars 4	USSR	orbiter	3,950	21.07.1973	10.02.1974	flyby instead of orbit insertion, min. distance: 2.200 km
Mars 5	USSR	orbiter	3,950	25.07.1973	12.02.1974	worked several days, data of atmosphere, images from southern hemisphere
Mars 6	USSR	lander	3,950	05.08.1973	12.03.1974	landing site: Maragritifer Sinus, contact lost
Mars 7	USSR	lander	3,950	09.08.1973	09.03.1974	orbit insertion failed, lander missed its target
Viking 1	USA	orbiter/lander	3,400	20.08.1975	19.06.1976	landing site: Chryse Planitia (20.7.1976)
Viking 2	USA	orbiter/lander	3,400	09.09.1975	07.08.1976	landing site: Utopia Planitia (3.9.1976), <i>Viking results (both orbiter/lander):</i> 55,000 images (also Phobos and Deimos), 100% of Mars surface at 100 – 200 m/pix, regional 30 m/pix, several images with 8 m/pix, panoramic images of landing sites

Phobos 1	USSR	Mars orbiter, Phobos flyby/lander	6,000	07.07.1988	---	contact lost
Phobos 2	USSR	Mars orbiter, Phobos flyby/lander	6,000	12.07.1988	29.01.1989	lander lost, temperature measurements of 1,500 km with in equatorial region, resolution: 2 km/pixel, 40 images of Phobos, lost on 27.03.1989
Mars Observer	USA	orbiter	2,573	25.09.1992	21.08.1993	contact lost, during MOI
Mars Global Surveyor	USA	orbiter	1,050	07.11.1996	12.09.1997	start of MOI (aerobraking), duration: 1 year (problems with solar panel)
Mars 96	Russia	orbiter/lander	6,180	16.11.1996	---	lost in Earth orbit
Mars Pathfinder	USA	lander/rover	276	04.12.1996	04.07.1997	landing site: Ares Vallis, 06.07.1997: rover touched Mars surface, 27.09.1997: contact lost
Nozomi (Planet - B)	Japan	orbiter	258	03.07.1998	---	December 2003: lost
Mars Climate Orbiter	USA	orbiter	338	11.12.1998	---	contact lost
Mars Polar Lander	USA	lander	290	03.01.1999	---	contact lost
Deep Space 2 (DS2)	USA	penetrators	4	03.01.1999	---	contact lost
Mars Odyssey	USA	orbiter	376	07.04.2001	24.10.2001	thermal infrared imaging spectrometer: 100 m/pix visible camera: 18 m/pix (5 wavelengths)
Mars Express	ESA	orbiter/lander	666	02.06.2003	25.12.2003	MOI successful
Spirit (MER-A)	USA	rover	185	10.06.2003	04.01.2004	landing site: Gusev Crater
Opportunity (MER-B)	USA	rover	185	07.07.2003		Mars Exploration Rover
Mars Reconnaissance Orbiter	USA	orbiter	1,925	10.08.2005		Mars Orbiter
Phoenix	USA	lander		Late 2007		Small Mars Scout Lander
Netlanders	Netherlands	orbiter/landers		Late 2007		Mars Netlanders
Mars 2009	USA	rover		Late 2009		Mars Science Laboratory Rover
Mars 2011	USA	orbiter/lander/ rover/return		2011		Scout Mission return Mars samples to Earth

## C Mars Express Fact Sheet

The listed characteristics of the Mars Express spacecraft are from the ESA website (ESA, 2004).

### **Mass Budget:**

Spacecraft Item	Mass at Launch
Spacecraft Bus	439 kg
Lander	71 kg
Payload	116 kg
Propellant	427 kg
Launch Mass	1,223 kg

### **Power Budget:**

Typical Mean Power Demand	Observation	Manoeuvre	Communication
Spacecraft	270 W	340 W	445 W
Payload	140 W	50 W	55 W
Total	410 W	360 W	500 W

### **Dimensions:**

Spacecraft bus dimensions	1.5 x 1.8 x 1.4 m
Thrust of main spacecraft engine	400 N
Attitude thrusters	8 at 10 N each
Propellant	267 litres
Pointing performance	0.15°

### **Power Source:**

Solar array area	11.42 m <sup>2</sup>
Lithium batteries	3 at 22.5 Ah each

### **Thermal Specification:**

Spacecraft bus	+10-20°C
PFS, Omega	-180°C
Thermal blanket	Gold-plated AlSn alloy

### **Nominal Operational Orbit Parameters:**

Orbital Inclination	86.3°
Apocentre	11,560 km
Pericentre	258 km
Period	7.5 h
Observational Phase at Pericentre	about 1 hour
Communications Phase	6.5 – 7.0 hours minimum

## **D Scientific Objectives of the I.P.F. as HRSC Co-Investigator**

The TMIS (Topographic Mars Information System) should be a package of methods and software that is a further development and augmentation of an already existing system for topographic data management on Earth. The Institute of Photogrammetry and Remote Sensing at the Vienna University of Technology has got great expertise in that field for years. The structure of the TMIS uses TopDM as kernel, where various spatially related datasets can be stored. The system is extended by additional functionality, for instance by a tool for geodetic transformations from one reference system and datum to another and from one map projection to another. Most importantly, the TMIS will also be open to external users who do not want to have an additional implementation of a stand-alone system. Library routines will be available for access from separately working programs or even from remote sites via communication networks. In addition to the central software, further software will be included as peripheral modules, such as ortho-photo generation, map composition, radiometric correction due to topographic influences, DTM interpolation and other features. Extensive import and export filters will provide off-line access to the contents of the database (Hoffmann and Neukum, 2003, p. 18).

## E HRSC Performance

Parameter	HRSC	SRC	Comments
<b>Mechanical and electrical parameters</b>			
Camera Unit envelope	515 mm x 300 mm x 260mm		length x width x height
Digital Unit envelope	222 mm x 282 mm x 212 mm		DU used for HRSC and SRC
mass	22.4 kg		
power consumption	43.4 W during imaging	5.3 W during imaging	joint ops: 48.7 W
<b>Electro-optical performance</b>			
detector type	THX 7808B	Kodak KAI 1001	
sensor pixel size	7 $\mu\text{m}$ x 7 $\mu\text{m}$	9 $\mu\text{m}$ x 9 $\mu\text{m}$	
pixel size on ground	10 m x 10 m	2.3 m x 2.3 m	at 250 km altitude
field of view per pixel	8.25 arcsec	2 arcsec	
active pixels per sensor	9 sensors a 5184	1024 x 1032	
image size on ground	52.2 km swath x [time]	2.35 km x 2.35 km	at 250 km altitude
radiometric resolution	8 bit before compress.	14 bit or 8 bit selectable	
sensor full well capacity	420,000 e <sup>-</sup>	48,000 e <sup>-</sup>	
signal chain noise	< 42 e <sup>-</sup> (rms)	-	
gain attenuation range	3.5 - 2528	-	corresp. to 10.5 dB-62 dB
spectral filters	5 panchromatic, 4 color	-	
nadir, 2 stereo, 2 photo	675 $\pm$ 90 nm	-	
Blue, Green, Red, near infrared	440 $\pm$ 45 nm, 530 $\pm$ 45 nm 750 $\pm$ 20 nm, 970 $\pm$ 45 nm	-	
center pixel MTF	0.40 at 50 lp/mm	-	
20° off nadir MTF	0.33 at 50 lp/mm		
SNR for panchr. lines	>>100 (no macro pixel)	>70	30° solar elevat., dark region
SNR for color lines	>80, blue >40	-	for 2 x 2 macro pixel
<b>Digital features</b>			
on-line compression	yes		DCT: table controlled JPEG
compression rate	2-20; bypass possible		
max. output data rate	25 Mbits/s after compression		only at pericenter, decreases at higher altitudes
<b>Operations</b>			
pixel exposure time	2.24 ms to 54.5 ms	0.5 ms to 50 sec	
pixel summation formats	1x1, 2x2, 4x4, 8x8	-	
compression rates	nominal: 6 ... 10		
typical image size	53 km x 330 km	2.4 km x 2.4 km	at 250 km altitude
typical data vol. per image	230 Mbit	8 Mbit or 14 Mbitt	
duty cycle	every orbit; several times/orbit		depends on memory budget
internal data buffer	no	4 images at 14 bit resoluition	
typical operations duration	3 to 40 min		
expected coverage	none	none	
operational lifetime	> 4 years		

(from: HRSC Science Performance Budget, Hoffmann et al., 2003, p. 17)

## F Scientific Publications and Public Relations

### **Scientific publications and presentations:**

- 23.-25. Sept. 2002: P. Dorninger: High Quality Visualizations of Mars Surface. IRSPS Workshop - Exploring Mars Surface and its Earth Analogons, September 2002, Sicily, Italy.
- 9.-13. Sept. 2002: C. Briese, N. Pfeifer, P. Dorninger: Applications of the Robust Interpolation for DTM determination. Symposium of ISPRS-Comm. III, Graz, September 2002. In: International Archives of Photogrammetry and Remote Sensing, Volume XXXIV / 3A, pp. 55 – 61
- Nov. 2002: P. Dorninger: Topographic Mars Information System (TMIS) - Aufbau eines globalen Bild- und Geländedatenarchivs des Planeten Mars unter Verwendung von XML Technologien. GeoNews - Software Magazin für Vermessung und Geoinformation, Heft4/2002, p. 12-13.
- 16.-22. Feb. 2003: P. Dorninger, C. Briese, J. Jansa, G. Mandlbauer: Modellierung der Marsoberfläche aus Laserscanner Daten. XII. 12. In: Chesl, Weinhold (Editors). Internationale Geodätische Woche, Obergurgl 2003, Weinhold-Verlag, pp. 21 – 30.
28. Feb. 2003: P. Dorninger: XML Technologies and Geodata. CORP 2003 - 8th international symposium on information and communication technologies in urban and spatial planning and impacts of ICT on physical space, proceedings, TU Vienna, 25. February-March 2003, pp. 223 – 229.
- Jan. 2004: P. Dorninger, J. Jansa, C. Briese: Visualizations and Analysis of Mars Surface. Planetary Space Journal, Volume 52, Issues 1-3, January-March 2004, pp. 249 – 257.
- Apr. 2004: P. Dorninger: Analyse und geomorphologische Verbesserung von Geländemodellen mittels Regensimulation, Sonderausgabe der Österreichischen Zeitschrift für Vermessung und Geoinformation (VGI) anlässlich des Hochschullehrganges Laserscanning (September 2003, I.P.F., TU Wien), Heft 4/2003, pp. 253 – 261.
- Jun. 2004: P. Dorninger: A Topographic Mars Information System, Dissertation Dorninger at the I.P.F., Technical University of Vienna

### **Public Relations:**

17. Jul. 2002: Presentation at the home page of the Technical University of Vienna in the TU science news.
17. Jul. 2002: Press release of the TU Vienna
17. Jul. 2002: Press release publicised by the Austrian Press Agency (Austria Presse Agentur – APA); The following media printed resp. publicised the information:
- Der Standard, 17. Juli 2002
  - Kurier, 18. Juli 2002
  - Profil, Heft 34/2002
  - Die Presse, 18. Juli 2002
- The following radio stations of the Austrian Broadcasting Cooperation (ORF) publicised the information:
- Radio Wien
  - Ö1 (Dimensionen: Mars Express – Die Erkundung des roten Planeten, 16. Oct.)
  - Radio 1476 (ORF Mittelwelle)
27. Sept. 2002: Presentation at the summer university „Graz in Space“:  
J. Jansa: Aufbau eines topographischen Mars-Informationssystems (TMIS) im Rahmen des Projekts "HRSC on Mars Express"
25. Nov. 2002: Presentation during the „University Meets Public“ program at the Volkshochschule Penzing:  
J. Jansa: Ein topographisches Informationssystem für den Mars
3. Mai 2003: Presentation at the ARGEOS 2003 at the TU Vienna:  
P. Dorninger: Entwicklung eines Topographischen Mars Informationssystems für Mars Express 2003
23. Mai 2003: Fernsehbeitrag in ‚Modern Times‘ – ORF 2 (Ivo Filatsch): Europa fliegt zum Mars
3. Juli 2003: Fernsehbeitrag in ‚Wien Heute‘ – ORF 2 Wien (Norbert Fiala): Die TU Wien und Mars Express
25. Aug. 2003: Der Standard
- 17.-19. Sept. 2003: "A Virtual 3D Model of Valles Marineris and Tharsis Highlands" (Internet3D), InterGEO 2003, Kongress und Fachmesse für Geodäsie, Geoinformation und Landmanagement, Hamburg
5. Okt. 2003: Invited talk and panel discussion at the „Kuffner Volkssternwarte“ (Michael Jensen)
27. Nov. 2003: Invited talk at the „16. Sitzung der Österreichischen Kartographischen Kommission (ÖKK)“
28. Nov. 2003: Format Science: Österreich am Mars
21. Dez. 2003: Die Krone: TU Wien und Mars Express

## Acronyms and Abbreviations

ADT	Abstract Data Types
ALS	Airborn Laser Scanning
API	Application Programming Interface
ASCII	American Standard Code for Information Interchange
BLOB	Binary Large Object
CLOB	Character Large Object
Co-I	Co-Investigator
CU	Computing Unit
DB	Database
DBMS	Database Management System
DBS	Database System
DDL	Data Definition Language
DLR	German Aerospace Center
DML	Data Manipulation Language
DOM	Document Object Model
DTD	Document Type Definition
DTM	Digital Terrain Model
EER	Enhanced Entity Relationship Model
ER	Entity Relationship Model
ESA	European Space Agency
FTP	File Transfer Protocol
GIF	Graphics Interchange Format
GIS	Geographic Information System
GML	Geography Markup Language
GUI	Graphical User Interface
HRSC	High Resolution Stereo Camera
HTML	Hypertext Markup Language
HTTP	Hypertext Transfer Protocol
I.P.F.	Institute of Photogrammetry and Remote Sensing
IAU	International Astronomical Union
IDL	Interactive Data Language
IQL	Interactive Query Language
ISO	International Organization for Standardization
JDBC	Java Database Connectivity
JPEG	Joint Photographic Expert Group
JPL	Jet Propulsion Laboratory
JSP	JavaServerPages
MDC	Metadata Catalogue

---

MER	Mars Exploration Rover
MEX	Mars Express
MGS	Mars Global Surveyor
MOC	Mars Orbiter Camera
MOLA	Mars Orbiter Laser Altimeter
MS	Microsoft
NASA	National Aeronautics and Space Administration
NF	Normal Form
NF <sup>2</sup>	Non First Normal Form Model
ODL	Object Definition Language
ODMG	Object Data Management Group
OGC	OpenGIS Consortium
OMG	Object Management Group
OO	Object-Oriented
OODBS	Object-Oriented Database System
OQL	Object Query Language
OR-DBS	Object-Relational Database System
OTF	on-the-fly
PDF	Adobe Portable Document Format
PDS	Planetary Data System
PI	Principal Investigator
PNG	Portable Network Graphic
RDBMS	Relational Database Management System
RDBS	Relational Database System
RDH	Random Digital Heights
RMS	Root Mean Square Error
SCOP++	Stuttgart Contour Program
SFTP	Secure File Transfer Protocol
SOAP	Simple Object Access Protocol
SQL	Structured Query Language
SRS	Spatial Reference Frame
SVG	Scalable Vector Graphics
TDS	Topographic Data Server
THEMIS	Thermal Emission Imaging System
TIFF	Tagged Image File Format
TIS	Topographic Information System
TMIS	Topographic Mars Information System
TMIS-EF	Topographic Mars Information System – Extended Functionality
TopDB	Topographic Database
TopDM	Topographic Data Management
TOPSQL	Topographic SQL



---

UDDI	Universal Description, Discovery and Integration
USGS	United States Geological Service
VICAR	Video Image Communication and Retrieval
VRML	Virtual Reality Modeling Language
WebCGM	Web-based Computer Graphics Metafile
WINPUT	Wiener Input Format
WMS	Web Map Services
WSDL	Web Service Description Language
X3D	Extensible 3D
XDK	XML Development Kit
XML	Extensible Markup Language
XSD	XML Schema Definition Language
XSL	Extensible Stylesheet Language
XSL:FO	Extensible Stylesheet Language: Formatting Objects
XSLT	Extensible Stylesheet Language - Transformations

## References

- Bancilhon, F., Delobel, C., Kanellakis, P. (Editors), 2004. Building an Object-Oriented Database System – The Story of O<sub>2</sub>. Morgan Kaufmann Publishers, San Mateo, CA, 1992.
- Battrick, B., Talevi, M., 2001. Mars Express – Europe goes to Mars!, ESA Publications Division, ESA BR-174, Noordwijk, The Netherlands, July 2001.
- Beaujardiere, J. (Editor), 2001. Web Map Service (WMS) 1.1.1, OpenGIS® Implementation Specification, OpenGIS Consortium Inc., 27 November 2001, OGC 01-068r2.
- Beaujardiere, J. (Editor), 2004. Web Map Service (WMS) 1.3.0, OpenGIS® Implementation Specification, OpenGIS Consortium Inc., 20 January 2004, OGC 03-109r1.
- Beck, M., 1999. World-View – Ein generisches Virtual Reality Framework für die interaktive Visualisierung grosser geographischer Datenmengen, Dissertation in Informatics at the University of Zurich. 1999.
- Beck, M., 2003. Real-time Visualization of big 3D City Models. International Workshop on "Visualization and Animation of Reality-based 3D Models", ISPRS Com. V, WG 6, 24. – 28.2.2003, Switzerland. International Archives of Photogrammetry and Remote Sensing, Vol. XXXIV-5/W10.
- Beeri, C.: Formal Models for Object-Oriented Databases. In: Kim, W., Nicolas, J., Nishio, S. (Editors). Proceedings of the 1<sup>st</sup> International Conference on Deductive and Object-Oriented Databases (DOOD'89), Kyoto, Japan. Elsevier Science Publishers, December 1989.
- Borgefors, G., 1986. Distance transformation in digital images. Computer Vision Graphics Image Processing 34 (3), pp. 344 – 371.
- Buchroithner, M., Waelder, O., 2002. Development of Methods for true 3D-Presentations of Mars Surface. Proceedings of InterCarto 8, GIS for Sustainable Development of Territories, 28.5.-1.6.2002, Helsinki - St. Petersburg, pp. 409 – 411.
- Briese, Ch., Pfeifer, N., Dorninger, P., 2002a. Applications of the Robust Interpolation for DTM Determination. Symposium of ISPRS Com. III, Graz, September 2002. International Archives of Photogrammetry and Remote Sensing, Graz, Austria, Vol. XXXIV/3A, pp. 55 – 61.
- Briese, Ch., Kraus, K., Pfeifer, N., 2002b. Modellierung von dreidimensionalen Geländemodellen in Laser-Scanner-Daten. Festschrift anlässlich des 65. Geburtstages von Herrn Prof. Dr.-Ing. habil. Siegfried Meier, TU Dresden, Inst. für Planetare Geodäsie, pp. 47 – 52.
- Cabrol, N., A., Grin, A., E., 1998. Ma'adim Vallis Evolution: Geometry and Models of Discharge Rate. International Journal of Solar System Studies (Icarus), Vol. 132, pp. 362 – 377.
- Carr, M.H. (Editor.), 1996. Water on Mars, Oxford University Press, New York, 1996.
- Cattell, R., G., G., Barry, D., K., Berler, M., Eastman, J., Jordan, D., Russell, C., Schadow, O., Stanienda, T., Velez, F., 2000. The Object Data Standard: ODMG 3.0. Morgan Kaufmann Publishers.
- Codd, E., F., 1970. A Relational Model of Data for Large Shared Data Banks. Communications of the ACM, Vol. 13, No. 6, June 1970, pp. 377 – 387

- Cox, S., Daisey, P., Lake, R., Portele, C., Whiteside, A. (Editors), 2004. Geography Markup Language (GML) 3.1, OpenGIS® Implementation Specification, committee draft, OpenGIS Consortium, 7 February 2004, ISO/TC 211/WG 4/PT 19136.
- Date, C., J., 1990. An Introduction to Database Systems, Vol I, Fill. Ed., Reading, Massachusetts et. al, 1990.
- Dorninger, P., 2004. Analyse und geomorphologische Verbesserung von Geländemodellen mittels Regensimulation. Hochschullehrgang Laserscanning, Vienna 2003, Österreichische Zeitschrift für Vermessung und Geoinformation (VGI), Heft 4/2003, pp. 253-261.
- Doyle, A., Cuthbert, A., 1998. Essential Model of Interactive Portrayal. OpenGIS Project Document 98-061.
- Duxbury, E., Jensen, D., 1994. VICAR User's Guide, Version 3, Jet Propulsion Laboratory, California Institute of Technology, Pasadena, California, 1994.
- Eisfeld, R., Jeschke, W., 2003. Marsfieber. Aufbruch zum Roten Planeten, Phantasie und Wirklichkeit, Droemer Verlag, München.
- Ehrig, H., Mahr, B., 1985. Fundamentals of Algebraic Specification 1. Equations and Initial Semantics. Springer-Verlag, Berlin.
- Eisfeld, R., Jeschke, W., 2003. Marsfieber. Aufbruch zum Roten Planeten, Phantasie und Wirklichkeit, Droemer Verlag, München.
- Engels, G., Gogolla, M., Hohenstein, U., Hülsmann, K., Löhr-Richter, P., Saake, G., Ehrich, H., 1992. Conceptual Modelling of Database Applications using an Extended ER Model. Data & Knowledge Engineering, North-Holland, Vol. 9, Nr. 2, pp. 157 – 204.
- Fitzke, J., Greve, K., Müller, M., Poth, A., 2004. Building SDIs with Free Software – the deegree project. In: CORP 2004, Proceedings of 9<sup>th</sup> symposium on Info- & Communication Technology in Urban- and Spatial Planning and Impacts of ICT on Physical Space, Vienna, 2004, pp. 97 – 103.
- Ferraiolo, J., Fujisawa, J., Jackson, D., (Editors), 2003. Scalable Vector Graphics (SVG) 1.1 Specification, W3C Recommendation 14 January 2003.
- Fuller, E., R., Head, J., W., 2001. Volcanism and Sedimentation: Origins of the Smoothest Plains on Mars. GSA Annual Meeting, Paper No. 178-0, November 5 – 8, 2001.
- Garvin, J., B., Sakimoto, S., E., H., Frawley, J., J., Schnetzler, C., C., Wright, H., M., 2000. Topographic Evidence for Geologically Recent Near-Polar Volcanism on Mars. International Journal of Solar System Studies (Icarus), volume 145, pp. 648 – 652.
- Gilbert, M., 2002. On-Line Distribution of Digital Topographic Data. In: International Archives of Photogrammetry, Remote Sensing and Spatial Information Sciences, ISPRS, Vol. XXXIV, Part 4, Com. IV, Ottawa, Juli 2002, pp. 185 – 189.
- Gottlob, G., Koch, Ch., Reinhard, P., 2002. Efficient Algorithms for Processing XPath Queries, Proceedings of 28th International Conference on Very Large Data Bases (VLDB), Hong Kong, China, August 2002.
- Gottlob, G., Koch, Ch., Pichler, R., 2003. Xpath query evaluation: Improving time and space efficiency. In Proc. IEEE Conference on Data Engineering.

- Grant, J., A., Golombek, M., P., Parker, T., J., Crips, A., J., Squyres, S., W., Weitz, C., M., 2004. Selecting landing sites for the 2003 Mars Exploration Rovers. *Planetary and Space Science*. Volume 52, Issues 1 – 3, January – March 2004. pp. 21 – 21.
- Gregg, T., K., P., Sakimoto, S., E., H., 2000. Marte Valles Lava Channel Flow Rates and Rheology from MOC and MOLA Data. *Lunar and Planetary Space Science Conference XXI*, No. 1758.
- Hartmann, W. K., Berman, D. C., 2000. Elysium Planitia lava flows: Crater count chronology and geological implications, *J. Geophys. Res.* 105, 15011-15026, 2000.
- Heuer, A., Saake, G., 2000. *Datenbanken: Konzepte und Sprachen*. 2. aktualisierte und erweiterte Auflage, mitp-Verlag, Landsberg, 2000.
- Heuseler, H., Jaumann, R., Neukum, G., 1997. *Die Mars Mission. Pathfinder, Sojourner und die Eroberung des Roten Planeten*, BLV Verlag, München.
- Hochstöger, F., 1996. Software for Managing Country-Wide Digital Elevation Data. *International Archives for Photogrammetry and Remote Sensing*, XXXI, Part B2, Vienna 1996, pp. 160 – 163.
- Hoffmann, H., Behnke, Th., Hauber, E., Flohrer, J., Matz, K.-D., Pischel, R., Jaumann, R., Neukum, G., 2003. Science Performance Budget for the HRSC on Mars Express.
- Hoffmann, H., Neukum, G., 2003. HRSC on Mars Express Co-Investigator Team: Experiment Implementation and Internal Management Plan
- Jaumann, R., Hauber, E., Lanz, J., Hoffmann, H., Neukum, G., 2001. Geomorphological Record of Water-Related Erosion on Mars, in Horneck, G., Baumstark-Khan, Ch. (Editors): *Astrobiology: The Quest for the Conditions of Life*, Springer Verlag, Köln, 2001, pp. 89 – 110.
- Kraus, K., 1998. Interpolation nach kleinsten Quadraten versus Krige-Schätzer. *Österreichische Zeitschrift für Vermessung & Geoinformation*. 86. Jahrg., Heft 1, pp. 45 – 48.
- Kraus, K., 2000. *Photogrammetrie Band 3. Topographische Informationssysteme*, 1<sup>st</sup> edition. Dümmler Verlag, Köln.
- Kraus, K., Briese, Ch., Attwenger, M., Pfeifer, N., 2004. Quality Measures for Digital Terrain Models. In: *Proceedings of 20<sup>th</sup> Congress of the International Society for Photogrammetry and Remote Sensing, ISPRS, Istanbul, July 2004*, in press.
- Kreger, H., 2001. *Web Services Conceptual Architecture (WSCA 1.0)*. IBM Software Group, May 2001.
- Kreslavsky, M., A., Head, J., W., 2000. Kilometer-scale roughness of Mars: Results from MOLA data analysis, *J. Geophys. Res.*, 101, 26,695-26,711, 2000.
- Li, N., Hui, J., Hsiao, H., Tijare, P., 2003. Cursor Management for XML Data. in *Database and XML Technologies (Bellahsene et al. Eds.)*, Database and XML Technologies, *Proceedings of First International XML Database Symposium, XSym 2003*, Berlin, Germany, September 2003
- Liu, C., Vincent, M., Liu, J., Guo, M., 2003. A Virtual XML Database Engine for Relational Databases. In: *Proceedings of Spatial Data 2000*, Department of Photogrammetry and Surveying, University College London, pp. 260-269.

- Loitsch, J., Molnar, L., 1991. A Relational Database Management System with Topological Elements and Topological Operators. In: Proceedings of Spatial Data 2000, Department of Photogrammetry and Surveying, University College London, pp. 260-269.
- Longley, P., Goodchild, M., Maguire, D., Rhind, D., 2001. Geographic Information Systems and Science. Chichester, John Wiley & Sons, Ltd, 2001.
- Mandlbauer, G., 2000. Verdichtung von Echolot Querprofilen unter Berücksichtigung der Flussmorphologie. Österreichische Zeitschrift für Vermessung & Geoinformation, 88. Jahrgang, Heft 4, 2000, pp. 211 – 214.
- Mertz, D., 2001. XML and Compression, Exploring the entropy of documents, Gnosis Software, Inc, September 2001
- Moritz, H., Sünkel, H., 1978. Approximation Methods in Geodesy. Sammlung Wichmann, Neue Folge, Band 10. Wichmann-Verlag, Karlsruhe.
- Morton, O., 2004. Mars Revisited. National Geographic. Official Journal of the National Geographic Society. January 2004. p2 – 31.
- Nebiker, S., 2003. Support for Visualisation and Animation in a Scalable 3D GIS Environment – Motivation, Concepts and Implementation. ", ISPRS Com. V, WG 6, February 2003, Switzerland. International Archives of Photogrammetry and Remote Sensing, Vol. XXXIV-5/W10.
- Oracle Spatial, 2003. Oracle Spatial – Users's Guide and Reference, Release 9.2, Part No. A96630-01, March 2002
- Plescia, J., B., 1990. Recent flood lavas in the Elysium region of Mars, Icarus, 88, pp. 465 – 490, 1990.
- Puttkamer, J., 1997. Jahrtausendprojekt Mars. Chance und Schicksal der Menschheit, Droemer Knauer Verlag, München
- Reichardt, M., 2001. OGC's GML 2.0 – A New Wave of Open Geoprocessing on the Web, GeoInformatics, Magazine for Geo-IT Professionals, Issue July/August 2001, pp. 18 – 21.
- Reinhart, M., 1995. Relationales Datenbankdesign, Verlag Franz Vahlen GmbH, München.
- Rieger, W., 1992a. Hydrologische Anwendungen des digitalen Geländemodelles. Dissertation at the Vienna University of Technology. 1992.
- Rieger, W., 1992b. Automated River Line and Catchment Area Extraction from DEM Data. International Archives of Photogrammetry and Remote Sensing, Washington, USA, Vol. XXIX/B4, pp. 642 – 649.
- Roatsch, T. (Editor), 2001. HRSC VICAR Label Description Document. HRSC-DLR-TN-4200-002, June 2001.
- Schneeberger, D., M., 1989. Episodic channel activity at Ma'adim Vallis [abstract]. In Lunar Planetary Science Conference, Vol. XX, pp. 964 – 965.
- Schrefl, M., Bichler, P., 1995. Modeling Reality in an Information System. in Frank, A., U. (Ed.): Geographic Information Systems, Vol. 1, Spatial Information,

- Scott, D. H., Tanaka, K. L., 1986. Geologic map of the western equatorial region of Mars, U.S. Geol. Surv. Misc. Invest. Map, I-1802-A.
- Smith, D.E., Zuber, M.T., Solomon, S.C., Phillips, R.J., Head, J.W., Garvin, J.B., Banerdt, W.B., Muhleman, D.O., Pettengill, G.H., Neumann, G.A., Lemoine, F.G., Abshire, J.B., Aharonson, O., Brown, C.D., Hauck, S.A., Ivanov, A.B., McGovern, P.J., Zwally, H.J., Duxbury, T.C., 1999. The global Topography of Mars and Implications for Surface Evolution, *Science*, 284 1495-1503, 1999.
- Tsichritzis, D., Klug, A., 1978. The ANSI/X3/SPARC DBMS Framework Report of the Study Group on Database Management Systems. *Information Systems*, Vol. 3, Nr. 3, pp. 173 – 191
- Wählisch, M., Niedermaier, G., van Gasselt, S., Scholten, F., Wewel, F., Roatsch, T., Matz, K-D., Jaumann, R., 2002. A new digital orthoimage map of the Martian western hemisphere using data obtained from the Mars Orbiter Camera at a resolution of 256 pixel/deg. 33<sup>rd</sup> Lunar and Planetary Science Conference, Houston, TX, March 2002.

## Web Links

ADOBE, 2004. The Adobe SVG Zone.

<http://www.adobe.com/svg/>

APACHE, 2004. The Apache Software Foundation.

<http://www.apache.org/>

ASU, 2004. Arizona State University.

<http://www.asu.edu/>

*(Portal site)*

<http://themis-data.asu.edu/>

*(THEMIS image archive)*

BZIP2, 2004. The Bzip2 Official Homepage.

<http://sources.redhat.com/bzip2/>

CARTONET, 2004. carto.net.

<http://www.carto.net>

CGM, 2004. CGM Open, an OASIS Community.

<http://www.cgmopen.org>

DIMENSION, 2004. Dimension, Stratasys Inc.

<http://www.dimensionprinting.com>

EOLI, 2004. EOLI-Web Envisat Catalogue.

<http://muis-env.esrin.esa.it/geteolisa/index.html>

ESA, 2004. European Space Agency, Science Programme Portal.

<http://sci.esa.int>

ESRI, 2004. Environmental Systems Research Institute.

<http://www.esri.com>

GEOMAGIC, 2004. Raindrop Geomagic GmbH, Cologne, Germany,

<http://www.geomagic.com>

GEONOVA, 2004. Internet3D, powered by GEONOVA, Geoinformation Solutions.

<http://www.geonova.at>

*(Portal site)*

[http://www.geonova.at/mars\\_gr/start.htm](http://www.geonova.at/mars_gr/start.htm)

*(Virtual Model of Valles Marineris)*

GNU, 2004. GNU General Public License. Free Software Foundation, Inc., Boston, USA, June 1991.

<http://www.gnu.org/copyleft/gpl.html>

GNU-ZIP, 2004. The Gzip Homepage.

<http://www.gzip.org/>

GRASS, 2004. Geographic Resources Analysis Support System.

<http://grass.itc.it/>

IBMDB2, 2004. IBM DB2 Product Family.

[www.ibm.com/software/data/db2/](http://www.ibm.com/software/data/db2/)

IDL, 2004. Research Systems Inc., The Interactive Data Language.

<http://www.rsinc.com/>

IPF-SCOP, 2004. Product info site of the I.P.F.

<http://www.ipf.tuwien.ac.at/products/products.html>

ISO, 2004. International Organization for Standardization, Geographic Information/Geomatics.

<http://www.iso.org>

<http://www.isotc211.org>

JAKARTA, 2004. The Apache Jakarta Project.

<http://jakarta.apache.org/tomcat/>

JAVA, 2004. Java Products and Technology.

<http://java.sun.com/>

JPEG2000, 2004.

<http://www.jpeg.org/jpeg2000/>

MACROMEDIA, 2004. Macromedia, Inc.

<http://www.macromedia.com/>

MOZILLA, 2004. The Mozilla Project.

<http://www.mozilla.org>

NASA-MER, 2004. Mars Exploration Rover (MER), Jet Propulsion Laboratory, California Institute of Technology, USA.

<http://marsrovers.jpl.nasa.gov/home/>

NASA-MGS, 2004. Mars Global Surveyor (MGS), Jet Propulsion Laboratory, California Institute of Technology, USA.

<http://mars.jpl.nasa.gov/mgs>

NASA-MOC, 2004. Mars Orbiter Camera (MOC), Malin Space Science Systems, San Diego, California, USA.

<http://www.msss.com/>

NASA-MOLA, 2004. Mars Orbiter Laser Altimeter (MOLA) Science Investigation Site, NASA's Goddard Space Flight Center, USA.

<http://ftpwww.gsfc.nasa.gov/tharsis/mola.html>

<http://www.wustl.edu/>

NASA-NSSDC, 2004. National Space Science Data Center, NASA Goddard Space Flight Center, Greenbelt, USA.

<http://nssdc.gsfc.nasa.gov/>

<http://nssdc.gsfc.nasa.gov/planetary/factsheet/marsfact.html> (Mars Fact Sheet)

[http://nssdc.gsfc.nasa.gov/planetary/chronology\\_mars.html](http://nssdc.gsfc.nasa.gov/planetary/chronology_mars.html) (Mars Express Fact Sheet)

NASA-ODYSSEY, 2004. Mars Odyssey Mission, Jet Propulsion Laboratory, California Institute of Technology, USA.

<http://marsprogram.jpl.nasa.gov/odyssey/>

OGC, 2004. OpenGIS Consortium.

<http://www.opengis.org>



ORACLE, 2004. Oracle Corporation.

<http://www.oracle.com>

PDS, 2004. The Planetary Data System, NASA.

<http://pds.jpl.nasa.gov>

POSTGIS, 2004. Refrations Research, PostGIS, Geographic Objects for PostGreSQL.

<http://postgis.refrations.net/>

POSTGRESQL, 2004. PostGreSQL.

<http://www.postgresql.org/>

SOAP, 2004. Simple Object Access Protocol.

<http://www.w3.org/TR/soap/>

SVGOPEN, 2004. SVG Open, Conference and Exhibition.

<http://www.svgopen.org>

USGS-NAMES, 2004. Gazetteer of Planetary Nomenclature, United States Geological Survey, Flagstaff, USA.

<http://planetarynames.wr.usgs.gov/>

W3C-DOM, 2004. W3C Architecture Domain, Document Object Model.

<http://www.w3.org/DOM/>

W3C-XML, 2004. World Wide Web Consortium. Extensible Markup Language.

<http://www.w3.org/XML/>

Web3D-X3D, 2004. Information Technology, Computer Graphics and Image Processing, Extensible 3D (X3D). ISO/IEC 19775:200x, Extensible 3D (X3D). Web3D Consortium.

<http://www.web3d.org/>

XMILL, 2004. XMill, An Efficient Compressor for XML.

<http://www.research.att.com/sw/tools/xmill/>

## Curriculum Vitae

*Name:* Dipl.-Ing. Peter Dorninger  
*Date and Place of Birth:* March 18, 1976 in Vienna  
*Marital Status:* married with Dr. Angela Dorninger

1982 – 1986 Elementary School, Biedermannsdorf  
1986 – 1994 BG/BRG Franz Keimgasse, Mödling (Grammar School)  
1994 – 1997 Surveying (Vermessungswesen), Vienna University of Technology (TU Vienna)  
1997 – 2000 Surveying and Geoinformation, TU Vienna  
1998 – 2000 Tutor at the TU Vienna  
1999 – 2000 Research assistant at the Institute of Photogrammetry and Remote Sensing (I.P.F.)  
16/05/2000 Dipl.-Ing. degree (M. Sc.) with honors from the Vienna University of Technology  
2000 – 2001 Military services  
since 2001 Research associate at the I.P.F. (TU Vienna) and  
Doctoral program in the frame of Mars Express